LUNG CANCER TARGETED CHEMOTHERAPY VIA HERCEPTIN BASED CHIMERIC ANTIGEN RECEPTOR (CAR) ENGINEERED T CELL MEMBRANE COATED SYNTHETIC NANOPARTICLES

by

SERKAN YAMAN

DISSERTATION

Submitted in partial fulfillment of the requirements

for the degree of Doctor of Philosophy at

University of Texas at Arlington

August 2019

Arlington, Texas:

Supervising Committee:

Kytai T. Nguyen, Supervising Mentor

Jon A. Weidanz, Co-Supervising Mentor

Justyn Jaworski

Liping Tang

Michael Cho

ABTRACT

LUNG CANCER TARGETED CHEMOTHERAPY VIA HERCEPTIN BASED CHIMERIC ANTIGEN RECEPTOR (CAR) ENGINEERED T CELL MEMBRANE COATED SYNTHETIC NANOPARTICLES

Serkan Yaman, Ph.D.

University of Texas at Arlington, 2019

Supervising Professors: Kytai T. Nguyen and Jon A. Weidanz

Cell membrane-derived nanoparticles recently caught attention due to their desirable features in drug delivery such as mimicking properties of native tissues and cells, avoiding systemic clearance, and alleviating foreign body responses. Besides nanoparticle technology, adoptive immunotherapy has emerged for its promising treatment modalities, including cancer specificity. Our long-term goal for this research is to develop a biomimetic drug carrier based on chimeric antigen receptor (CAR) transduced T cell membranes. In the study, anti-cancer drug afatinib loaded poly(D,L-lactide-*co*-glycolide) (PLGA) nanoparticles (NPs) co-extruded with anti her-2 based chimeric antigen receptor (CAR) engineered Jurkat T cell membranes. Anti-her-2 CAR-T cells were produced by lentiviral transduction of anti-her-2 chimeric antigenic receptor coding lentiviral plasmids. Anti-her-2 CAR-T cells were characterized by their specific activities against Her-2 antigen and used for cell membrane extraction. Anti-her2 CAR-T cell membrane coated PLGA nanoparticles (CAR-T-MNPs) characterized and confirmed via fluorescent spectral microscopy and flow cytometry. Membrane coated NPs showed sustained drug release over the course of 21 days and were stable up to 5 days. Afatinib loaded CAR-T-MNPs inhibited the growth

of A549 lung, breast and ovarian cancer cells *in vitro*. In addition, *in vitro* uptake studies revealed that CAR-T-MNPs showed an increased uptake by A549 cells. These results also confirmed, via *in vivo* biodistribution studies using subcutaneous lung cancer model in nude mice that, of all studied groups, CAR-T-MNPs localized more at tumor areas compared to those of other studied groups. Therefore, new CAR modified cell membrane coated NP drug-delivery platform has shown its efficacy *in vitro* and *in vivo.* Proposed CAR based NPs are promising biomimetic delivery with its long circulation time and tumor site accumulation while opening a new way to personalized medicine and tumor specific targeting by patient's own cell membrane coated NP delivery.

Keywords: Nanoparticles, CAR-T cells, membrane-based drug delivery, cancer chemotherapy

Acknowledgements

My deepest gratitude goes first and foremost to my advisors, Drs. Kytai T. Nguyen and Jon A. Weidanz, for their constant guidance, encouragement, and patience during the entire period of my PhD program. Without them and the knowledge that they have delivered to me, this thesis work could not be completed. I am grateful to them for giving me an opportunity to work in their laboratories as a graduate student.

Similarly, very special thanks go to Dr. Manoj K. Sabnani, who helped me with several techniques used in this project. I am also very thankful to Harish Ramachandramoorthy, who I worked as a graduate student under during most of the time of this work. Moreover, I am greatly indebted to all my laboratory colleagues, and it is an honor for me to remember all of the good memories associated with Dr. Nguyen's and Dr. Weidanz's group members.

Finally, I would like to dedicate this thesis to my family members, who have always believed in me despite my situations and struggles and motivated me to pursue this PhD journey. Their support and encouragement in hard times has motivated me to keep working towards my goals.

-Serkan Yaman August 2019

TABLE OF CONTENTS

LIST OF FIGURES

LIST OF TABLES

CHAPTER 1

Background of lung cancer and its current therapies

1.1) Lung cancer: background and statistics

The lungs are the respiratory organ located in the chest. They have a cancellous structure and are protected by the ribs. Lungs are consisted of two parts: the right and the left lung. Because of the heart's location, the left lung has two lobes and the right has three. The overall anatomy of the lung can be seen in **Figure 1** [1]. Air follows a path through the nose or mouth, then the trachea, and ends up in the alveoli. From the trachea to the alveoli, air follows a path called the bronchi, which creates a tree like structure from the trachea to the alveoli by forming a tube-like structure. At the alveoli, the gas exchange takes place where oxygen transports the air to the alveoli epithelium and carbon dioxide is expelled from the epithelia to the alveoli space [1].

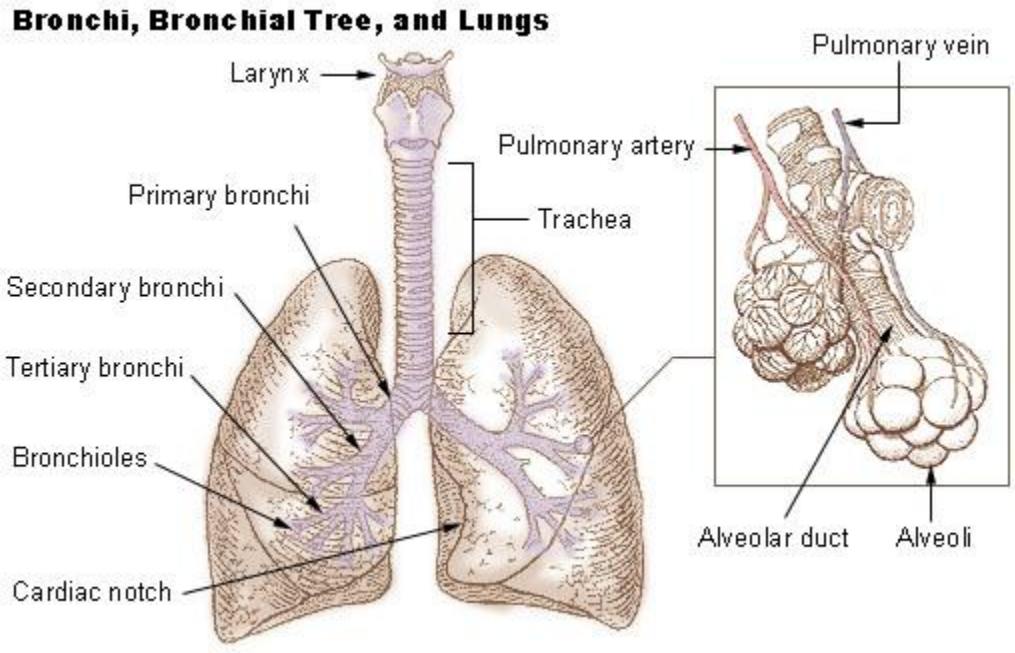

Figure 1: Anatomy of Normal Human Lung [1].

The number one reason for cancer deaths in the United States is lung cancer, which accounts for one fourth of every cancer related death each year with the lowest 5-year survival rate (18%) and costs more lives every year than breast, prostate, ovarian and colon cancers together [2]. In 2015, about 218,527 new cases of lung cancer were reported, and 153,718 people died from lung cancer in the United States [3]. Small cell lung cancer (SCLC) and non-small cell lung cancer (N-SCLC) are seen as the two main types**.**

1.1.1) Small cell lung cancer

Small cell lung cancer accounts for 10-15 percent of lung cancers. Usually, it begins in the bronchi and tends to grow more quickly than N-SCLC tumors. Small cell lung cancer is frequently metastatic to lymph nodes; however, it is more responsive to chemotherapeutic drugs than non-small cell lung cancer [4].

1.1.2) Non-small cell lung cancer (N-SCLC)

Non-small cell lung cancer is the most common lung cancer with about 85-90% of all lung cancers. SCLC grows relatively slower compared to that of N-SCLC, and histologically N-SCLC has three sub-types:

- **Adenocarcinoma** consists from gland like cells and develops in small airways around the outer edge of the lung. Adenocarcinoma accounts for 40% of all N-SCLC tumors.

- **Squamous cell carcinoma** hails from squamous tissues in which cells looks like fish scales under the microscope. It is usually seen in the central part of the lung or as a line inside the main airways. Squamous cell carcinoma accounts for 25% of N-SCLC tumors.

- **Large cell carcinoma** is distinguished histologically from other types by the large round size. This type of lung cancer can be found anywhere in the lung and tends to grow rapidly and spread quickly compared to other types. Large cell carcinoma accounts for about 10-15% of all N-SCLC tumors. If a lung cancer has characteristics of two types, it is called a mixed small cell/large cell cancer, however, this variant is not common [4].

1.2) N-SCLC staging

Lung cancer staging is classified based on whether the tumor remains local or has spread from its original place to other systems or organs. Due to the relatively big volume of the lungs, N-SCLC tumors can grow for a long time before they are able to be diagnosed. Moreover, its symptoms might be confused with other lung related diseases such as coughing, fatigue and so on. Thus, diagnosis of early-stage lung cancer (stages I and II) is also another hurdle needed to be overcome.

N-SCLC staging is classified as follows:

- **Stage I**: The tumor is localized in a specific area in the lungs and has not expanded to any surrounding tissue.

- **Stage II**: The tumor is still localized in the lung but has spread nearby to lymphatic tissues/nodes.

- **Stage III**: In this stage, the tumor has spread within the lung and the lymph nodes. This stage is also described as a locally advanced stage, which has two subtypes called stage IIIA and stage IIIB.

Stage IV: This is the last stage of N-SCLC. Cancer has already metastasized to all lobes, and to other parts/organs of the body, and cancer cells are also found in body fluids [5].

1.3) The risk factors and incidences

1.3.1) Smoking

Lung cancer is strongly correlated with smoking, and smoking is responsible for 90% of all lung cancer incidents. The risk of lung cancer increases with overall smoking time and smoke exposure. Researchers have proven that exposure to tobacco smoke as a nonsmoker increases the risk of lung cancer by 24%. Tobacco smoke has more than 4,000 chemicals, and many of them have been shown to be carcinogenic [6].

1.3.2) Inhalation of asbestos dust

Asbestos inhalation is also another risk to develop N-SCLC. Asbestos silicate consists of fibers ranging in sizes from 100 nm to 10 μm and can stay for a longtime in the lung tissue. This material was commonly used in the past as an insulation material. When it is exposed to lungs, the fibers damage the lung tissue and lead to lung/mesothelioma cancer. Nowadays, use of asbestos based materials is strictly prohibited around the world [7].

1.3.3) Exposure to radon gas

Radon is an invisible and odorless gas, which is released from uranium containing rocks/soils. About 12% of lung cancer deaths is thought to be related with radon exposure. Radon gas can leak from soil through homes, which were built on a soil naturally containing radon and/or the ones on the lower levels. One out of every 15 houses in the US has exceeded a critical level in terms of radon gas according to the U.S. authorities [4].

1.3.4) Familial genetic inheritance

In addition, individual genetic susceptibility may take place for lung tumor development. Various researchers have shown the development of lung cancer likely happens in relatives, who inherit certain genes/mutations, compared to the overall population, and this is not related with their smoking history [6].

1.3.5) Lung diseases

Individuals who have a history of certain lung related diseases such as tuberculosis, pulmonary fibrosis, or chronic obstructive pulmonary disease (COPD) are also considered as another risk factor for the development of lung cancer [6].

1.3.6) Air pollution

Air pollution caused by heavy industrial processes, power plant wastes, and diesel exhaust is also creating a huge risk factor for developing lung cancer in exposed people. Around 1%-2% of all lung cancer related deaths is associated with polluted air exposure. All other risk factors can be listed including: radiation/industrial/military chemical exposure [8].

1.4) Current treatment options and limitations

Treatment methods for N-SCLC depend on different factors such as disease types and stages as well as whether the tumor is metastasized or not. Currently, different treatment options available for N-SCLC are listed below [9, 10]:

- Surgery
- Chemotherapy
- Radiotherapy
- Targeted Therapy
- Immunotherapy

1.4.1) Lung cancer surgery

Surgery is the removal of tumor tissues while minimally affecting the healthy tissue. Surgery is advised if the tumor has not spread to multiple areas. In this case, surgery is the best option to treat non-small-cell lung cancer. Four different surgery types to remove the tumors include [11]:

- Wedge resection: removes only affected tissues with very small sections of healthy ones.
- Partial resection: removes a relatively large portion of the lung, which is affected from cancer spread.
- Lobectomy: removal of an entire lobe.
- Pneumonectomy: removal of the whole lung.

If lung cancer can be diagnosed early, surgical options provide a better chance for survival from N-SCLC. However, if there is a risk of recurrence from the cancer cells which are left behind,

chemotherapy or radiation therapy should be used as a combination after surgery. Furthermore, due to patient specific circumstances (e.g. age, overall health, and others), surgery might not be a good option for advanced staged and metastatic cancer cases.

1.4.2) Chemotherapy

Chemotherapy uses chemical drugs to kill or inhibit growth of cancer cells. During chemotherapy, either a single type chemo-drug or a mixture of different formulations can be introduced via intravenous or oral routes. Usually, it is given periodically over weeks or months, with intervals of cease to assure patient recovery. Chemotherapy either can be used as a stand-alone therapy option or it can be combined with surgery or radiation therapy. In combination with surgery, it helps regression of the tumor size prior to operation or destroying any remaining cancer cells in the body. In advance-staged lung cancers, chemo-drugs might also be used as a pain/symptom reliever. The advantage of chemotherapy includes that it is applicable to different tumor scenes and can be combined with different treatment options. However, most of the chemotherapeutic drugs fall short for adequate response rates and have very serious side effects due to low and non-specific drug delivery. Emerging drug resistant cancer cell populations from lung tumors also make the cancer resistant to the chemotherapy option [12, 13].

1.4.3) Radiotherapy

Radiotherapy utilizes high-energy waves such as positron or X-ray to tumor cells to precisely aim and kill lung cancer cells. In general, radiotherapy is considered effective against both SCLC and N-SCLCs [14]. Radiotherapy can be used for locally advanced tumors if the surgery is not an option to be utilized. In addition, radiotherapy can be used with surgery to shrink the tumor or to kill any remaining cancer cells after the surgery. Radiotherapy is often considered

as a combinatorial treatment option with either surgery or chemotherapy. However, radiotherapy falls short in some cases. For instance, there is a risk for creating new tumors during this therapy. Cells are also resistant to radiation therapy in hypoxic areas [15].

1.4.4) Targeted drug therapy

Targeted drug treatments use distinctive markers for the tumor and its microenvironment to deliver anti-cancer drugs for more effective delivery, tumor growth inhibition and treatment outcomes. For this, specific abnormalities presented within cancer cells are being exploited to inhibit tumor growth and differentiate drug accumulation at the tumor region by either passive or active targeting strategies [16]. So far, various targeted drug therapy options are on the market, and they serve better treatment options for advanced lung tumors. However, some of them only work in some patients with certain mutations. In addition, it is hard to find these distinctive markers, which are emerging from the healthy cell population. Furthermore, tumor specific markers vary from patient to patient and tumor to tumor, and an effective targeting is still the remaining challenge to overcome [17-19].

1.4.5) Immunotherapy

Immunotherapy in general aims to utilize the immune system to deal with cancer. Most of the time, the patient's immune system is not able to cope with the tumor because of an immune suppressive microenvironment. Therefore, immunotherapy focuses on removing immune suppressive obstacles for the patient's immune system [20, 21]. In addition, either chemotherapy or radiotherapy is often combined with immunotherapy for a robust treatment outcome. Immunotherapy is generally applied to patients only when they are responsive and have advanced

stage lung cancer. Its applications can be classified under two main classes: cell-based therapies and humoral-based therapies.

1.4.5.1) Cell based therapies

One particular focus of immunotherapy is cell based therapy [22]. Immune cells from cancer patients are being isolated for *in vitro* reprogramming to gain anti-tumor effector functions. CD4+/CD8+ T, NK and dendritic cells are currently the main cell types for researchers to utilize this strategy [23-25]. Lymphocytes are collected from patients, expanded *in vitro*, and genetically engineered to generate specific receptors on the cell surface to target cancer cells. These cells are called Chimeric Antigenic Receptor T cells (CAR-T cells). These specific receptors recognize and help activate T cells, which can kill cancer cells. In recent years, CAR T-cell based therapies have been used for treating various cancers effectively [26]. Another approach is to use dendritic cells (DC) as natural adjuvants to create tumor specific T cells *in vivo*. Dendritic cells are specialized on antigen presentation to immune effector cells (e.g. CD4+ and CD8+). The main purpose of DC vaccination is to emerge tumor specific CD8+ T cells, which can recognize and destroy the tumor *in vivo* and maintain immunological memory to prevent relapse. DCs are a crucial player of the immune system in terms of creating immunity and self-tolerance [23], making them a suitable tool for researchers to create effective therapeutic immunity against cancer cells.

1.4.5.2) Humoral based therapies

In cancer immunotherapy, monoclonal antibodies have proven their effectiveness. The main idea of using therapeutic antibodies is to inhibit tumor growth by either blocking the growth/signaling pathways of the tumor or facilitating immune cells for binding/killing cancer cells [27]. Another approach is recovering the body's own anti-tumor immunity via blockage of

checkpoint markers. Immune checkpoints control the inhibitory pathways of the immune system that are crucial for preventing tissue damage during the physiological immune responses and maintaining self-tolerance. Cancer cells also exploit these immune checkpoint pathways to survive under the immune system surveillance [28]. Therapeutic monoclonal antibodies can serve as antagonists to those inhibitory receptors by blocking their inhibitory molecules. Today, coping with cancer via monoclonal antibodies applies from broadened direct actions (e.g. blockage and recognition) to specific payload delivery (e.g. targeted drug delivery, antibody drug conjugates) or uses in specialized effects on the tumor microenvironment (as imaging agents) [27, 29]. Successful development of therapeutic antibodies involves complex processes such as chemical and physical characterization of antibodies, analysis of antigen binding specificity, immune effector functions, toxicity assessment, *in vivo* bio-distribution, and therapeutic efficacy in tumor transplanted animal models. EGFR (ERBb1), HER-2 (ERBb2), VEGF, CD20, CD30 and CD52 can be given as examples of tumor specific targets, which are successfully targeted by therapeutic monoclonal antibodies. Currently, there are several therapeutic antibodies that the FDA has approved to be used for various hematological and solid cancer types and a large number of additional ones are currently being developed [30].

Even though the above-mentioned immunotherapy applications have been shown to be effective in specific treatment options, they still have several limitations. Apart from costly complex development procedures, their long-term effects *in vivo* cause some concerns [2, 31]. For instance, long term existence of engineered cells might lead to health complications such as autoimmune diseases and other side effects [32]. Moreover, some immunotherapy treatment options still fall short to treat particular types of solid tumors whereas engineered cells are still vulnerable by various factors of the tumor microenvironment [33]. To cope with the above-

mentioned drawbacks, novel nano/bio technological applications are being developed for successful introduction of immunotherapy for clinics.

1.5) Active targeting drug delivery in lung cancer treatment

Nanoparticle-based drug delivery applications have a vast potential for better effective treatment due to their unique properties compared with traditional drug formulations. Controlled and sustained release, increased stability and circulation time, enhanced bioavailability, altered organ distribution to reduce side effects, improved drug solubility, facilitated target site accumulation, and reduced administration frequency can be counted as advantages of nanoparticle-based drug delivery systems [34]. Active targeted drug delivery utilizes targeting ligands via conjugating them on synthetic drug carrier nanoparticle surfaces to enable active seeking of targeted molecules on the intended cells. Moreover, active targeted nanoparticles today can be utilized not only as drug delivery agents but also as diagnostic tools via incorporation of specific dyes and/or imaging agents. In addition, they can be designed as hybrid systems called theragnostic nanoparticles to fulfill both of the above-mentioned duties at the same time [7].

So far, nano carrier systems for N-SCLC treatment can be classified into 4 sub-classes:

1- Lipid based nano carriers. Anionic/cationic liposomes, micelles, and temperature-sensitive liposomes are being developed for the N-SCLC treatment [8, 9]. DOXIL and Lipoplatin can be given as FDA approved examples of liposomal drug carriers to treat N-SCLC.

2- Polymeric based nano carriers. PLGA (polylacti-co-glycolic acid), PLA (polylactic acid), polycaprolactone, gelatin, alginate and albumin have been utilized extensively as polymeric drug carriers due to their biocompatibility, biodegradability and sub cellular size. FDA approved Abraxane can be given as an example of polymeric nanoparticles to treat N-SCLC [10].

3- Metal based nano carriers. In particular, gold and silver nanoparticles have been used for both N-SCLC treatment and diagnostic purposes [35].

4- Other type nano carrier systems. Magnetic (SPIO) and mesoporous silica nanoparticles (MSNs) are some examples of other nano carrier systems, which are being used to treat N-SCLC [12, 13, 36].

Nanocarrier-based drug carrier active targeting efficacy heavily depends on ligand selection, conjugation chemistry, and nanocarrier architecture. Major factors, which play important roles on active targeted nanocarrier systems, include size, shape, charge, and hydrophobicity/hydrophilicity of the carrier as well as size, type, charge, and density of the targeting ligands used on the carrier [43]. Several novel modifications have also been applied to improve properties of nano carriers such as induced active targeting and escaped RES uptake and immune surveillance. Lipid-polymer hybrid polymeric systems, polymer based polymerosomes, polyethylene glycol (PEG) modification and chemical ligand conjugation techniques can be given as examples. However, they still fall short in satisfying some of the clinical needs due to their limitations including low circulation time, host immune response, RES clearance, complex NP structure, conjugation chemistry, and ligand interactions [37, 38].

1.5.1) Ligands in active targeting drug delivery

Active targeted drug delivery aids drug carriers in identifying cell or tissue specific cell membrane receptor expression [39]. Modification of the NP surface with targeting moieties is significantly enhancing its targeting ability to specifically bind to certain cancer cells. Furhermore, this specific ligand-receptor interaction facilitates the uptake of NPs inside cytoplasm via receptor-mediated endocytosis [40]. The efficiency is defined as capability of delivering nanocarriers selectively to

the targeted tissue. Aptamers, antibodies, peptides, nucleic acids, growth factors [41] and various small molecules can be given as examples for targeting moieties utilized in active drug delivery applications [42-46]. Monoclonal antibodies are the main component of active drug targeting strategies, which include whole antibodies or binding fragments conjugated to drug carriers and/or therapeutic molecules. These antibody conjugated drug carriers expedite delivery of active molecules whereas the payload is released upon reaching its final destination. Trastuzumab (antiERBB2), Cetuximab (anti-EGFR) and Bevacizumab (anti-VEGF) can be given as examples for the treatment of various cancers [30].

1.5.2) Limitations of ligand functionalized active targeting drug carriers

Despite promising results, targeting ligand conjugated synthetic drug carriers have multiple challenges and limitations such as NP architecture, ligand target interactions, conjugation chemistry used, and host immune responses. Active and effective targeting mainly relies on carrier-target molecule interaction. Besides the above-mentioned limitations of active targeted drug carriers, another limitation is targeting efficiency of synthetic NP drug carrier systems. Structural characteristics of NPs have great effects on *in vivo* targeting. For instance, targeting ligands are very prone to shed off from surface during degradation in surface eroding polymeric carriers. Low density of ligands conjugated on the NP surface is another factor, resulting in an ineffective targeting. This is generally because of competitive inhibition, unwanted targeting ligand orientation and steric blockage of targeting moieties [47]. On the contrary, increased uptake by the immune system [48], reducing adverse effects due to target binding kinetics [49], and minimizing non-specific binding to off-target cells [50] are some of the results from having a high ligand density on the NP surface.

In terms of size, small sized NPs have better accumulation in tumors. However, their relatively high surface curvature affects their functionalization [51]. Conversely, while larger carriers are suitable for ligand conjugation, they are handicapped for effective internalization by several types of cancer cells. In addition, conjugating ligands, which have a high radius, can also affect NP size to increase, leading to decreased tumor accumulation [52]. Conjugation of targeting moieties on the NP surface is also another factor affecting targeting efficacy. There are several different strategies to couple ligands on NPs such as bifunctional (i.e. EDC, NHS functional groups), and thioester/thioether cross-linkers (i.e. 2-iminothiolene, maleimide functional groups), and click chemistry (i.e. dibenzocyclooctyne) applications [47]. Some of the mentioned conjugation approaches have resulted limitations like immunogenicity or inter crosslinking of NPs [53].

Several different types of ligands (antibodies, peptides, aptamers, and so on) have been investigated over decades to improve targeting strategies for drug delivery applications. Antibodies, targeting ligands and proteins have limitations despite their favorable features, which help to increase targeting specificity. For instance, undesirable effects of nanoparticle aggregation is a big hurdle to control drug carrier's size and stability due to inter-crosslinking of nanoparticles in the presence of various functional groups [37, 47, 52]. Small targeting peptides (such as TAT or RGD), on the other hand, have non-specific binding to healthy tissues [54]. In addition, during conjugation or physiological circulation, unfavorable environmental factors (i.e. ionic strength, enzymes, or pH) may decrease ligand binding functions [47]. Within a tumor, there are heterogeneous cell populations, which might express different cell surface receptors. When this heterogeneity is considered, single ligand targeting falls short to actively deliver the drug to entire tumor populations. Therefore, while utilizing ligand targeted drug carriers, there is a risk to

increase “target-negative” cells in the heterogenious tumor population which might cause drug resistance over time as a result of induced adaptation.

From both cancer biology and drug delivery points of view, functional and adaptive drug carriers like cell membrane-based NPs have many advantages due to their desirable features to overcome the above-mentioned limitations. For instance, they have been proven to provide better RES avoidance, flexible modifiability, versatility, and potential to have multiple targeting ligands at one carrier unit in addition to improving biocompatibility and stealth properties [55]. Therefore, this advancement opens a new horizon for the nanotechnology-based drug delivery applications called biomimetics in nanotechnology and drug delivery.

1.6) Biomimetic nanoparticles in cancer treatments: cell membrane coated nanoparticle-based applications for cancer therapy

Designing a platform that can specifically deliver the payload, mimic/manipulate biological interactions, and avoid systemic side effects is one of the major challenges in the drug delivery field. Recent advances in nano-/bio-technology, material science and bioengineering led to the development of many polymers, metallic or lipid based biomimetic carriers. However, efficient bioavailability of those platforms has not been achieved yet due to their relatively simple structure compared to biological systems. These artificial drug delivery platforms suffer from their “foreign-body” features, leading to serious side effects *in vivo*. On the contrary, the biomimetic compound-based carriers are considered as the “self” that helps reach acceptable toxicity and better biocompatibility. Among the biomimicry field, immunological biomimicry has a crucial important role in developing better therapeutic modalities in the field of immunotherapy, immunomodulation and vaccine delivery by increasing bioavailability and mimicking complex interactions of immune

system elements. Therefore, researchers put their spotlight on engineering and using cell or cell derived sources. They can be used as an anti-cancer drug, immune-modulator, therapeutic/modulator/antigen peptide and/or vaccine loaded carriers, including engineered whole cells, cell membranes and exosomes. Cell or cell membrane-based delivery platform engineering can be utilized in various ways as to gain/loss of bio–functions, target/manipulate their destination or combine their critical features for obtaining desired responses (**Figure 2**). Recently, cell membrane-coated particles or drug carrier cells have been investigated for their effects on anti-cancer, immunotherapy, immunomodulation, artificial antigen presentation (aAPC) and cancer

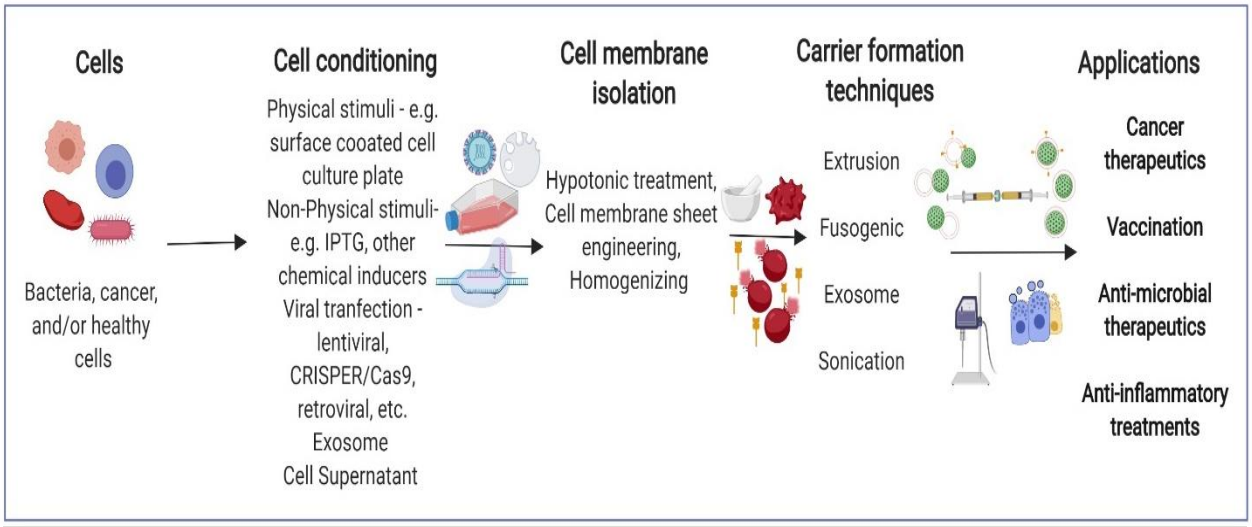

Figure 2: Illustration showing techniques and applications of cell membrane-based nanocarriers.

vaccines.

1.6.1) Principle mechanisms motivating cell membrane based carriers for immunomodulation/immunotherapy

Multi-cellular organisms undergo complex biological reactions between the host cell and the pathogen or diseased cells, leading to abnormal conditions such as high acidity inside the cells,

dysregulated proliferation, release of inflammatory molecules, and others. Most of the regulatory molecular interactions take place in the immune system in response to diseases such as cancer, autoimmune diseases, and so on. Recently, discovered information of these molecular mechanisms is being exploited by nanoparticle technology to develop novel therapies (**Figure 3**). NPs loaded with drugs can be directed towards a specific target using various moieties involved in the complex

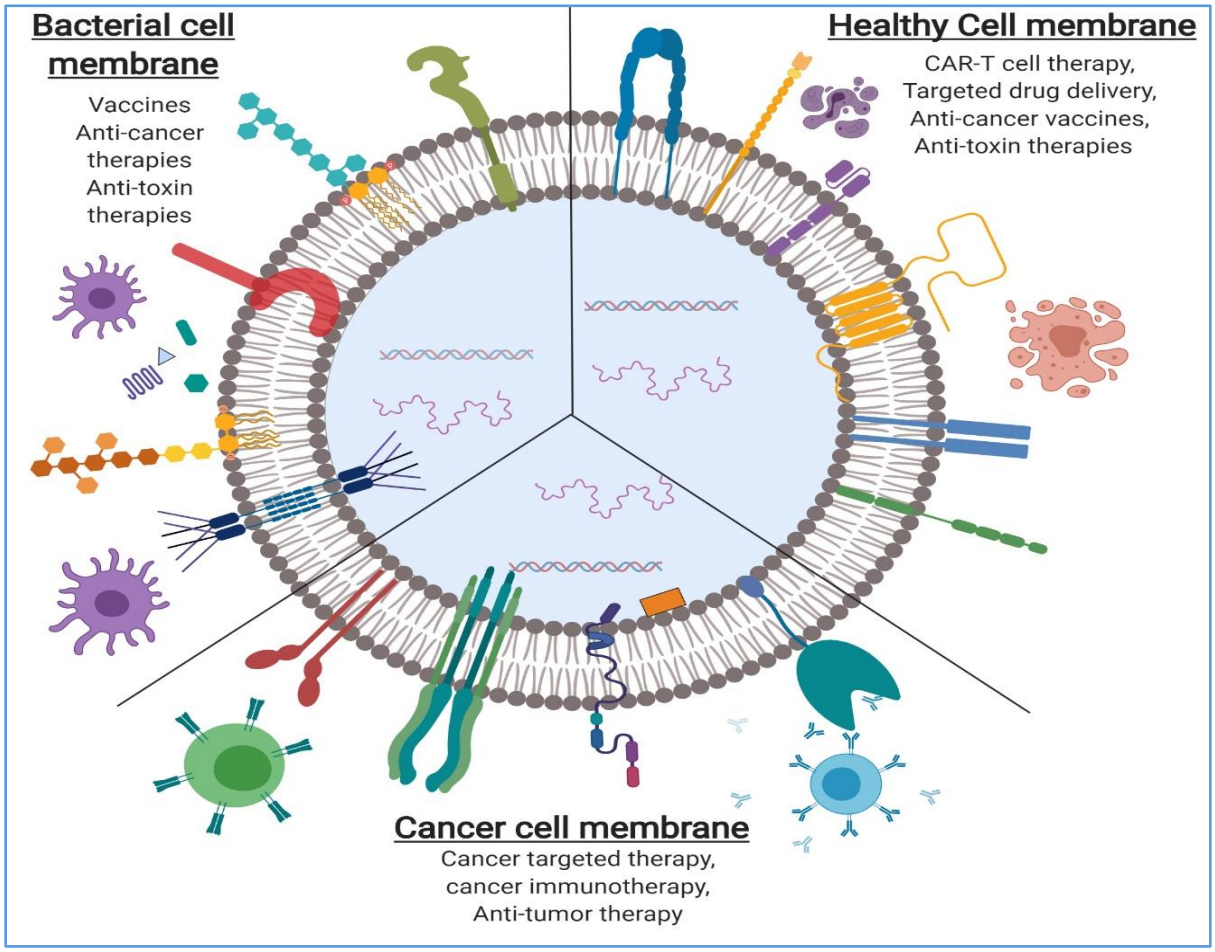

Figure 3: Illustration showing three major cell types and their applications on cell membrane-based drug delivery immunotherapy and immunomodulation.

biological mechanisms.

A bottom-up approach of surface functionalization is commonly adopted in the NP fabrication for targeted drug delivery. Surface functionalization incorporates the functional moieties such as enzymes, imaging agents, biopores, ligands and other functional target molecules.

These moieties are chemically conjugated or noncovalently absorbed onto the nanoparticle surface [56]. Though nanoparticles have provided a significant therapeutic outcome, they lack in some multi-functional applications such as targeting, homing and immunomodulation. Cell membrane-coated nanoparticles (CMCNP) have been increasingly studied for their mimicry of cell surface functionality to help in reducing the immune response of nanoparticles *in vivo* and introduce the capability of combining natural and synthetic materials. Efficient navigation and pathologically significant interactions within complex biological mechanisms can be achieved using cell membrane-coated nanoparticles with a relatively higher circulation time [57].

1.6.2) Cell membrane-based payload delivery applications

Cell membrane coated nanoparticles are getting more and more attention due to their mimicry of the cell surface functionality to reduce immune responses toward nanoparticles *in vivo* and to provide the capability of combining natural and synthetic materials. Cell membrane-coated nanoparticles have been shown to consist of a relatively higher circulation time [54]. In this section, we summarized different bio-mimetic drug carrier systems and discussed their advantages and limitations.

1.6.2.1) Cell based therapeutic delivery systems

The ability of the immune system to survey and sense pathogens and other dysregulated homeostasis is highly evolved. Due to the discoveries in immunobiology and cancer biology, immune cell-based therapies have emerged as new therapy options in the clinic, especially hematological cancers. In the last decade, engineered lymphoid cells have been developed with various different approaches to recognize specific disease antigens via their naïve receptor called “T-cell receptors” (TCRs) or via novel engineered synthetic receptors called “chimeric antigenic

receptors" (CARs). Novel approaches using such engineered T-cells to give synthetic NPs a hitching ride to their destination are showing promising results in targeted drug delivery. Many advances in directing T-cells to the tumor environment have been studied. However, immunosuppression of the tumor microenvironment remains challenging [58]. T-cell engineering of SynNotch circuits, where T-cells when in contact with a specific antigen promote cleavage of the transmembrane SynNotch receptor and release the transcriptional domain attached intracellularly, lead to its entry into the nucleus followed by activation of targeted gene expression. This can be used to overcome hurdles such as tumor immunosuppression and autoimmune activation and to successfully deliver molecules of interest at pathologically specific locations while circumventing the issues such as dilution and circulation half-life often faced in the direct injection of nanoparticle delivery [59]. Another novel strategy has used on nuclease-deficient synthetic receptors (dCas9-synR) to accommodate combinatorial inputs (proteins, lipids or sugars) for intracellular signal transduction module of antigen/antibody specific cellular responses [60]. Very recent approaches like engineering CAR-T cells to express "*a la carte* responses at the action site" promote activation of interested genes to overcome the mentioned tumor immunosuppression and autoimmune activation. Cellular engineering techniques like these also have such potential to be used in the design of new signal pathway circuits to improve cell differentiation where required, and supplement antibody expression for regulatory feedback mechanisms, immunosuppressive factors e.g. autoimmune diseases.

Some other strategies have used cells as a carrier for targeted delivery of payloads such as immunomodulatory drug loaded nanoparticles. As we know, the tumor microenvironment (TM) is hard to reach and possess immunosuppressive factors. Bypassing these factors might increase the efficacy of current applied therapies. For instance, targeting CTLA-4 and PD-1 expressing

lymphocytes in the TM might be a good option. Conjugating immunomodulatory drug loaded NPs on cell surfaces (such as R848- toll-like receptor agonist, SD-208-inhibitor of TGFβ kinase) creates such advantages like actively seeking cancer cells compared to only targeting ligand conjugated NPs. At the same time, immunomodulatory drugs loaded into NPs can induce checkpoint blockade and inhibit immunosuppressive mediators via autocrine and paracrine routes, leading to infiltration of CD8+ T cells into tumors [61].

Limitations of whole cells as carriers

Attaching and/or loading drug loaded NPs to the cell may lead toxicity to the cell itself and alter its functions because chemotherapeutic drugs are toxic to all kind of cells in some extent. It is reported that RBC stability and plasticity have been affected due to chemical modifications of cell membranes. For instance, glycophorin A expression patterns have changed after crosslinking NPs on the cell surface [62]. This change may lead RBCs to release damage associated patterns (DAMP) and result in immune activation or opsonization by humoral elements [63]. In addition, unusual releases of internal proteins from modified cells might cause immune reactions such as hemoglobin [64]. In the case of using bacterial mediated drug delivery, immune reactions are also quite common [65]. Mesenchymal stem cell (MSC) mediated drug delivery has also been used to deliver payloads to tumor regions. However, it is reported that MSCs might be responsible for contributing to tumor metastasis via releasing chemokines and growth factors. In addition, they help tumors to suppress the immune system, differentiate epithelial cells to become cancer-associated fibroblasts and retain the stemness of cancer cells [66]. This aspect of live cell-based drug delivery requires a thorough consideration of cell type selection. Keeping limited surface availability and cells own vital interactions in mind, holding released drug concentration in the

therapeutic window while avoiding cytotoxic effects to its carrier would make drug dosage optimization very hard to achieve for cell based delivery [55].

1.6.2.2) Cell membrane coated NP (CMCNP) based drug delivery systems

Advantages of cell membrane coated nanoparticles

Cell membrane coated biomimetic nanoparticles have made an impressive contribution to the improvement of cancer therapy. Due to the cell membrane structure and the retained cellular antigens, biomimetic NPs carry special advantages, such as long blood circulation, ligand recognition, immune escape, homotypic targeting, and the ability for sustained drug delivery [67]. Recently, cell membrane coated nano-systems with unique features and functions such as coating of nanoparticles with different cell lines, such as red blood cells, platelets, and lymphocytes, have been studied. Among the various physiological motives considered in fabricating a nanoparticle for drugs or specific molecules, having a longer circulation time will have a major clinical impact as it would increase the chances of better delivery and targeting with active and passive mechanisms such as enhanced permeability and retention effect (EPR) and other mechanisms such as reticuloendothelial system (RES) clearance [68]. Exploiting these mechanisms for more specific targeting and biomodulation are the major advantages provided by the biomimetic CMCNP.

Current applications of cell membrane based therapies

First, CMCNP was developed by coating erythrocyte membranes on PLGA NPs, which increased the nanoparticle retention in the blood to 72 hours against 15.8 hours of conventional synthetic stealth featured PEG-coated NPs [69]. RBC cell membrane-mimetic poly(lactic-co-glycolic acid) NPs with perfluorocarbon core (PFC@PLGA-RBCM) use the membrane camouflaging to deliver oxygen into solid tumors as another application of cell membrane coated NP delivery [70].

Prolonged blood circulation for cancer treatment and mimicking the cell surface functionality in navigating and reaching the specific target are major advantages of the CMCNP research.

Few novel approaches of fusing two different natural cell membranes have been reported. Diana Dehaini *et al.* have fused RBC and platelet cell membranes and coated the hybrid onto PLGA nanoparticles [71]. This approach not only improves the circulation by inhibiting the RES clearance, but also consists of an additional functionality produced by the platelet cell membrane, which has cancer cell specific binding molecules such as P-selection and CD44 receptor to target cancer cells. Hybrid approaches of using RBCs and various cancer cell membranes have also shown to inhibit tumor growth. Strategies like copper sulfide nanoparticle coating with RBC and melanoma cancer cell membrane fused hybrid vesicles exhibit immunosuppression mechanisms such as macrophage phagocytosis inhibition and homotypic targeting achieved by homologous surface adhesion domains on the cancer cell membranes [72, 73].

Not only showing its efficacy for cancer therapy, cell mimicry-based delivery is also very promising in toxin neutralization. A nanosponge made of RBC coated PLGA with α-toxin incorporation reduced staphylococcal α-haemolysin when it was administered into a toxin-challenged mouse, showing the capability of arresting toxins while taking advantage of the biomimicking nature of RBC membranes in avoiding immune clearance [74]. Leukolike vectors such as the one developed by Kang *et al.* used neutrophils' membrane coated nanoparticles (NM-NP) for targeting metastatic niches where NM-NP had 2.12 to 3.02-fold accumulation in the metastatic foci in comparison with bare NPs and PLGA-PEG-NPs, respectively [75]. This affinity towards metastatic niches is facilitated by the Mac-1, N-Cadherin and other adhesive proteins expressed on neutrophil membranes in higher than conventional PEG coating used for increasing circulation half-life and avoiding clearance [76, 77].

Other mechanisms being exploited in cancer cell-membrane coated nanoparticle mediated therapeutics include the capability to induce immune responses either by stimulating immune cells or by blocking major checkpoints in the immune pathways of cytotoxic T-cell associated proteins and other immunomodulatory molecules. Specificity of the antigenic profile presented by the cell membrane can be used in training the immune system to fight cancers, bacterial infections and other pathogens [78-80]. Cancer cells evade elimination and survive via various mechanisms by immunomodulation via loss or dysregulation of major histocompatibility complex expression (MHC), decrease in immunogenicity such as upregulation PD-L1, immunosuppression by taking advantages of anergic pathways of tumor-infiltrating lymphocytes, and immunosuppression of tumors via the active sites of "immune privilege" formed by tumor-infiltrating lymphocytes [81]. Along with the before mentioned evasive strategies, cancer cells agglomerate with constitute solid tumors via strong adhesion using their surface membrane proteins, which makes the infiltration restricted. In addition, unorganized and poor vasculature inhibits exploitation of the EPR effect of NP delivery in some cancer types. In this manner, Cao *et al.* have used the macrophage α4 protein and VCAM-1 of metastatic cancer cell interactions to deliver cytotoxic anticancer drugs for metastatic inhibition of breast cancer metastasis to lungs [82]. Fang *et al.* also showed cell membrane coated NPs to have homotypic tumor targeting by means of galectin-3 and Thomsen-Friedenreich antigen (T antigen) adhesion properties of cancer cell membranes [78]. Zhu *et al.* used cracked cancer cell membrane coated magnetic iron oxide NPs for targeting tumors and showed the greater potency for homing ability towards homologous tumors *in vivo* than other active targeting strategies, which depend on recognition selectivity and receptor density [83]. There was a 40-fold and 20-fold increase in uptake of cell membrane coated NPs in comparison with RBC coated NPs and bare PLGA NPs, respectively, in the MDA-MB-435 cells, showing the

affinity of cancer cell membrane coated nanoparticles towards cancer cells in attribution to the cell adhesion molecules which help in homotypic binding.

In addition to drug delivery and targeting applications, the membrane coating approach has emerged as a great tool for the development of cancer vaccines. In this regard, Kroll *et al.* encapsulated an immunological adjuvant called CpG oligodeoxynucleotide 1826 (CpG), which can trigger maturation of antigen presenting cells into a PLGA nanocore, and then PLGA-CpG NPs were coated with B16-F10 mouse melanoma cell membranes containing tumor associated antigens [84]. In another novel biomimetic platform, cytotoxic T-lymphocyte coated NPs in combination in with low-dose irradiation were used for targeting and treating gastric cancer [85]. The low dose irradiation increased the chemoattractant such as IFN-γ production and upregulated adhesion molecule expression facilitating the CD8+ T cells increase in the tumor environment along with homing and localization of T-lymphocyte membrane-encapsulated PLGA NPs by avoiding opsonization via highly abundant serum proteins such as CD45 and CD3z. This strategy demonstrated a 50-75% decrease in uptake when compared to bare NP via vascular extravasation by LFA-1 or CD11a. In addition, other literature work reported that T-lymphocyte membrane-encapsulated PLGA NPs were able to avoid being sequestered by lysosomes and retained their lymphocyte coating while NPs were seen to be trapped among the endolysosomal compartments with a two-fold increase in particle density across tumors in mice in comparison to bare NPs [86]. Cancer conditions such as breast cancer metastasis to lungs are hard to target using regular nanotherapeutics because of the poor vasculature inhibiting from exploiting the EPR effect of NP delivery. The above-mentioned cell membrane coated NPs have shown to have greater targeting and localizing capabilities than the conventional bottom-up approach of functionalized nanoparticles employed in the treatment of cancer. All of these examples of biomimicry-based

nanoparticle binding to cancer cells provide a significant targeting advantage over conventional targeting carrier fabrications such as antibody/peptide decorated nanoparticles used to target cancer cells where unknown cell membrane protein interactions are lost. **Figure 4** demonstrates potential cell surface proteins that could be used in immunomodulation, immunotherapy, and targeted drug delivery applications.

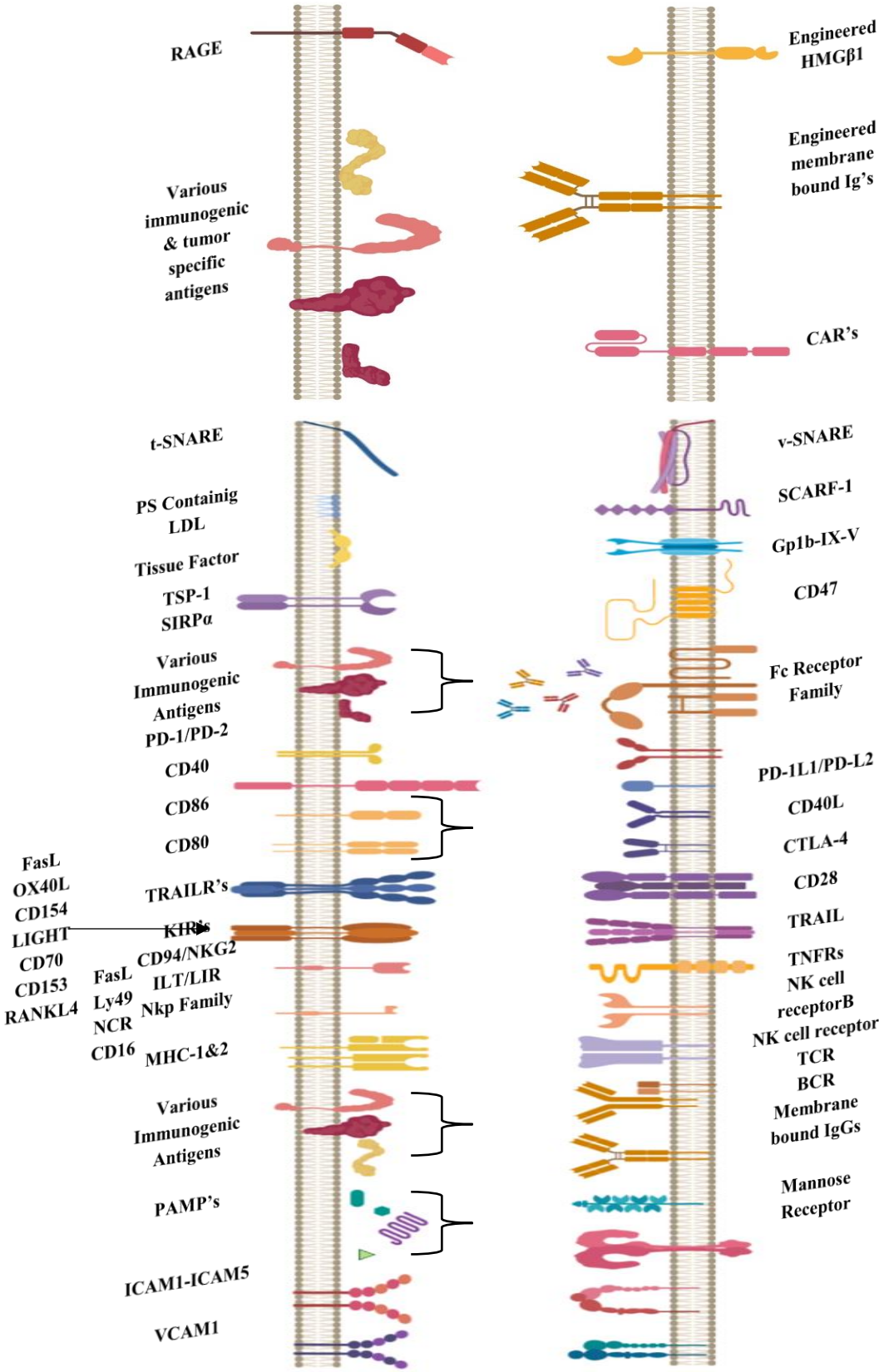

Figure 4: Potential cell surface proteins to be used in immunomodulation, immunotherapy, and targeted drug delivery applications.

1.6.3) Cell types used in cell membrane-based drug delivery applications

1.6.3.1) T-cells

T-cells carry out a variety of immune functions within the body because of the large amount of proteins found on their membrane. T-cell proteins have been found to play important roles in the MPS (i.e. mononuclear phagocyte system) uptake, immune tolerance, and targeting of endothelium/tumors. Furthermore, T-cells and their membranes increase blood circulation. Coating the membranes with NPs does not affect the membrane's biological activity. The combination of T-cell targeting and permeability along with NP modulation makes T-cells attractive candidates for cancer therapies [87]. Stephan *et al.* have reported synapse directed delivery of immunomodulator drugs via T-cell surface conjugated nanoparticles [88]. In the research, nanoparticles attached to T-cell membrane proteins so that molecular interactions could be regulated to prevent autoimmunity or boost immunity against tumor cells. Lipid nanoparticles were prepared from maleimide-functionalized liposomes through extrusion and then conjugated to effector T-cell membranes through incubation. NP covered T-cells were transferred into the prostate cancer developed model mice. The treated group consisted of a 5.2-fold reduction in tumor volume and had a survival advantage of over 14 days over mice treated with just T-cells and T-cells assisted with nanoparticles [88]. Mitchell *et al.* showed that TRAIL-coated lymphocytes kill cancer cells in the circulation [89]. Cancer cells and blood cells can use a selectin-based adhesion to interact between each other. With this knowledge, liposomes with E-selectin adhesion receptors and TNF-related apoptosis inducing ligand (TRAIL) are present on its surface and conjugated with lymphocytes to provide the cell with the ability to stick and destroy any circulating colon or prostate tumor cells in the bloodstream. Control mice had ~130,000 cancer cells/ml of blood while

TRAIL-coated lymphocyte treated mice had <2000 cancer cells/ ml. The lymphocytes were still functionalized even after 2.5 hours of circulating in the mice [89].

Another new biomimetic platform uses the cytotoxic T-lymphocyte coated NPs in combination with low-dose irradiation for targeting gastric cancer [85]. In this study, human cytotoxic T-lymphocyte (hCTL) membranes were used due to their ability to circulate in the blood longer and to localize at tumor sites. The low dose irradiation is used not only in attacking cancer cells but also increasing chemoattractants such as IFN-γ production and upregulating adhesion molecule expression which facilitates the CD8+ T cells increase in the tumor environment. PLGA nanoparticles were coated with hCTL membranes through co-extrusion. PLGA nanoparticle covered hCTL membranes decreased the cellular uptake rate and targeted tumors after 24 hours. The growth inhibition rate was 57% and with LDI; 89%. About a 50-75% decrease was seen in uptake of these NPs when compared to bare NPs, and vascular extravasation was facilitated by LFA-1 or CD11a [85]. Parodi *et al.* used lymphocyte properties to investigate particle uptake between host and donor cells and the accumulation of lympholike vectors (LLV) in melanoma tumors because lymphocytes can pass through biological barriers and accumulate at target tissues [86]. Researchers showed that nanoporous silicon particles can also perform similar actions when coated with cell membranes from human THP-1 and murine J774 cells. A decrease in uptake for the LLV coating was seen twhen the donor membrane matched with the host membrane ranging from ~50% to ~75%. Murine J774 LLVs had delayed accumulation in the liver for up to 40 minutes *in vivo* and can also bind to the murine B16 melanoma tumor in a non-destructive manner [86]. In comparison of subcellular localization, LLVs were able to avoid being sequestered by lysosomes and retained their lymphocyte coating while NPs were seen to be trapped among the

endolysosomal compartments, and there was a two-fold increase in particle density across tumors in mice compared to bare NPs [86].

1.6.3.2) Macrophages and dendritic cells

Macrophages are a type of immune cell that secrete cytokines and chemokines and come from monocytes, the largest type of white blood cells, to deal with damaged tissue or infections. Besides their ability to locate and eat foreign particles such as bacteria, viruses, fungi and parasites, macrophages are known to cross biological barriers and are present in tumor masses making them potential drug delivery carriers. In tumor sites, macrophages can release chemoattractants for more macrophages and monocytes. Furthermore, macrophages can operate under hypoxic conditions. Combined with drug-loaded nanoparticles, macrophages and their membranes are a potent drug delivery vehicle [90]. Xuan *et al.* prepared doxorubicin-loaded mesoporous silica nanocapsules (MSNCs) camouflaged with a macrophage cell membrane (MPCM) [91]. More than 30% of MPCM-camouflaged MSNCs were phagocytized by macrophages. MPCM-camouflaged MSNCs remained in circulation after 24 and 48 hours of treatment with 36% and 32% retention, respectively whereas bare MSNCs were cleared after 24 hours. An *in vitro* study showed 4T1 mice breast cancer cells took up the DOX-loaded MPCM-camouflaged MSNCs. An animal study was followed by injecting DOX-loaded MPCM-camouflaged MSNCs into 4T1 tumor bearing mice. DOX fluorescence could be detected for 72 hours in the tumor site. Tumors treated with DOX-loaded MPCM-camouflaged MSNCs had their volumes decreased and, in some cases, regressed almost completely [91].

In another study, Thamphiwatana *et al.* prepared macrophage mimicking nanoparticles (MM-NPs) by using J774 mouse macrophage cell membranes and fusing them with PLGA cores [92]. The MM-NPs contained LPS binding proteins like CD14 and TLR4 along with cytokine

binding receptors CD126, CD130, CD120a, and CD120b. The MM-NPs were mainly distributed in the blood, liver, and spleen. The LPS removal capacity of the MM-NPs was measured using assays which indicated 62.5 ng of LPS were removed per milligram of MM-NPs. The MM-NPs were then measured for their ability to sequester proinflammatory cytokines in a mixture. The MM-NPs removed 105.1 pg of IL-6, 4.3 pg of TNF, and 6.5 pg of IFN-y corresponding to 53%, 12%, and 15%, respectively. Injecting mice with LPS followed by MM-NPs showed no increase of cytokines. Further study revealed 60% of mice survived lethal LPS levels. A lethal dose of *E. coli* was administered to mice followed by MM-NPs treatment. The number of bacteria in key organs and proinflammatory cytokines were significantly lower compared to that of 10% sucrose treatment where 4 out of 10 mice survived up to 60 hours [92].

Dendritic cells (DC) have the ability of expressing ligands capable to activate various immune cells like natural killer (NK) cells responsible for killing tumor cells. Dendritic cells are often the target for antigen presenting vaccines, but the cells can be used for other purposes like targeting cancer. Dendritic cells possess the ability to process a variety of antigens and as shown by Munich *et al.* exosomes derived from dendritic cells directly kill tumor cells and activate NK cells via TNF superfamily ligands like TNF, FasL, and TRAIL [93]. Mature DCex (mDCex) exposed to melanoma cells through incubation induced significant cell death at 24 hours and increased at 48 and 72 hours. mDCex is also capable of killing other cancer cell types like lung carcinoma KLN205 and colon carcinoma MC38 cells. NK cell exposure to mDCex and immature DCex (iDCex) through incubation shows greater NK cell activation when exposed to mDCex than iDCex [93].

1.6.3.3) Neutrophils

Neutrophils like their other white blood cell counterparts, macrophages and T-cells, play an active role in the body's immune system and have similar advantages for using in therapeutic purposes. Neutrophils sets themselves apart from the other cells for having the capability to travel to places in the body that other cells cannot access like the brain. For example, neutrophils have the capability to penetrate inflamed brain tumors as reported by Xue *et al.* who used neutrophil-mediated anticancer drug delivery for suppression of malignant glioma [94]. In this research, neutrophils loaded with paclitaxel (PTX) carrying liposomes suppressed glioma in mice after a tumor was surgically excised to induce inflammation. PTX-CL and neutrophils were incubated together so the liposomes could be taken up by the neutrophils. PTX-CL/neutrophils brain-target efficiency was determined, and PTX-CL/neutrophil treatment ensured a 50% survival rate of up to 61 days in treated mice compared to those of Taxol and PTX-CL, which ensured 29 and 38 days survival, respectively. In addition, 25% of mice treated with PTX-CL/ neutrophils survived more than 4 months [94]. Kang *et al.* developed a nanosized neutrophil-mimicking drug delivery system (NM-NP) that was produced by coating neutrophil membranes on carfilzomib-loaded PLGA nanoparticles in order to neutralize circulating tumor cells (CTCs) and inhibit formation of the metastatic niche [75]. NM-NPs are loaded with carfilzomib (NM-NP-CFZ) and circulating tumor cells (CTC) were incubated together. *In vitro* study showed the NM-NPs attached to endothelial cells (HUVEC cells) more than 2.9-fold compared to blank NPs. For *in vivo* studies, mice were administered with 4T1 lung cancer cells followed by either NM-NPs or NPs. The study showed NM-NPs accumulating in the metastatic foci was 2.12- and 3.02- fold compared to NPs and PLGA-PEG-NPs, respectively, after 24 hours of intravenous administration. NM-NP-CFZ were administered to mice four times on days 0, 7, 14, and 21. Early metastatic

nodule formation was found to be significantly lower. The next animal study showed NM-NP-CFZ reducing 4T1 metastasis foci by 87% [75]. Krishnamurthy *et al.* synthesized nanoghosts by using a monocyte cell membrane shell and doxorubicin loaded PLGA core [95]. Using flow cytometry, the uptake of the dox loaded nanoghosts by MCF-7 breast cancer cells was higher than PLGA NPs. An MTS cytotoxicity assay using MCF-7 cells revealed free dox to have an IC_{50} of 0.5 μM while nanoghosts and PLGA NPs had IC_{50} values of 4 μM and 12 μM, respectively [95].

1.6.3.4) Red blood cells (RBCs)

Red blood cells are natural circulating carriers due to their long circulation times allowing for tumor targeting and efficacy [96]. Furthermore, RBCs can be type-matched to enhance biocompatibilty [97]. Their availability and lack of intracellular organelles makes their membranes easy to collect for combining with drug-loaded nanoparticles. The long circulation time combined with NPs can lead to prolonged drug release. Luk *et al.* combined red blood cell membranes and doxorubicin loaded PLGA nanoparticles as an anti-tumor drug delivery system [98]. The RBC-NP(DOX) were tested on EL4 mouse lymphoma cells. While cancer cell killing tests revealed free DOX working more effectively than the RBC-NP(DOX), the formulation had better uptake by EL4 cells compared to free DOX. Mice were then implanted with EL4 cells and allowed to grow for 9 days. Afterwards, the mice were treated with RBC-NP(DOX). The formulation-controlled tumor growth and almost doubled the median survival from 24 to 47 days [98].

RBC membrane coated NPs have also been used for vaccine applications. Toxoid vaccines are developed from the inactivated toxins, but the processes used for preparation of these vaccines are difficult and often cause the improper denaturing of the toxin protein structure, leading to altered antigen presentation while compromising immunogenicity. Nanotoxoids can circumvent these preparation processes used in presenting the toxins by detaining them inside the cell

membrane and delivering them safely *in vivo.* Wang *et al.* have developed a nanoparticle-based anti-virulence vaccine to target methicillin-resistant staphylococcus aureus skin infections [99]. RBC membranes were fused with the surface of poly (PLGA where RBC membrane coating was functional for pore-forming α-hemolysin (Hla) (heptameric cell membrane pore forming factor) insertion. In the study, nanotoxoid (Hla) when injected in the mouse showed induction of Hla corresponding antibodies and showed a germinal center formation characteristic in draining lymph nodes. There was almost no drop in anti-Hla titers over a five-month period. When nanotoxoid(Hla) vaccinated mice where challenged with MRSA bacteria, there was clear attenuation of lesion formation with a 5-fold decrease in the dermonecrotic area, and inhibition of Hla-mediated skin damage showing high extravascular neutralization activity of the titers produced from the vaccine induction [99].

Hu *et al.* developed another biomimetic approach that RBC based nanosponges can absorb pore-forming toxins (PFTs), which are the most common toxic proteins generated by pathogenic bacterial infections. A nanosponge made of RBC coated PLGA reduced staphylococcal α-haemolysin when administered into toxin-challenged mice showing the capability of arresting toxins taking advantage of the biomimicking nature of RBC membranes [74]. A natural RBC bi-layer membrane was fused onto PLGA NPs to form these nanosponges, and the nanosponges have shown reduced toxicity towards cells when absorbed by α-toxins into the NP core [74]. The same group also reported a biomimetic approach to functionalize NPs by coating them with RBC membranes for anti-cancer drug delivery. Results showed that RBC membrane coating increased the nanoparticle retention in the blood to 72 hours against 15.8 hours of PEG-coated NPs by avoiding the clearance by macrophage engulfment via the “self” CD47 receptor recognition [69].

Danesh *et al.* reported the use of RBC exosomes, which cause monocytes to release proinflammatory cytokines for boosting lymphocyte responses *in vitro* [100]. Mixing these cells with extracellular vesicles (EVs) resulted in secretion of proinflammatory cytokines and increased survival of peripheral blood mononuclear cells (PBMCs). EVs also increased CD4 and CD8 T-cell proliferation, induced significant upregulation of various cytokines, especially IL-1β, and stimulated PBMCs. EVs were incubated with both monocytes and T-cells and were found to interact with monocytes instead of T-cells and this interaction induced the production of TNF- α via exosomes [100]. Gao *et al.* reported surface functionalization of gold nanoparticles (AuNPs) with RBC membranes to improve their biocompatibility and reduce macrophage uptake *in vivo* [101]. AuNPs are used for their modifiable surfaces, optical properties, and biocompatibility. Red blood cells (RBCs) contain membrane proteins that protect them from macrophage uptake. Coating AuNPs with RBC membranes via extrusion effectively shield AuNPs from phagocytic uptake. RBC-AuNPs were incubated with J774 murine macrophage cells and cell uptake of RBC-AuNPs was measured after 30 minutes. RBC-AuNPs had an uptake of 3.2 ng/1000 macrophage cells whereas uncoated AuNPs had an uptake of 13.5 ng/1000 macrophage cells [101].

1.6.3.5) Stem cells

Mesenchymal stem cells (MSCs) are used as drug delivery systems for their innate targeting ability towards inflammation and lesions. MSCs can also penetrate solid tumors and interact with target cells. Plus, MSCs can be genetically modified to express therapeutic genes and can be enhanced with nanoparticles. Their membranes retain much of their natural ability and can be used for membrane-based drug delivery systems [102]. Sadhukha *et al.* engineered mesenchymal stem cells as tumor-targeted therapeutic carriers and treated human MSCs with paclitaxel-loaded polymeric nanoparticles [103]. Nano-engineered MSCs were cytotoxic towards A549 lung adenocarcinoma

cells and MA148 ovarian cancer cells *in vitro.* This was determined via MTS analysis, which showed an IC_{50} of 6.71 nM and 4.52 nM in A549 cells and MA148 cells, respectively. Both cell types maintained substantial cell death as nano-engineered MSCs were present. Animals studies using infrared fluorescence revealed that nano-engineered MSCs initially travelled to the lungs but then distributed to the liver, spleen, and lungs [103].

Wang *et al.* used bone marrow derived MSCs loaded with paclitaxel (PTX) encapsulated PLGA nanoparticles for glioblastoma therapy in rats [104]. The MSC NPs were injected into contralateral brain hemispheres. MSC NPs (1 pg drug/cell) decreased C6 glioma cell survival by 40%-50% compared to 100% C6 cell survival demonstrated by untreated MSCs. Red fluorescent probe, CM-Dil, was used to stain MSC NPs for *in vivo* distribution. After injecting the right brain hemisphere with Cm-Dil-stained MSC NPs, in two days about 44% ± 5.4% of drug-loaded MSC migrated towards gliomas. After 12 days, mice injected with MSC-NP had no abnormal consciousness or motor response. Plus, the median survival time for the tumor-bearing mice was 35.5, 24.5, 22.0, 13.5, and 14.5 days for MSC NPs, MSC Ptx, Ptx-PLGA NPs, MSCs, and saline, respectively. The MSC-NP group exhibited the most significant reduction in glioma areas [104].

Gao *et al.* developed bone marrow derived mesenchymal stem cell membrane-coated gelatin nanogels (SCMGs) as a tumor-targeting drug delivery system [105]. Gelatin nanogels were loaded with anticancer drug, doxorubicin (gelatin-DOX) and then coated with stem cell membranes (SCMGs-DOX). SCMGs-DOX were incubated with HeLa human cancer cells for 24 hours. An MTT assay showed an IC_{50} of 0.63 μg mL^{-1} and 2.55 μg mL^{-1} for SCMGs-DOX and gelatin-DOX, respectively. HeLa cells uptake of SCMGs-DOX was almost 100% after 0.5 and 1 hour. SCMGs-DOX were injected into mice bearing HeLa tumor and showed delayed tumor

growth for 15 days. The average tumor weight for the SCMGs-DOX treated mice was smaller compared to the control groups [105].

1.6.3.6) Cancer cells

Cancer cells as therapeutic carriers are unique candidates. They can be easily cultured to harvest a good amount of their membranes. The cancer cells target other cancer cells like themselves, which enhances tumor interactions, and they can escape the immune system for longer circulation in the bloodstream. Cancer cell membrane-coated nanoparticles (CCMNPs) can deliver tumor-associated antigens to antigen presenting cells and be used as immunomodulatory, anti-cancer drug or vaccine delivery platforms. Fang *et al.* have showed cancer cell membrane coated nanoparticles can be used as an anti-cancer vaccine and drug carrier [78]. Monophosphoryl lipid A (MPLA- boosts immune response of antigens) modified mouse melanoma cancer cell membranes extruded with drug loaded PLGA nanoparticles (110 nm). These CCMNPs have a dual functionality of both tumor antigen presentation for immunotherapy and homotypic targeting of cancer cells to deliver the payload. Incubation of Monophosphoryl lipid A incorporated CCMNPs with dendritic cells was shown to upregulate maturation markers such as CD40, CD80, and CD86 in the dendritic cells. Co-culture of MPLA-CCMNPs pulsed dendritic cells and splenocytes with gp100 epitope showed T-lymphocyte crowding around dendritic cells where their activation was later quantified by IFN-γ confirming antigen-specific response elicited by MPLA- CCMNPs [78]. In another study, MDA-MB-435 human cell line membrane was coated onto PLGA with fluorescent dye loaded in the core. There was a 40-fold and 20-fold increase in uptake of CCMNP in comparison with RBCNPs and bare PLGA cores in the MDA-MB-435 cells. Results show the affinity of cell membrane coated nanoparticles towards cancer cells in attribution to the cell adhesion molecules which help in homotypic binding. As mentioned above, Kroll *et al.* developed

an anticancer vaccine by coating Cpg-loaded PLGA (CpG-CCNPs) with B16-F10 mouse melanoma cell membranes [84]. CpG-CCNPs were successful in getting bone marrow-derived dendritic cells to secret interleukin-6 (IL-6) and IL-12 more than free CpG, and the CpG-CCNPs managed to induce dendritic cell maturation after *in vivo* administration. Later, T-cell based assays were used to confirm the CpG-CCNPs anti-tumor vaccination capabilities. Mice with wild-type B16-F10 were vaccinated with CpG-CCNPs. A high T-cell proliferation was observed on CpG-CCNP treatment with T-cells generation of multiple tumor antigen specificities such as enhanced production of IFN-γ and IL-2. The vaccine prevented tumor occurrence for 86% of mice after 150 days of administration. CpG-CCNPs extended the median survival from 20 days for untreated groups to 40 days, whereas CpG-NPs treated mice had a median survival of 22 days [84]. Sun *et al.* developed a drug delivery system using doxorubicin-loaded gold nanocages (AuNs) as an inner core and 4T1 cancer cell membranes (CMVs) as the outer core [106]. The CDAuNs utilize the homotypic targeting of the cancer cell membranes and the hyperthermia-responsive ability of the AuNPs for thermal-triggered drug release. In *in vitro* studies, the CDAuNs released DOX under hyperthermia and targeted 4T1 cells. Furthermore, the CDAuNs inhibited tumor volumes and metastatic nodules by 98.9% and 98.5%, respectively, using a 4T1 breast tumor model [106].

1.6.3.7) Bacteria

Bacterial outer membrane vesicles (OMVs) have been used as vaccine platforms for decades due to their ability to carry surface antigens, be readily phagocytosed by cells, and stimulate innate immunity and promote adaptive immune response. In addition, bacterial outer membrane vesicles (OMVs) are being investigated as therapeutic delivery systems just as OMVs and/or in combination with nanoparticles. Bacterial OMVs are attractive for their high, uniform yield. Compared to other cells and their membranes, OMVs carrying drug-loaded nanoparticles

have two potential positive therapeutic effects: immunostimulation and payload delivery. The featured properties of nanoparticles such as the ability to carry antigens and immunostimulatory adjuvants can be used to elicit immune responses by mimicking natural microbe activities. This mechanism is gaining attention to produce more robust therapeutic delivery platforms. Bacterial membranes also provide immunogenic antigens and pathogen associated-molecular patterns, which help to stimulate immune responses and associated pathways [107-109].

Gao *et al.* have used an *Escherichia coli (E. coli)* bacteria pathogen model to study bacteria membrane coated NPs [110]. They have collected bacterial membranes and fused them on the surface of AuNPs (gold nanoparticles). Injection of these bacterial membrane-coated AuNPs showed boosted activation of CD11c+ dendritic cells in lymph nodes with upregulation of costimulatory molecules (CD40, CD80, and CD86) and elicited B-cell responses (increased IgG levels) and T-cell responses (increased levels of IFN-γ and interleukin 12 on vaccination with BM-AuNPs). Salmonella enterica OMVs expressing pneumococcal PspA are also used to probe antibody responses [111]. Mice immunized with PspA engineered OMVs triggered immune responses in contrast with no responses coming from only OMVs or only PspA groups. Bacterial outer membranes have also shown to suppress tumors like murine colon adenocarcinoma tumors [112]. In this study, mice were transplanted with cancer cells and treated with the genetically engineered *E. Coli* outer membrane, leading to inactivated lipopolysaccharide (LPS). Naturally, LPS binds to TLR4 receptors, which in turn produces IL-8 cytokines. The modified *E. Coli* OMVs showed decent prevention of tumor growth for murine carcinoma and B16BL6 melanoma cells compared to functionalized nanoparticles [112]. In another study conducted by Gujrati *et al., E. coli* is engineered to express human anti Her-2 protein with reduced endotoxicity toward human

cells to kill cancer cells by delivering small interfering RNA (siRNA) via targeting kinesin spindle protein (KSP) [113]. OMVs have an affinity towards HER-2-overexpressing tumors, resulting in greater tumor inhibition by 66% compared to the control mice. Modified OMVs did not show induction of a severe immune response or prolonged inflammatory responses and were safe at any dose [113]. Fantappie *et al.* engineered *E. coli o*uter membrane vesicles to carry heterologous antigens: SpyCEP, Streptolysin O, Spy0269, SAM_1372, and R-TEM b-lac [114]. These antigens were chosen for their ability to induce immune responses, their measurable functional activities, and for belonging to different compartments of the cell. The recombined OMVs are capable of inducing antibody responses especially from those immunized with Slo-OMVs and SpyCEP-OMVs. Those OMVs gave mice a >80% survival rate [114]. **Table 1** presents a summary of research studies associated with cells incorporated with NPs and cell membrane coated NPs for drug delivery and therapeutic applications.

Ligand	Cell/cell membrane	Advantages	Application	Ref.
CD47	RBC membrane coated PLGA NPs	Increased circulation half-life of NPs with an immunosuppressive CD47 marker towards SIRP-α in phagocytic cells such as macrophages	Personalized medicine and Drug delivery system (DDS)	[69, 115]
CD47, CD235α, CD61 and CD41	RBC-Platelet coated PLGA NPs	CD235a marks a species-specific marker on RBC along with CD47 an immunosuppressive marker, CD41, CD61 making up the $\alpha_{IIb}\beta_3$ assists in hemostasis and thrombosis of platelets.	Personized medicine and anti-cancer therapies	[71, 116]
Cadherins and Glycoprotein100	Mouse melanoma and cell membrane coated PLGA NPs	Induction of dendritic cell maturation and stimulation of antigen-specific T cells by gp100 epitope	Cancer immunotherapy	[78]
CD45, CD3z and CD11a	Cytotoxic T-lymphocyte membrane PLGA NPs	Ability to avoid opsonization via CD45 and CD3z markers and facilitate vascular extravasation via LFA-1 or CD11a	Cancer immunotherapy and radiotherapy	[85]
α4 integrin	Liposome coated with macrophage membrane for targeting metastatic cancer cells	Macrophage α4 interactions with metastatic cancer cell VCAM-1 molecules to target and inhibit metastasis.	Drug deliver for anti-metastatic cancer immunotherapy.	[82]
Mac-1, N-cadherins	PLGA NPs coated with neutrophil membranes	Neutrophil membrane proteins such as Mac-1 and N-cadherin facilitate CTC-targeting properties and help design DDS for targeting metastatic niches.	Anti-metastatic cancer immunotherapy	[75]

Table 1: Table summary of cell/cell membrane based therapeutic applications utilizing cell membrane proteins as either targeting, therapeutic or modulatory purposes.

Ligand	Cell/cell membrane	Advantages	Application	Ref.
FGFRs, EGFRs	Stem cell membrane coated nanoparticles	Stromal cell proliferation signal responsive receptors such as FGFRs and others on MSCs home them to the tumors, and this phenomenon is being used for tumor targeting.	Targeted tumor therapy	[105]
FAKs, RHO	Cancer cell membrane coated magnetic iron oxide NPs	Surface specific proteins such as integrins, FAKs and RHO proteins provide homing ability of cancer cell membrane coated NPs in tumor-self targeting.	Homotypic cancer targeting. Cancer cell therapy.	[78, 117]
Anti-CD19 synthetic notch receptor	T-cell expression via SynNotch receptors	Antigen specific expression (input) of desired proteins at desired locations via T cells.	Cancer immunotherapy, CAR-T cell therapy	[59]
RTK-based and GPCR-based chimeric receptors	DCas9-SynR in HTLA /HEK293 cells	Combinatorial antigen inputs for site specific cellular responses/delivery of therapeutic agents.	CAR-T cell therapy, Regeneration, Immunotherapy	[60]
PD-1 antibody, CD8	T-cells as carriers for PLGA/PEG NPs loaded with immunomodulatory drugs	Improved antitumor immunity and qualitative delivery of drugs in tumor microenvironment via PD-1 binding of CD8+ cells.	Cancer immunotherapy, Antitumor immunity	[61]
Neutrophil extracellular traps (NETs)	Neutrophil cell membrane coated nanoparticles	Natural binding of NETs to circulating tumor cells by selective adhesion is targeted to deliver therapeutic drugs inhibiting CTCs.	Anti-metastatic therapy	[75, 118]

Table 1: Table summary of cell/cell membrane based therapeutic applications utilizing cell membrane proteins as either targeting, therapeutic or modulatory purposes (Cont.).

Ligand	Cell/cell membrane	Advantages	Application	Ref.
MSR, MMR, VCAM-1	Macrophage coated nanoparticles	The macrophage membrane actively targets cancer by the respective ligands adhesion and delivers the therapeutic drugs via the nanoparticle release.	Cancer immunotherapy	[119]
CXCR4 and CD44	Cancer cell and glioma cell membrane coated nanoparticles	Disruption of cancer cell migration towards fibroblasts by internalization of NPs with CXCR4 and CD44.	Anti-metastatic therapies. Cancer therapy	[120]
MPLA	Cancer cell membrane, MPLA functionalized PLGA NPs.	Maturation of dendritic cells via MPLA functionalized cancer cell membrane.	Antitumor therapy	[78]
PAMPs (Pathological associated	Outer membrane vesicle of Salmonella	PAMPs bind to PRRs and stimulate innate immunity activities.	Immunotherapy with bacterial OMVs	[121]
HER-2-specific affibody	E. coli K-12 W3110 strain OMV.	HER-2-homing AffiHer-2 OMVs siRNA delivery to target cancer cells.	Cancer immunotherapy	[113]
Inactivated LPS	Salmonella enterica	Tumor treatment of colon adenocarcinoma, metastatic murine carcinoma and B16Bl6 melanoma via antitumor cytokines CXCL10 and interferon (IFN-ϒ)	Antitumor immunotherapy	[121]

Table 1: Table summary of cell/cell membrane based therapeutic applications utilizing cell membrane proteins as either targeting, therapeutic or modulatory purposes (Cont.).

CHAPTER 2

Herceptin-based CAR transduced T lymphocyte membrane camouflaged nanoparticles. A new approach to enhance drug targeting and circulation time in lung cancer

2.1) Introduction

As mentioned earlier, particle based drug delivery has not yet fully been controlled and applied clinically for reasons of the opsonization, non-specific clearance [122], relatively short circulation time [123], and limitations of fabricating actively targeted drug carriers. Blood component interactions of these synthetic NPs, on the other hand, is another factor that affects the NP's fate in the body. This interaction creates a layer on the surface of NPs called "protein corona" (PC) [124]. The PC is responsible for cellular uptake, physiological features, immune responses, and targeting efficiency of the particles [125-127]. For these reasons, using very well characterized carrier materials and identifying the blood component interactions as well as their PC composition are needed for the targeted drug delivery applications [128-134]. Above-mentioned short-comings in the synthetic particle-based drug delivery field make the use of biomimetic materials to create advanced drug delivery systems more and more popular [135-138]. Bacteria or virus-based carriers [134, 139], hybrid nano-bio systems [140, 141], and cell based drug delivery vehicles [69, 82, 105] have been reported to have potential applications for biomimetic targeted drug delivery. Among

these, development of cell membrane coated synthetic polymeric nanoparticles as drug carriers also has broad application potential in the field. Furthermore, this type of cell based biomimetic drug delivery application might provide a new way for individualized medicine applications by applying the patients' own cells for their own treatments [69, 78, 86, 142, 143].

Here we describe a unique approach, combining afatinib loaded PLGA NPs with CAR-T cell membranes from genetically engineered human Jurkat lymphocytes to target Her-2 positive lung cancer for therapy. Co-extrusion methods were used to fabricate targeting nanoparticles with prolonged circulation and avoiding systemic clearance and undesired PC formation. Thus, there was a potential of increased ability of anti-her-2 CAR-T-MNPs to migrate and localize at tumor sites that is not otherwise achievable through current modification and bioconjugation techniques. Afatinib is the FDA approved chemotherapeutic drug used in the study, which is effective against lung and breast cancer treatment. These new nano drug carriers, called CAR-T-MNPs, are produced by camouflaging PLGA NPs with Her-2 ScFv expressing cellular membranes isolated from genetically modified lymphocytes. Several *in vitro* and *in vivo* experiments were performed to determine if CAR-T-MNPs could increase circulation time and actively accumulate on her-2 expressing tumor tissues.

2.2) Overview of research project

This research project has been designed to develop CAR T-cell membrane coated PLGA NPs for N-SCLC treatment. The overall goal of the project described here is to develop anti her-2 CAR T-cell membrane-coated PLGA nanoparticles for targeted chemotherapeutic treatment of N-SCLC. The overall design is presented in **Figure 5**.

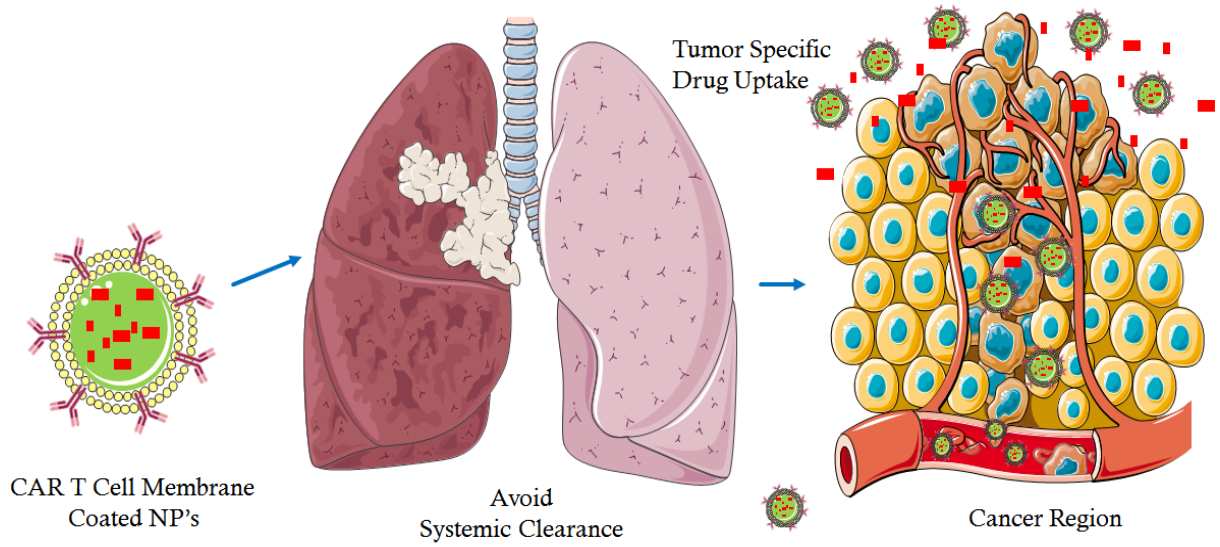

Figure 5: Overall view of proposed CAR-T-MNPs for targeted N-SCLC therapy.

CART-cell-based immunotherapy is being applied successfully in immunotherapy treatment modalities. Target-specific CAR T-cell genetically engineered to express a ligand for the target in the form for chimeric antigenic receptor. In this project, anti her-2 CAR T-Jurkat cell membrane was used for coating PLGA NPs to be utilized as targeted chemotherapeutic drug delivery platform for her-2 positive lung cancer.

PLGA NPs are chosen due to their:

- Sustained drug release profile
- Biocompatibility and biodegradability
- Proven efficacy and approval to be used as chemo drug carrier systems

- Wide variable drug loading capacities.

Chemotherapeutic drug afatinib was selected due to its effectiveness against variable cancer cell lines via selective inhibiting ERBB protein family phosphorylation. Afatinib can also be used in combination with immunotherapeutic antibodies and/or with other chemo-drugs. The specific cell signaling mechanism effected by afatinib is represented in **Figure 6** [144].

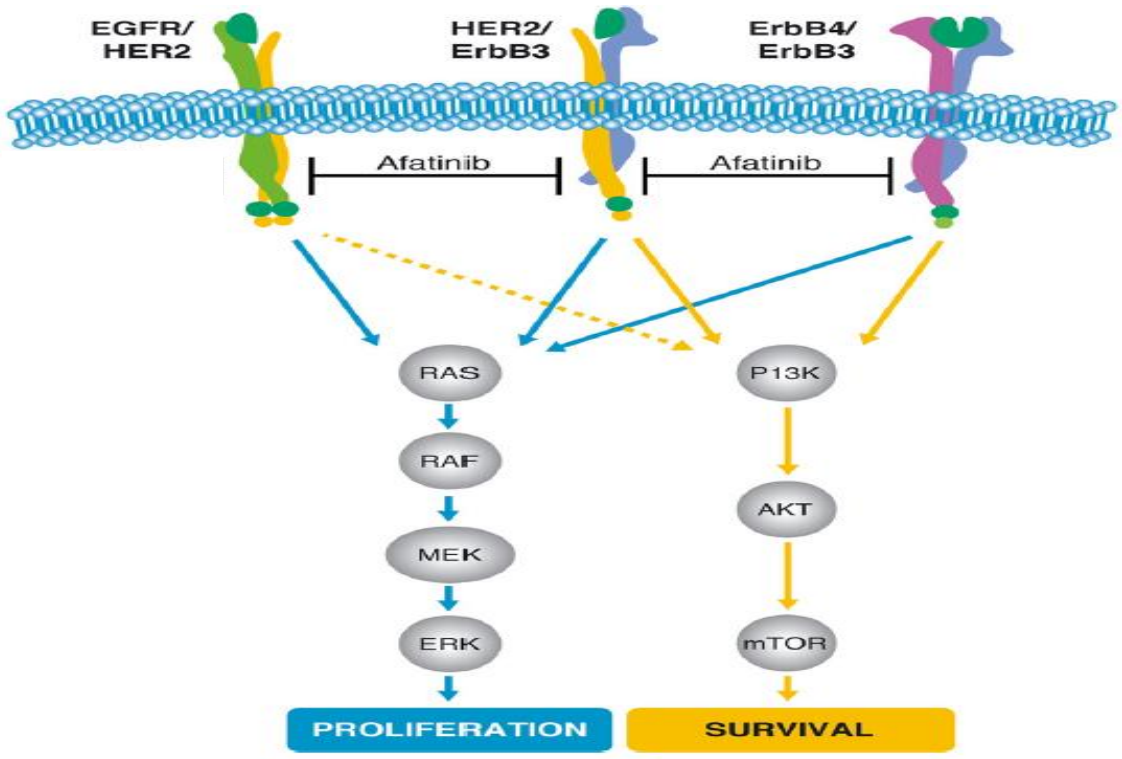

Figure 6: Irreversible inhibition of ErbB receptor family signaling by afatinib.

It was hypothesized that the presence of anti-her-2 CAR on T-MNPs would specifically target her-2 expressing lung cancer cells and enhance cellular uptake. The chemotherapeutic drug afatinib is proposed for inhibition of ERBB protein family phosphorylation in lung cancer cells to inhibit cell survival and proliferation. It was also hypothesized that the therapeutic efficiency of CAR-T-MNPs was significantly enhanced when compared to those of non-specific membrane coated (Plain Jurkat T-MNPs) and only afatinib-PLGA NPs.

2.3) Advantages of using CAR-T-MNPs

The concept of using cell membranes as drug delivery vehicles is becoming more and more popular [145-147]. As mentioned earlier, cell membrane coated drug carriers might ensure unique drug delivery features and functions via coating of nanoparticles with different cell lines, such as red blood cells, platelets, and lymphocytes. Among these cell types, lymphocyte cell membranes have major advantages as they improve drug delivery efficacy, provide better targeting of cancer cells via camouflaging, and consist of minimal unwanted interactions with complements, reticuloendothelial and renal system components. Lymphocytes express different types of proteins on their membrane surface to detect diseased or inflamed tissues [148, 149]. In addition, human lymphocytes express high levels of adhesion molecules to reach affected or activated tissues [150, 151] and are more effective to target tumor sites [152, 153]. Thus, the coating of lymphocyte membranes on the surface of a drug carrier would increase the specific tumor accumulation and facilitate targeted tissue interactions via cell native lymphocyte cell membrane adhesion molecules [68]. Exploiting these features of the biomimetic lymphocytes membrane coated drug carriers can provide superior drug carrier abilities for more specific targeting and biodistribution over conventional drug carriers. Examples from current applications of lymphocyte membrane coated carriers include neutrophil membrane coated nanoparticles for targeting metastatic tumors [75]. Metastatic tumor cells are expressing ligands for the adhesive proteins expressed on neutrophil membranes [76, 77]. In another application, cytotoxic T-lymphocyte coated NPs were used for targeting and treating gastric cancer [85]. In addition, T-lymphocyte membrane-encapsulated PLGA NPs were able to avoid being segregated by lysosomes and retained their lymphocyte coating on the NPs while trapped in the endolysosomal compartments [86]. Furthermore, tumor-associated carcinoembryonic antigen (CEA) chimeric antigen receptor (CAR) engineered jurkat cells were actively accumulated *in vivo* on liver tumors compared to originaljurkat cells for cell

based viral therapeutic delivery [154]. Therefore, the strategy of targeting molecule (CAR, TCR, and ScFv) engineered jurkat cell membrane coated drug delivery is a promising approach for the biomimetic drug delivery field to be carried further.

2.4) Specific aims

1. **Aim 1:** Development, optimization and characterization of N-SCLC targeting anti her-2 CAR T Jurkat cells.

   In this aim, N-SCLC specific CAR T-cells is going to be developed via lentiviral engineering method. Transfection studies are going to be optimized with isolated anti her-2 CAR plasmids, and the binding to its target is going to be demonstrated. After engineering jurkat cells, the expression of anti her-2 chimeric antigenic receptor is going to be measured via flow cytometry. Cell sorting and stable expression experiments with high efficiency is going to be assessed.

2. **Aim 2:** a) Fabrication and characterizations of CAR-T-MNPs as drug carriers

   b) *In vitro* evaluation of CAR-T-MNPs as a drug carrier system against N-SCLC.

   In Aim 2, membranes are going to be isolated from CAR-T-cells and coated on PLGA nanoparticles to form CAR-T-cell membrane coated PLGA NPS (CAR-T-MNPs). CAR-T-MNPs are going to be characterized in terms of morphology, drug loading/release, blood clotting and hemocompatibility. Flow cytometric and microscopic analysis is going to be done to prove membrane coating on NPs and also ligand existence on their surface. As *in vitro* characterizations, their uptake by A549 cells will be measured via comparing control groups (Jurkat cell membrane and anti-her-2 antibody conjugated PLGA NP groups). In

addition, *in vitro* killing efficacy of CAR-T-MNPs will be assessed against her-2 overexpressing cell lines *in vitro* and compared with other treatment groups.

3. **Aim** 3: *In vivo* targeting efficacy evaluation of CAR-T-MNPs on xenograft tumor models. *In vivo* near infrared imaging studies will be done on xenograft tumor model on nude mice. CAR-T-MNPs group will be compared to control groups (Anti her-2-PLGA and Jurkat T-MNP). On *in vivo* images, fluorescence intensities from tumors going to be measured. *Ex vivo* organ imaging and fluorescent accumulation are also determined to evaluate biosdistribution of CAR-T-MNPs. At the end point of the studies, spectrophotometric analysis of homogenized organs will be done to confirm the findings of *in vivo* and *ex vivo* image analysis. NP distribution of all organs and tumors will be plotted and analyzed to reveal the effect of CAR-T membrane coating on PLGA NPs.

2.5) Innovative aspects

The novelty of this project involves the development of a drug-delivery platform fabricated from targeted specialized human cytotoxic CAR-T-cell membranes. The CAR-T-cell membrane-coated NPs will enlarge the concept of individualized therapy with high integrity and functionality. Up to now, such an approach to use targeted specialized cell membrane coated nanoparticles for cancer chemotherapy has not been reported. The results would aid in future research in the development of better chemotherapeutic drug delivery systems with prolonged circulation time and enhanced tumor site accumulation. Furthermore, this project might open a new way to individualized and tumor specific targeting by patient's own ligand and membrane coated NP delivery.

2.6) Successful outcomes

The successful completion of this research will assist in the design and development of CAR-T-MNPs, which have superior tumor targeting and accumulation, RES and immune system avoidance, and minimal cytotoxicity compared to the current chemo-loaded NP systems. If successful, the CAR-T-MNPs developed in this research will be able to provide a better tumor regression, can be degraded at a controlled rate, and will be biocompatible for *in vivo* use.

2.7) Materials and Methods

2.7.1) Cell lines and culture conditions

Lentiviral packaging cell line Lenti-X 293 T was provided by Takara-Clontech. HEK 293 T, her-2 positive tumor lines SKOV-3, MCF-7 and her-2 negative tumor lines, MDA-MB-231 and Jurkat E6-1 were provided by American Type Culture Collection (ATCC). All cell lines were cultured in medium consisting of RPMI 1640 (or DMEM) supplemented with 10% heat inactivated FBS (Corning), 100 U/ml penicillin, and 100 µg/ml streptomycin (Invitrogen). Lymphocytes and Jurkat cells were cultured in GT-T551 medium (Takara) supplemented with 10% FBS (Corning) and 50 IU/ml IL-2 (Miltenyi) at 37°C and 5% CO2.

2.7.2) Materials

Poly(lactic-co-glycolic acid) ((PLGA),LG 50:50, (M_n 25,000-35,000 Da)) and poly(lactic-co-glycolic acid)-NHS ((PLGA-NHS),LG 50:50 (M_n 25,000-35,000 Da)) were obtained from PolySciTech, whereas polyvinyl alcohol (PVA), NHS, bovine serum albumin (BSA), and

fluorescein from Sigma, dichloromethane from Merck, and EDC (1-ethyl-3-(3-dimethylaminopropyl)-carbodiimide) from Fluka Chemie. All reagents were of analytical grade.

2.7.3) Preparation of PLGA nanoparticles

Briefly, Afatinib (10 mg) was added dropwise to 3 mL of dichloromethane containing PLGA (90 mg) sonicated for 3 minutes and resultant emulsification was added dropwise to 20 mL of aqueous phase containing 5% poly(vinyl alcohol) and emulsified using ultrasonication for 10 minutes at an 1.30 on 0.30 off. The mixture was subsequently stirred overnight in the fume hood at room temperature to evaporate organic solvents. The nanoparticles were washed three times with ultra-pure water using ultracentrifugation at 15.000 rpm 15 min and freeze-dried (− 57 °C, 0.090 mbar, 24 h, Labconco). For *in vitro* and i*n vivo* particle tracking purposes, 10 μg of coumarin-6 green dyes or ICG infrared dyes was added to the PLGA dichloromethane solution prior to PLGA nanoparticle synthesis (without drug/water phase). To determine loading efficacy, afatinib encapsulated in the PLGA was measured using UV-VIS Spectrophotometer.

2.7.4) Hybridoma cell culture, purification and characterization of 4D5 anti her-2 antibodies

4D5 hybridoma cells were thawed rapidly, then transferred to 5 ml warm RPMI 1640 medium containing 10% FBS and 1% P/S (Gibco) and plated onto 25 cm tissue culture flasks. Cells split 1:5 every 3 days to keep the cell density 10^6 cells/ml. Split cells into larger plates every-time by adding cells to fresh 10 ml medium in 75 cm2 flasks and 25 ml in 175 cm2 flasks. Gradually, the FBS amount decreased in hybridoma culture from 10% to 0%, and all supernatant was maintained in 4 degrees for purification. For antibody concentration, all the cells collected and spun down at 3000 rpm for 5 minutes at 4°C. Collected supernatant was filtered through 0.22 μm filter and concentrated using Amicon (Millipore). Cells were stirred via ultracel ultrafiltration disc

(Millipore 100kDA cutoff membrane). For purification step, 1 ml HiTrap Protein G HP column (GE healthcare 17-0404-03) was equilibrated via filtering 10 ml pH PBS. Concentrated superanatant was mixed 1:1 with binding buffer pH7.2 and applied to column at 1 ml/min. Column was washed with 20 ml PBS, and antibodies were eluted with 5 ml 100 mM Glycine pH 3. 0.5 ml fractions were collected into tubes containing 50 µL 0.5M Tris (pH 9.5) and gently mixed to neutralize pH. Protein contents in purified fractions were measured via nanodrop (280 Abs), and functionality of the antibodies was tested via flow cytometer on A549 cells. Fractions containing high concentrations of antibody were kept at 4°C until used.

2.7.5) Lentiviral vector production and transduction of T-cells

2.7.5.1) Lentiviral vector production

pHR_PGK_antiHer-2_synNotch_Gal4VP64 lentiviral plasmid (used as backbone for expressing anti her-2 specific CAR plasmids) and pHR_Gal4UAS_tBFP_PGK_mCherry (used as fluorescent reporter for transduction) lentiviral plasmids were a gift from Wendell Lim (Addgene plasmid # 85423) [59]. Pantropic VSV-G pseudotyped lentivirus was produced via transfection of either HEK 293T (ATCC) or Lenti-X 293T cells (Clontech #11131D) with anti her-2 CAR plasmids and/or pHR_Gal4UAS_tBFP_PGK_mCherry expression vectors and the viral packaging plasmids psPAX2 and pLP-VSVG using Lipofectamine 3000 (Invitrogen). Supernatants containing lentivirus were collected 24, 48 and 72 hours later. Collected viruses were concentrated using Amicon Ultra -15 (10.000 kDA cut off) centrifugal filter tubes and frozen at -80^{o}C degree.

2.7.5.2) Lentiviral transduction of Jurkat T-cells

For transduction of Jurkat T-cells, Jurkat T-cells were thawed, and culture started for lentiviral transduction. At day 4, CD4+ Jurkat cells were spinoculated (2000 rpm 90 minutes) and co-

cultured for 24 hours with lentiviral supernatants in the presence of 8 µg polybrene (Merck). After transduction, the cells were cultured in the presence of 10% FBS until use. T-cell surface markers were later detected via anti-human CD3, CD4 antibodies (Biolegend) using flow cytometry methods. Her-2 cell surface expression of various cancer cell lines (MDA-MB-231, A549, SKOV-3) was detected using isolated anti her-2 4D5 mouse antibodies and anti-mouse IgG (H+L) (Jackson laboratories). Her-2 specific CAR expression was detected by Anti-Myc Tag-Alexa 647 (Cell Signaling). Fluorescence response analysis and sorting of live cells were performed using a BD LSR II & BD melody flow cytometer and analyzed with FCSlyzer software (Becton Dickinson).

2.7.6) CAR-T membrane isolation

Cells (10^8) were washed three times with cold PBS (1X). Before the last spin, cells were counted and resuspended in cold hypotonic buffer Tris-HCl (10mM, pH7.5) in 10 mL. Protease and phosphatase inhibitor cocktail (PIC) was added (5 µL/million cells) and incubated at 4°C for 20 minutes. The mixture was centrifuged at 4000 g for 10 minutes. The resulting pellet was resuspended in cold PBS 0.25X + PIC at 1 ml/10 million cells and incubated for another 20 minutes at 4°C. The mixture was centrifuged at 4000 g for 10 minutes, then the pellet was resuspended in cold PBS 1X + PIC and kept on ice. DNAse reaction was performed on the samples based on their DNA contents (for 20 million cells: 20 IU DNAse for 4 hours). After using DNAse, mixture was centrifuged at 4000 g for 10 minutes. The isolated membranes were collected, lyophilized overnight and stored at 4°C. Right before use, membrane lyophilates were weighed and resuspended in a PBS solution.

2.7.7) Coating PLGA nanoparticles with CAR-T membranes and nanoparticle characterization

CAR-T membrane-derived nanovesicles were prepared as follows; drug loaded PLGA nanoparticles were added via hydrating these NPs with freeze-dried CAR-T membranes, whereas the CAR-T membrane amount was slightly more than the calculated amount of lipid molecule derived from cells to cover all amount of PLGA nanoparticle surface. The mixture was sonicated for 5 minutes using a probe sonicator. Subsequently, the mixture was co-extruded using an Avanti mini extruder, as previously reported [69]. The size distribution and polydispersity of these particles were measured via dynamic light scattering. The *in vitro* release profile of Afatinib from the CAR-T-MNPs was performed using dialysis method and UV-VIS Spectrophotometer.

2.7.7.1) Flow cytometry and Western Blot

After extrusion, membranes were stained with lipophillic DiD dye to detect coating efficacy (APC channel), and stained NPs were run on the flow cytometry. To identify the specific anti her-2 CAR receptor in the CAR-T-MNPs formulations, the particles were stained with anti c-myc tag antibody to detect ScFv on the particle surface. The samples were analyzed using a flow cytometer without SSC threshold.

Western Blot analysis was done to confirm the existence of anti her-2 CAR molecule on isolated membranes. In Western Blot analysis, isolated membranes were run on SDS-PAGE gels under denaturing conditions. Samples were mixed with laemmli buffer containing 10% β-mercaptoethanol, 4% SDS, 125 mM Tris-HCl, 20% Glycerol, 0.004% bromophenol blue and run on gel; then transferred onto nitrocellulose membranes. Membranes were incubated with primary antibodies against mouse anti-human CD3 and anti-mouse IgG (heavy chain light chain) (Jackson

laboratories). Blots were visualized using the ECL (Millipore) with ChemiDoc Imager (Bio-Rad). Non-conjugated nanoparticles were used as a control.

2.7.8) Conjugation of anti her-2 antibodies with PLGA NPs

To covalently attach mAbs onto the nanoparticle surface, NHS conjugation chemistry was employed. Right after synthesis of PLGA NPs (20% PLGA-NHS and 80% PLGA), washed particles were added to 1 ml of a 0.3 M MES buffer. Different weight ratios of 1 mg nanoparticles to 5, 50 and 100 µg of mAb were used in conjugation experiments. The reaction mixture was stirred gently for 3 hours at room temperature. Excess linking reagents and soluble by-products were separated by centrifugation at 13,200 rpm for 10 minutes, and the pellet was washed three times with 1 ml PBS, pH 7.4. Finally, mAb conjugated nanoparticles were re-dispersed in 300 µl of PBS, and the protein content was determined by ELISA and nanodrop (280nm Abs).

2.7.9) Detection of mAb on the surface of nanoparticles

2.7.9.1) Indirect ELISA Assay

Microtiter ELISA well plates were coated with 100 µl of the Her-2 antigen solution at a concentration of 1 ug/ml in coating buffer. Samples were incubated overnight at 4°C. After incubation time, they were washed with 300 ul wash buffer three times and blocked with 300 ul blocking buffer at 37°C for 1.5 hours. Plates were washed 3 times and incubated 1.5 hour at 37°C with different concentrations of unconjugated PLGA, anti her-2 antibody conjugated PLGA and with standard anti her-2 antibodies alone. After repeating the washing step, 100 µl of HRP-conjugated secondary antibody (anti-mouse H+L chain, 0.1 ug/ml in dilution buffer) was added to each well and incubated for 1 hour at 37°C. After washing 3 times with the washing buffer, 100 µl TMB substrate solution was added to each well and incubated at room temperature for 30

minutes after adding stop solution to each well. That was followed by the measurement of absorbance values at 450 nm wavelength (Tecan).

2.7.9.2) Western Blot

Western Blot analysis was done to confirm the conjugation of anti her-2 antibody on PLGA NPs. In Western Blot analysis, antibody conjugated nanoparticles were run on SDS-PAGE gels under denaturing conditions. Samples were mixed with laemmli buffer containing 10% β-mercaptoethanol, 4% SDS, 125 mM Tris-HCl, 20% Glycerol, 0.004% bromophenol blue and run on gel then transferred onto nitrocellulose membranes. Proteins/membranes were analyzed by western blotting. Membranes were incubated with primary antibodies against anti-mouse IgG (H+L chain) (Jackson laboratories). Blots were visualized using the ECL (Millipore) with ChemiDoc Imager (Bio-Rad). Non-conjugated nanoparticles were used as a control.

2.7.10) Characterization of nanoparticles

2.7.10.1) Particle size and zeta potential analysis

Freeze-dried nanoparticles were dispersed in deionized water. Their mean particle diameter and the width of the particle distribution (polydispersity index) were determined by photon correlation spectroscopy or dynamic light scattering (DLS) using a Nanobrook 90 plus PALS (BrookHaven Instruments). The particle charge was quantified as zeta potential by Nanobrook 90 plus PALS zetasizer using the Nanobrook 90 plus. All measurements were made in triplicate.

2.7.10.2) Surface morphology

The surface morphology of the formulated nanoparticles was visualized by transmission electron microscopy (TEM). Before observation, freeze-dried nanoparticle samples in DI water were fixed onto ozone treated copper grids and stained with uranyl acetate (0.5%). A H-7500 TEM (Hitachi) transmission electron microscope was used to visualize the particle morphologies.

2.7.10.3) Drug loading efficacy and *in vitro* drug release profile

The supernatant solution obtained after ultracentrifugation of NPs during the formulation process was stored at −20°C until being used for loading efficiency determination. For the drug release studies, suspensions of Afatinib loaded NPs in PBS (pH 7.2) were added to dialysis bags (Spectrum Laboratories Inc.) with a molecular weight cut-off (MWCO) of 8000 Da. The experiment was done in quadruplicates. Dialysis against PBS was carried out at 37°C up to 21 days. At pre-determined time points, dialysate was collected and stored at −20°C for later analysis. The absorption of Afatinib was measured using the spectrometer at λ 345 nm. A standard curve was plotted by measuring the absorbance of known concentrations of Afatinib. The amount of Afatinib released was then determined against the standard curve and was correlated to the Afatinib loading efficiency, which was determined using the formula given below.

$$\%\ Loading\ efficiency = \frac{Total\ Afatinib\ used - Afatinib\ in\ supernatant}{Total\ Afatinib\ used} X\ 100$$

2.7.10.4) Hemocompatibility studies

Human blood from donors was collected and handled by following methods. Informed consent was obtained from the study participants before drawing blood for the hemocompatibility studies. After collection, human blood was incubated with CAR-T-MNPs at different concentrations (0, 250, 500, 750, and 1000 µg/ml), 0.9% saline (negative control), or distilled water (positive control) for 2 hours. Following centrifugation at 1000 g, absorbance readings were taken at 545nm. The percentage of hemolysis was calculated using the equation below:

$$\%\ Hemolysis = \frac{(sample\ OD - Negative\ control\ OD)}{(Positive\ control\ OD - Negative\ control\ OD)} X\ 100$$

To study blood clotting kinetics, CAR-T-MNPs of varying concentrations (0, 250, 500, 750, and 1000 µg/ ml) were added to blood that was activated with CaCl2 (n=9). At pre-determined time points (10, 20, 30, and 60 minutes), the red blood cells (RBCs) not involved in clot formation were lysed. Absorbance readings of supernatant were taken at 540nm. The absorbance readings were inversely proportional to clot formation.

2.7.10.5) Binding kinetics of fabricated anti her-2 PLGA NPs via competitive ELISA assays

To measure whether fabricated NPs were able to engage with her-2 protein, competitive ELISA assays were performed with anti her-2 conjugated PLGA NPs. Microtiter ELISA plate wells were coated with 100 µl of the her-2 antigen solution at a concentration of 0.1 ug/ml in coating buffer. Plates were incubated overnight at 4°C, washed with 300 ul wash buffer three times, and blocked with 300 ul blocking buffer at 37°C for 1.5 hours. Plates were washed 3 times and incubated with different concentrations of anti her-2 antibody conjugated PLGA NPs in the presence of biotinylated anti her-2 antibodies (0.05 µl/ml) for one hour at 37°C. After repeating the washing steps, 100 µl of HRP-conjugated streptavidin (0.1 ug/ml in dilution buffer) was added to each well and incubated for 1 hour at 37°C. After the washing steps, 100 µl TMB substrate solution was added to each well and incubated at room temperature for 30 minutes, and then the absorbance values were measured on 450 nm wavelength (Tecan). Data was normalized against bare PLGA NPs and analyzed for experimental and control groups.

2.7.11) *In vitro* cellular uptake studies

For fluorescent uptake microscopy imaging (EVOS Floid, Invitrogen) studies, A549 were seeded on a glass bottomed six well tissue culture plate (Corning). Jurkat-T-MNPs, anti her-2-PLGA NPs or CAR-T-MNPs were added and incubated with cells for 30 minutes at 37°C. Cells were then

washed using PBS and were fixed using 5% formaldehyde for 20 minutes. The cell nuclei were stained using NucBlue (Thermo), and cells were imaged using the inverted fluorescent microscopy. For the spectrophotometric analysis of uptake, Coumarin-6 (C-6; fluorescent drug) loaded Jurkat-T-MNPs, anti her-2 PLGA NPs and CAR-T-MNPs at different NP concentrations (100 µg/mL, 250 µg/mL, 500 µg/mL, 750 µg/mL) were exposed to cells in 96 well plates for 30 minutes and subsequently washed with 1X PBS and lysed with 250 µl/well of 1% Triton® X-100 (approximately 30 min incubation). Cell extracts were then analyzed for protein content using the Pierce BCA protein assay kit (Thermo Scientific, Rockford, IL) and C-6 fluorescent intensity (emitted from particles uptaken inside the cell) using a UV-vis Spectrophotometer (458/540 em/ex). Total protein concentration in each lysate was calculated using a BSA standard curve. The uptake of the nanoparticles was calculated by normalizing the particle concentration (determined from fluorescence intensity in a lysate) in each sample with total cell protein, which correlated to the number of cells in the sample.

2.7.12) *In vitro* cytotoxicity assays

A549, MDA-MB-231 and SKOV-3 cells were seeded (5×10^3 cells/well) in 96-well plates and incubated overnight. Free Afatinib, Afatinib loaded PLGA NPs, anti her-2 PLGA NPs, Jurkat-T-MNPs, and CAR-T-MNPs were added to the seeded cells (n=4). After incubation for 48 hours, the absorbance at 490 nm was measured using UV-VIS Spectrophotometer (Tecan) after incubating with MTT reagent (Promega) for one hour. Cell viabilities were calculated via normalizing to the control group (cells exposed to complete media, 100% viability).

2.7.13*) In vitro* live-dead and LDH release assays

2.7.13.1) *In vitro* live-dead assays

A549 cells were seeded at a density of 5×10^3 cells/well in 96-well plates and incubated overnight. Free Afatinib, Afatinib loaded PLGA NPs, anti her-2 conjugated PLGA NPs, Jurkat-T-MNPs, and CAR-T-MNPs were added to the seeded cells (n=4). After incubation for 48 hours, cells were stained with enzo live-dead staining kits following the company's instructions. Cells were incubated with permeable Live-Dye™ and the cell non-permeable PI (red) dyes in staining buffer for 15 minutes at 37°C. Following incubation with the staining solution, cells were visualized using the inverted fluorescent microscope, and images were recorded.

2.7.14) *In vivo* biodistribution of CAR-T-MNPs in tumor implanted mice

The biodistribution study was examined whether intravenously injected CAR-T-MNPs targeted subcutaneous tumors in the tumor implanted mice. A549 cells were injected into NGC mice at 2 $\times$ 10^6 cells/mouse via subcutaneously to develop a lung cancer model. Prior to the distribution assay, tumor volumes measured regularly to determine the optimal experimental start point. ICG-loaded CAR-T-MNPs or anti her-2 conjugated PLGA NPs were prepared in the same formulation procedure mentioned earlier. Saline, ICG-loaded PLGA NPs, anti her-2 PLGA NPs, Jurkat-T-MNPs and CAR-T-MNPs were intravenously given to mice at 5 mg of ICG loaded particles (n = 3). At 1, 4, 8, and 16 hours, images of animals for all groups were monitored and recorded by the Kodak FX/Pro imaging system. At the end point of the experiment, mice were autopsied, and tumors and major organs were carefully collected and weighed. Then the tumor tissue sections were carefully frozen in OCT, and sectioned at 10 μm (CM1950, Leica). The fluorescence signals of tumors and each organ were recoded using the Kodak FX/Pro imaging system for quantification. Furthermore, some weighted tumors and organs were homogenized for 2 minutes using a tabletop

Precellys homogenizer (Bertin Instruments). Homogenates were centrifuged at 4000 rpm for 10 minutes, and fluorescent measurements of supernantants were taken at λex 786 nm and λem 825 nm using spectrophotometer (Tecan). Effective nanoparticle accumulation on all organs and tumors (μg NP per mg of organ) were determined using standard curve of ICG PLGA NPs and normalized against saline group.

CHAPTER 3

Results and Discussion

3.1) Fabrication, purification and characterization of 4D5 anti her-2 antibodies

4D5 hybridoma cell line was tested for the secreted antibody existence in culture supernatant. For this, 1x10^6 A549 cells were stained for flow cytometric analysis. As seen in the flow cytometry

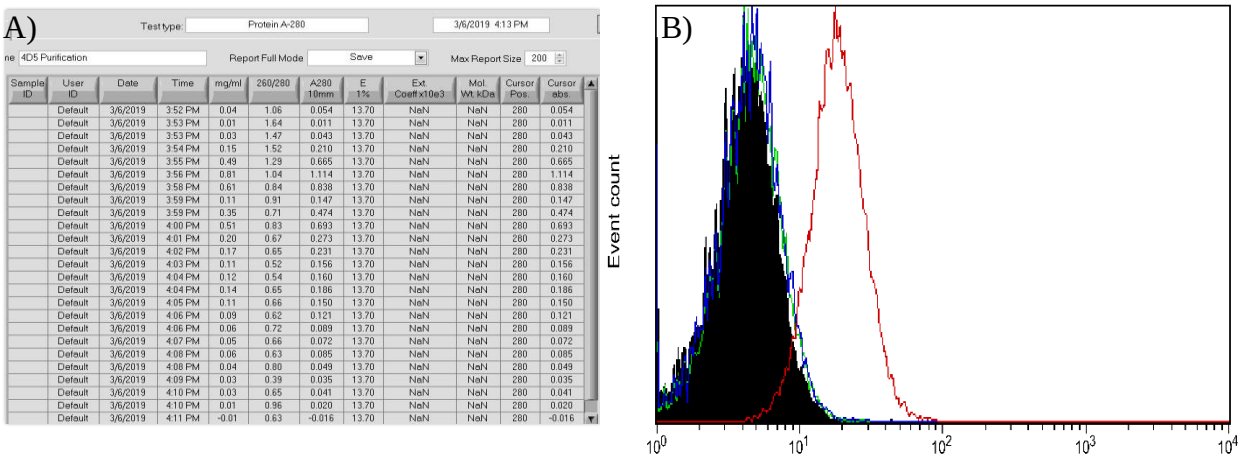

Sample ID	User ID	Date	Time	mg/ml	260/280	A280 10mm	E 1%	Ext Coeff x10e3	Mol. Wt. kDa	Cursor Pos.	Cursor abs.
	Default	3/6/2019	3:52 PM	0.04	1.06	0.054	13.70	NaN	NaN	280	0.054
	Default	3/6/2019	3:53 PM	0.01	1.64	0.011	13.70	NaN	NaN	280	0.011
	Default	3/6/2019	3:53 PM	0.03	1.47	0.043	13.70	NaN	NaN	280	0.043
	Default	3/6/2019	3:54 PM	0.15	1.52	0.210	13.70	NaN	NaN	280	0.210
	Default	3/6/2019	3:55 PM	0.49	1.29	0.665	13.70	NaN	NaN	280	0.665
	Default	3/6/2019	3:56 PM	0.81	1.04	1.114	13.70	NaN	NaN	280	1.114
	Default	3/6/2019	3:58 PM	0.61	0.84	0.838	13.70	NaN	NaN	280	0.838
	Default	3/6/2019	3:59 PM	0.11	0.91	0.147	13.70	NaN	NaN	280	0.147
	Default	3/6/2019	3:59 PM	0.35	0.71	0.474	13.70	NaN	NaN	280	0.474
	Default	3/6/2019	4:00 PM	0.51	0.83	0.693	13.70	NaN	NaN	280	0.693
	Default	3/6/2019	4:01 PM	0.20	0.67	0.273	13.70	NaN	NaN	280	0.273
	Default	3/6/2019	4:02 PM	0.17	0.65	0.231	13.70	NaN	NaN	280	0.231
	Default	3/6/2019	4:03 PM	0.11	0.52	0.156	13.70	NaN	NaN	280	0.156
	Default	3/6/2019	4:04 PM	0.12	0.54	0.160	13.70	NaN	NaN	280	0.160
	Default	3/6/2019	4:04 PM	0.14	0.65	0.186	13.70	NaN	NaN	280	0.186
	Default	3/6/2019	4:05 PM	0.11	0.66	0.150	13.70	NaN	NaN	280	0.150
	Default	3/6/2019	4:06 PM	0.09	0.62	0.121	13.70	NaN	NaN	280	0.121
	Default	3/6/2019	4:06 PM	0.06	0.72	0.089	13.70	NaN	NaN	280	0.089
	Default	3/6/2019	4:07 PM	0.05	0.66	0.072	13.70	NaN	NaN	280	0.072
	Default	3/6/2019	4:08 PM	0.06	0.63	0.085	13.70	NaN	NaN	280	0.085
	Default	3/6/2019	4:08 PM	0.04	0.80	0.049	13.70	NaN	NaN	280	0.049
	Default	3/6/2019	4:09 PM	0.03	0.39	0.035	13.70	NaN	NaN	280	0.035
	Default	3/6/2019	4:10 PM	0.03	0.65	0.041	13.70	NaN	NaN	280	0.041
	Default	3/6/2019	4:10 PM	0.01	0.96	0.020	13.70	NaN	NaN	280	0.020
	Default	3/6/2019	4:11 PM	-0.01	0.63	-0.016	13.70	NaN	NaN	280	-0.016

Figure 8: Testing the purified antibodies. A) Nanodrop results of purified antibody fractions. B) Flow cytometric analysis of A549 cells with purified 4D5 antibodies.

histogram (**Fig. 7)**, 4D5 cell culture supernatant treated cells with anti her-2 staining show a significant shift. Therefore, the existence of anti her-2 antibody in the supernatant was demonstrated, and thereby antibody

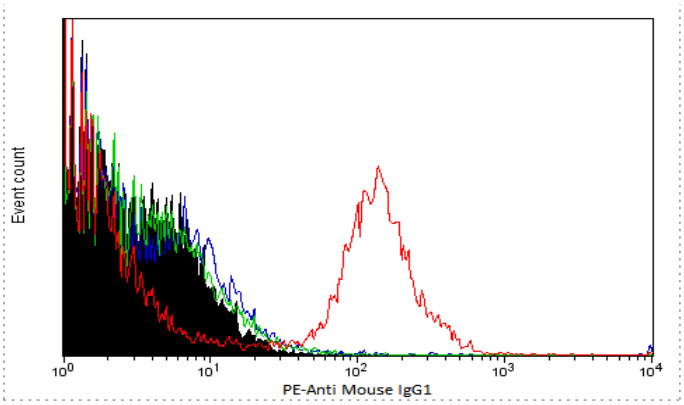

Figure 7: Flow cytometry confirmation of anti her-2 antibodies in hybridoma cell culture supernatants.

collection and purification steps were performed. The purified antibody product was also validated (**Fig. 8**).

After purification steps, positive fractions were selected based on their 280 nm absorbance on nanodrop and total concentration of purified antibody was calculated. Following, obtained antibodies were tested to assess their binding functionality against A549 cells. For this binding study, A549 cells were stained with purified antibodies and PE-anti mouse secondary antibody. As shown in the histogram (**Fig. 8**), purified antibodies showed a significant shift in PE channel for the stained A549 group.

3.2) Plasmid purification, digestion and confirmation

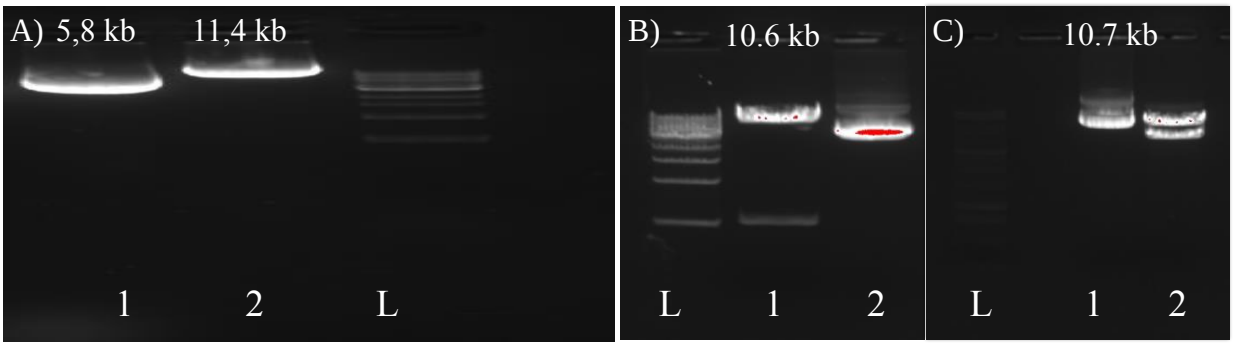

Figure 9: Plasmid purification. A) Line 1: pLP/VSVG, Line 2: AntiHer-2-SynNotch. B) Line 1: psPAX, Line 2: EcoRI digested. C) Line 1: 4Gal_UAS_mCherry_tBFP, Line 2: EcoRI digested plasmids L: 1kb step DNA ladder.

Transformed bacterial cultures were grown in lab, and PCR confirmed positive colonies were expanded further and used for purifying plasmids (Qiagen Mega plasmid DNA isolation kit). These purified plasmids were confirmed by PCR, enzyme digestion (EcoRI) and gel electrophoresis (by size) as shown in **Figure 9**.

3.3) Lentiviral vector production

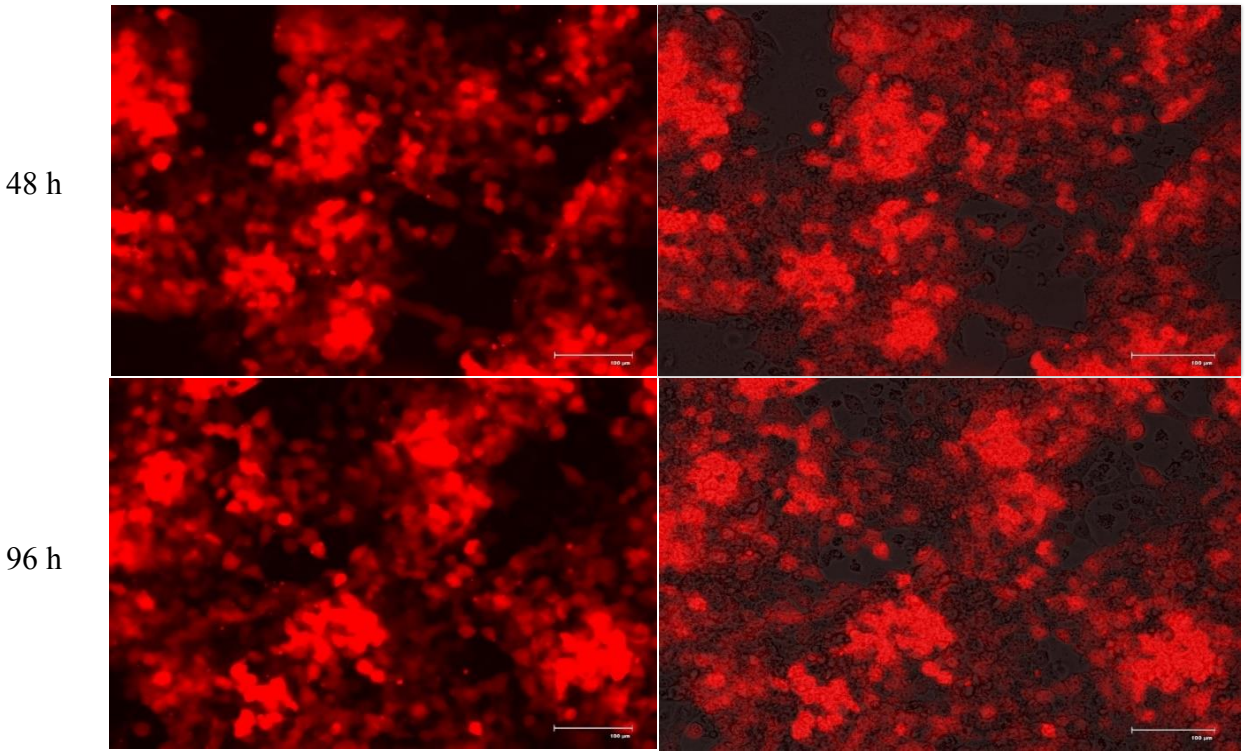

Figure 10: Lentiviral vectors produced in Lenti-X 293T packaging cell line.

Lipid-based plasmid DNA transfection methods were followed for lentiviral transfection studies. Lenti-X 293T cells grown in 6 well plates were exposed to psPAX + pLP/VSVG+ 4GalUAS_tBFP_mCherry +anti her-2SynNotch plasmids together as equimolar mass in total of 3 ug. After transfection, constitutive mCherry fluorescence (**Fig. 10**) was observed, and culture supernatant was collected over the course of 3 days. Cell culture supernatants were then used to transduce Jurkat T-cells to express mCherry and anti her-2 CAR proteins.

3.4) p24 ELISA Lentiviral Tittering Studies

Lentiviral tittering studies have been done to optimize CAR T-cell transductions. Two different cell types and three different transfection reagents have been used. Packaging cell media was collected over the course of 3 days and subjected to anti-p24 ELISA Lentiviral tittering study.

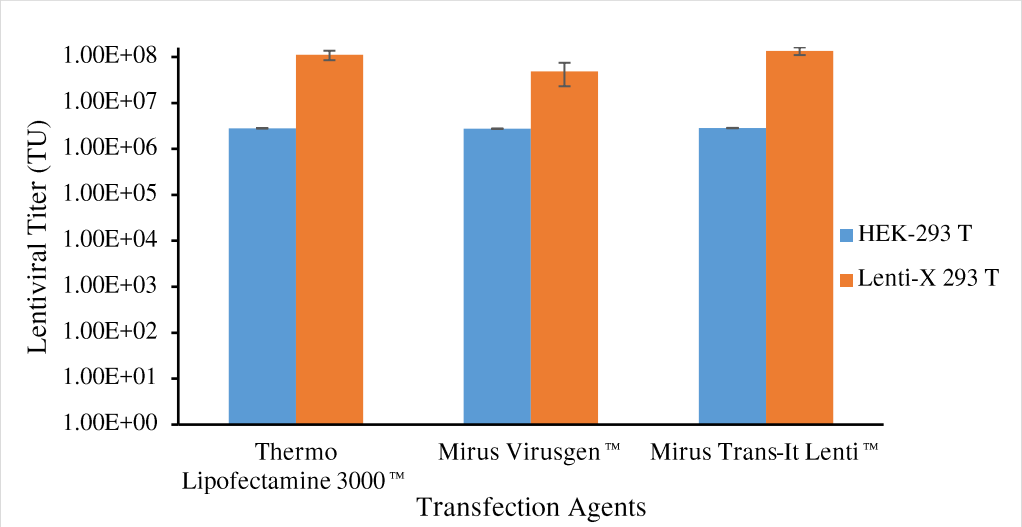

Figure 11: Viral titer measurement via p24 ELISA lentiviral tittering study.

As a result (**Fig. 11**), Lenti-X 293 T and Thermo Lipofectamine 3000 were chosen as the packaging cell line and transfection reagent. Furthermore, Lentiviral titer and multiplicity of infection (MOI) were calculated to match the viral titer requirement for each cell line which was going to be transduced.

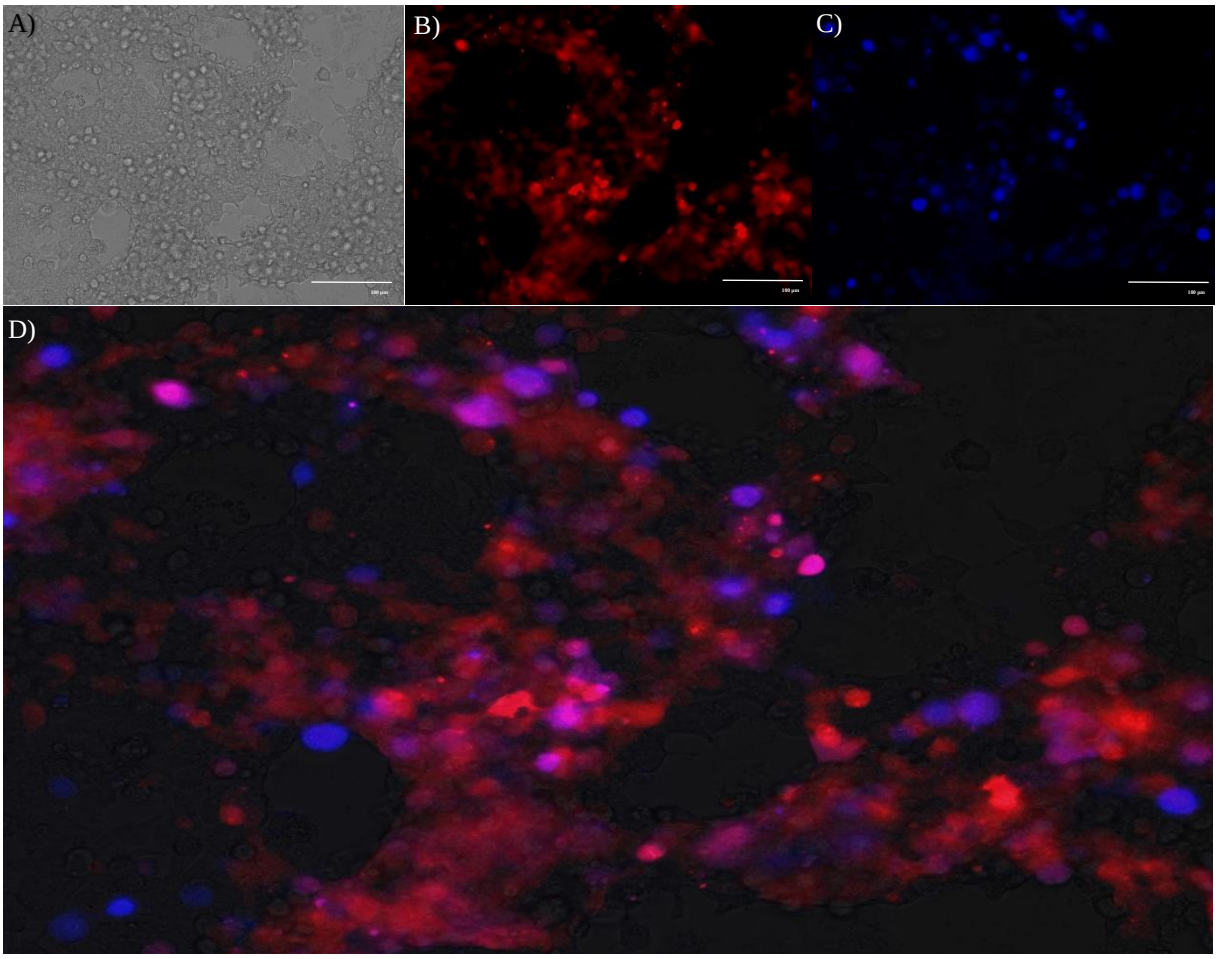

Figure 12: Plasmid transfection of cells. Her-2-synNotch-Gal4 and pHR_Gal4UAS_tBFP_PGK_mCherry transfected HEK 293T cells subjected to Her-2 expressing A549 co-culture for BFP reporter expression. (A: DIC, B: Red, C: Blue, and D: Merged).

3.5) Anti her-2 expression on transfected HEK293 T-cells

A transfection system uses two different transfer plasmids; one encodes the anti her-2 ScFv antigen binding SynNotch receptor, whereas the other plasmid is used as a reporter plasmid. In this very specific plasmid set, whenever there is binding to the SynNotch receptor, it releases Gal4VP intracellular transcription activator portion to activate the expression of blue fluorescent protein (tBFP) in the other reporter plasmid. A reporter plasmid has two distinct colors; one is mCherry (red) for anti her-2, and the other is tBFP (blue) for the binding. mCherry is the constitutive reporter for the transfection monitor and tBFP is the reporter for binding monitoring purposes. Therefore, in this microscopic study, transfected HEK-293T cells were co-cultured with Her-2

positive A549 cells for 24 hours. As shown in **Figure 13**, microscopic images were taken in three different channels to prove the integrity of the plasmids and their transfection potential.

3.6) Lentiviral transduction of Jurkat T-cells

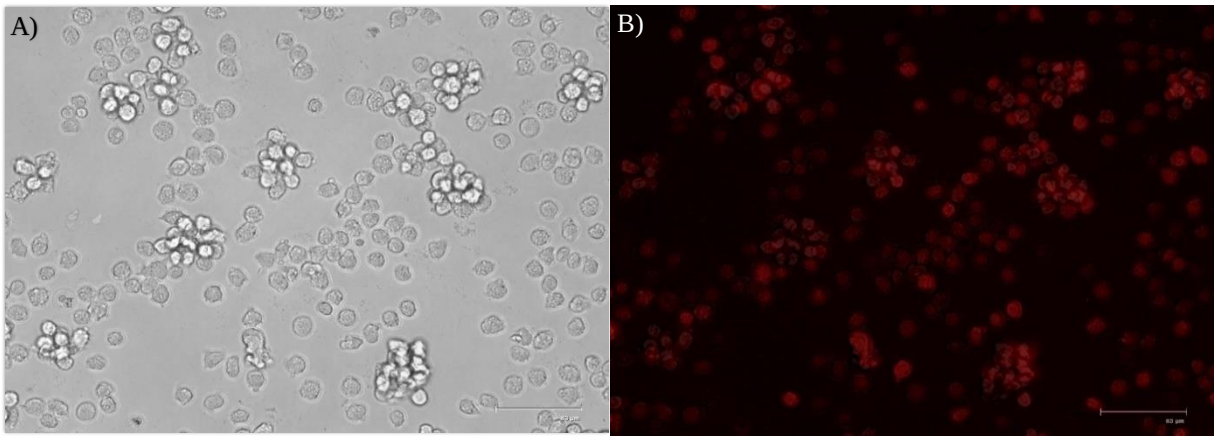

Figure 13: Collected viral particles via centrifuge, concentration applied to cells with +8 µg/ml Polybrene for 48 hours. (A: DIC and B: Red channel).

Collected viral particles were applied to cells with +8 µg/ml Polybrene for 48 hours. After viral transduction, fluorescent microscopic pictures were taken of anti her-2 +mCherry expressing Jurkat cells. After transduction confirmation via fluorescent microscopy, transduction of cells was confirmed and characterized via flow cytometry. In this case, anti-CD3-PE antibody (PE channel) was used to characterize Jurkat cells, whereas internal mCherry fluorescent protein (PerCP-Cy5.5 channel) was used for transfection.

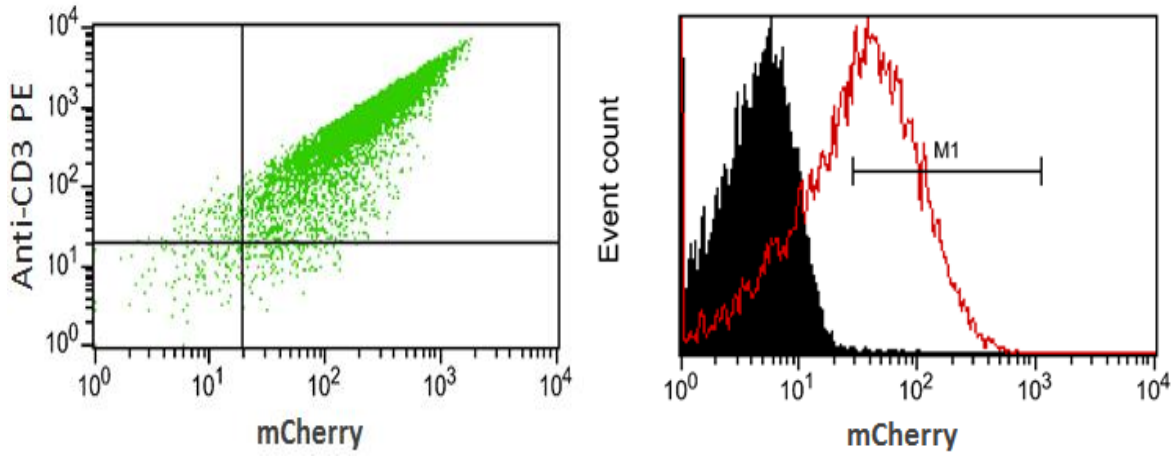

Figure 14: Flow cytometric confirmation of Jurkat cell transduction.

As shown in **Figure 14**, cells were showing a distinctive shift (by 50% increase) in the mCherry spectra compared to the non-transduced group, and they were able to stain with anti-CD3 PE antibody as well. The results indicated that Jurkat cells were successfully transduced with produced lentiviral particles.

3.7) Anti her-2 TCR receptor confirmation on Jurkat cell surface

After confirmation of reporter plasmid transduction and stable mCherry protein expression, the same set of experiments was used for anti her-2-CAR receptor encoding transfer plasmid transduction studies. In the extracellular portion of anti her-2 CAR receptor, a small tag called c-myc was placed as an extra sequence in the plasmid to detect the receptor easily on the cell surface. In this case, instead of fluorescent protein mCherry, Alexa fluor 647 anti myc-tag antibody was used.

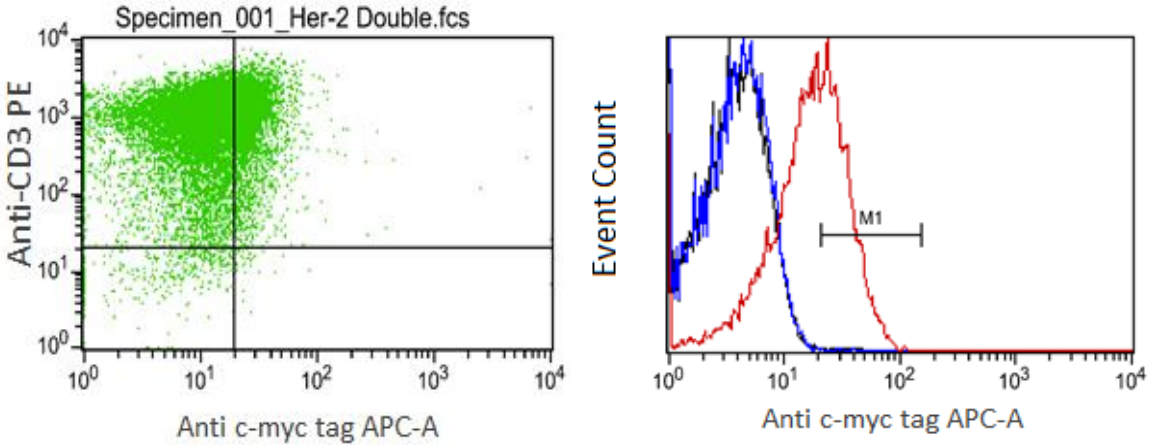

Figure 15: Flow cytometric confirmation of anti her-2 expression on Jurkat cells.

As shown in **Figure 18**, Jurkat cells were successfully transduced to express anti her-2 CAR receptor on their cell surface. They were also characterized by their CD3 expression as well. Again, a distinctive shift was seen in the anti myc-APC channel compared to the non-transduced anti-myc tag stained group. As transduction efficacy, around 40-50% of all the cell population were found to express anti her-2 CAR receptor on the surface.

3.8) Transduced Jurkat sorting (mCherry based)

Transduced cells were sorted via BD melody cell sorter. For the sorting experiment, mCherry was used to sort out mCherry tranduced cells from the negative population. As shown below (**Fig. 15**), almost half a million Jurkat cells were sorted by using PERCP-Cy5.5 channel with around 70-80% efficiency. Cells had been sorted with BD melody using aseptic techniques and negative/positive fractions were cultured further.

CYTOMETER INFO

User Name:	Core User	Application Name:	BD FACSChorus	Cytometer Serial Number:	P6617590005
Experiment Name:	Serkan-Jurkat Sorting	Application Version:	1.1.15.0	Cytometer Name:	BD FACSMelody

SORT DETAILS

Sort Mode:	Purity	Sort Status:	Stopped by System	Start Date Time:	08/03/2018 05:40PM
Sort Device:	Tubes 5.0mL	Nozzle Size:	100 micron	End Date Time:	08/03/2018 05:46PM
Total Events:	840,305	Pressure:	22.83 PSI		
Processed Events:	100.0%	Drop Frequency:	34.0 kHz		

SORT STATISTICS

Tube	Population	Target Count	Sort Count	Sort Rate	Efficiency	Time
1	P1	1,296,000	117,094	648	72%	3m 0s
2	P2	1,296,000	289,362	1602	81%	3m 0s

CYTOMETER SETTINGS

Fluorochrome	PMT Voltages
FSC	95
SSC	447
FITC	409
PE	525
PerCP-Cy5.5	662
APC	615
APC-Cy7	509

Compensation: Spillover Values

Into (Detectors)	From (Fluorochromes)				
	FITC	PE	PerCP-Cy5.5	APC	APC-Cy7
FITC	100.00	0.14	0.00	0.00	0.01
PE	106.05	100.00	0.00	0.01	0.05
PerCP-Cy5.5	42.64	52.10	100.00	5.20	0.35
APC	0.03	0.02	0.20	100.00	3.84
APC-Cy7	0.01	0.01	1.46	15.48	100.00

Threshold: FSC @ 10000

POPULATION HIERARCHY

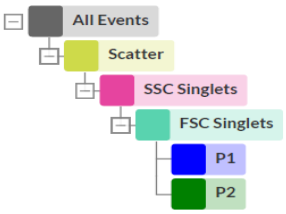

Figure 16: Jurkat cell sorting report for mCherry based sorting experiment (BDmelody).

Later, fluorescent images were taken of cultured positive and negative cell fractions to show sorting efficacy of transduced Jurkat cells.

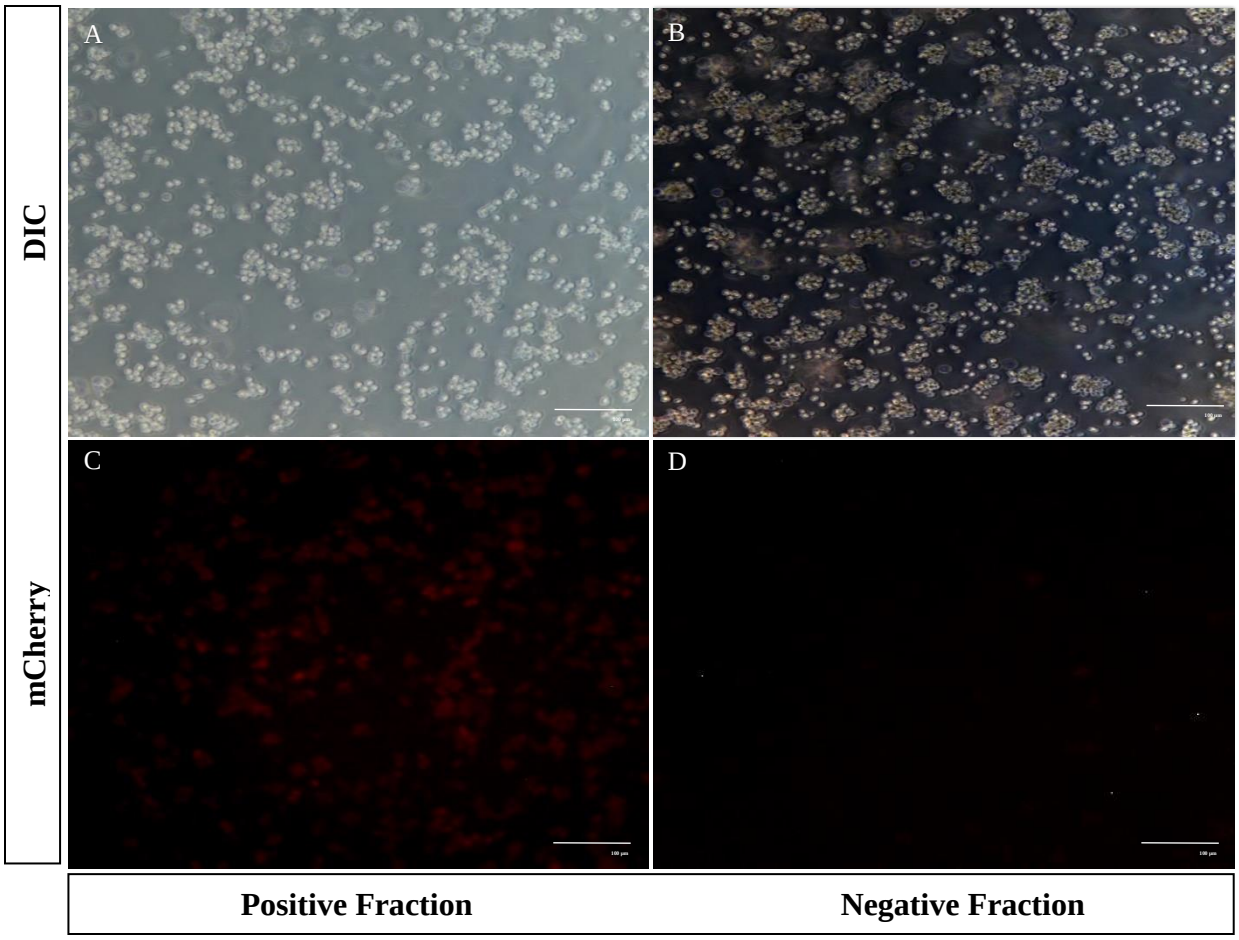

Figure 17: Sorted fractions of transduced Jurkat cells in further culture.

As shown in **Figure 16**, sorted positive fraction shows mCherry expression compared to the negative sorted group. The next step was to check whether transduced Jurkat cells were these plasmid ORFs stable in a long-term. For this, transduced, sorted cells were cultured at least two weeks to confirm their expression stability. Their stable gene expressions were confirmed via fluorescent microscopy and flow cytometry. After this confirmation, cells were further sorted and characterized by their her-2 expressions and further cultured for their membrane isolation.

3.9) Long term stable mCherry ORF expression after sorting

Cells after two weeks of subculture were imaged under the fluorescent microscopy, and their mCherry expression was also confirmed via flow cytometry.

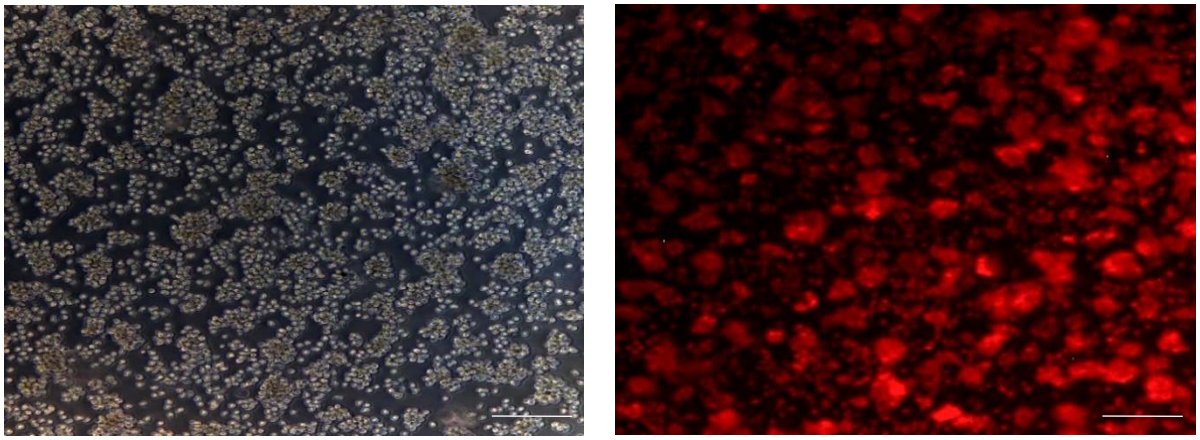

Figure 18: Fluorescent microscopic and flow cytometric confirmation of stable mCherry expression on Jurkat cells.

As shown in **Figure 17**, mCherry transduced Jurkat cells were able to express transduced genes over two weeks. In fluorescent microscopy, almost all the cells were showing mCherry expression (red). In flow cytometry result, cells again showed a distinctive shift compared to the non-transduced Jurkat cell group and having more than 87% mCherry positive cell population.

3.10) Transduced Jurkat sorting (her-2 expression based)

CYTOMETER INFO

User Name:	Core User	Application Name:	BD FACSChorus	Cytometer Serial Number:	P6617590005
Experiment Name:	Serkan-Jurkat 4D5 Sorting	Application Version:	1.1.15.0	Cytometer Name:	BD FACSMelody

SORT DETAILS

Sort Mode:	Purity	Sort Status:	Stopped by System	Start Date Time:	09/11/2018 05:49PM
Sort Device:	Tubes 5.0mL	Nozzle Size:	100 micron	End Date Time:	09/11/2018 05:58PM
Total Events:	839,917	Pressure:	22.76 PSI		
Processed Events:	100.0%	Drop Frequency:	34.0 kHz		

SORT STATISTICS

Tube	Population	Target Count	Sort Count	Sort Rate	Efficiency	Time
1	P2	1,296,000	123,437	236	93%	8m 41s
2	P1	1,296,000	504,193	966	97%	8m 41s

CYTOMETER SETTINGS

Fluorochrome	PMT Voltages
FSC	116
SSC	469
APC	811

Compensation: Spillover Values

Into (Detectors)	From (Fluorochromes)
	APC
APC	100.00

Threshold: FSC @ 10000

POPULATION HIERARCHY

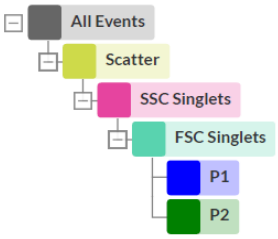

Figure 19: Jurkat cell sorting report for anti her-2 based sorting experiment (BD melody).

In the second set of cells sorting experiments, anti her-2 expressing cells were sorted by using Alexa fluor 647 anti-myc tag antibodies. As shown in **Figure 19**, more than half a million Jurkat cells were again sorted by using APC channel with around 93-97% efficiency.

3.11) Long term stable mCherry & her-2 ORF expression after sorting

Stable anti her-2 CAR expression in the cultured cells after 2 weeks of expansion was confirmed via flow cytometry. As seen in **Figure 20**, mCherry and anti her-2 CAR transduced Jurkat cells were able to express transduced genes that were stable after two weeks.

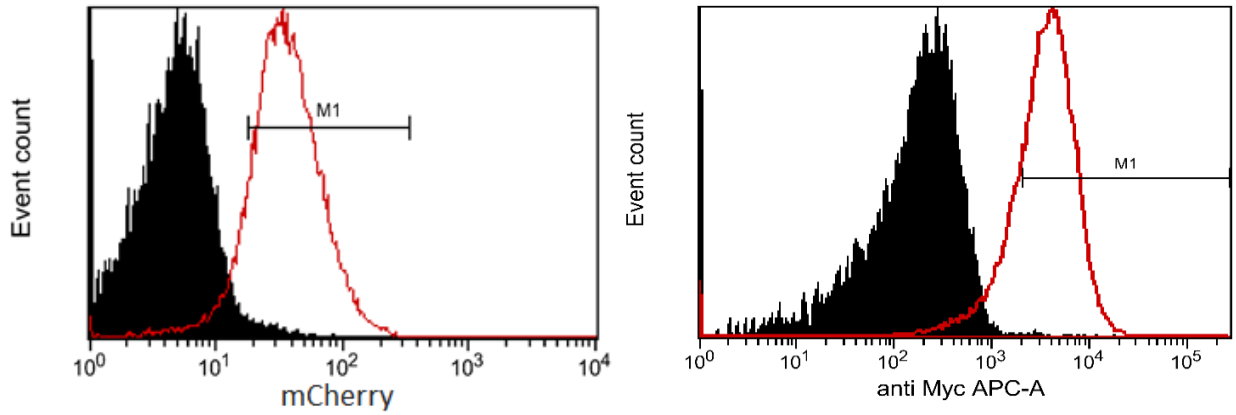

Figure 20: Based on the flow cytometry results, both mCherry and anti Her-2 CAR transduced cells showing a distinctive shift compared to the non-transduced Jurkat cell group and having more than 90% positive cell population.

3.12) Assessment of anti her-2 CAR receptor binding function of transduced Jurkat cells

The next question of anti her-2 CAR receptor and CAR-T-cell development for membrane isolation is whether anti-her2 ScFv's derived from anti her-2 SynNotch receptors are functional or not. To answer this question, the advantage of the reporter plasmid has been used. As earlier mentioned, the reporter plasmid used in the design has two distinct fluorophores which are constitutively active (mCherry); the other one is only activated if GAL64VP protein is translocated to the nucleus from the anti her-2-SynNotch receptor. GAL64VP is only releasing from the first plasmid when there is a binding to the anti her-2 receptor and thus activating the promoter for the BFP fluorophore.

Therefore, mCherry and anti her-2 sorted Jurkat cells were exposed either to SKOV-3 or HEK293T cells over the course of 24 hours. As shown in **Figure 21**, SKOV-3 exposed Jurkat cells were showing a remarkable tBFP expression compared to HEK293T cell exposure.

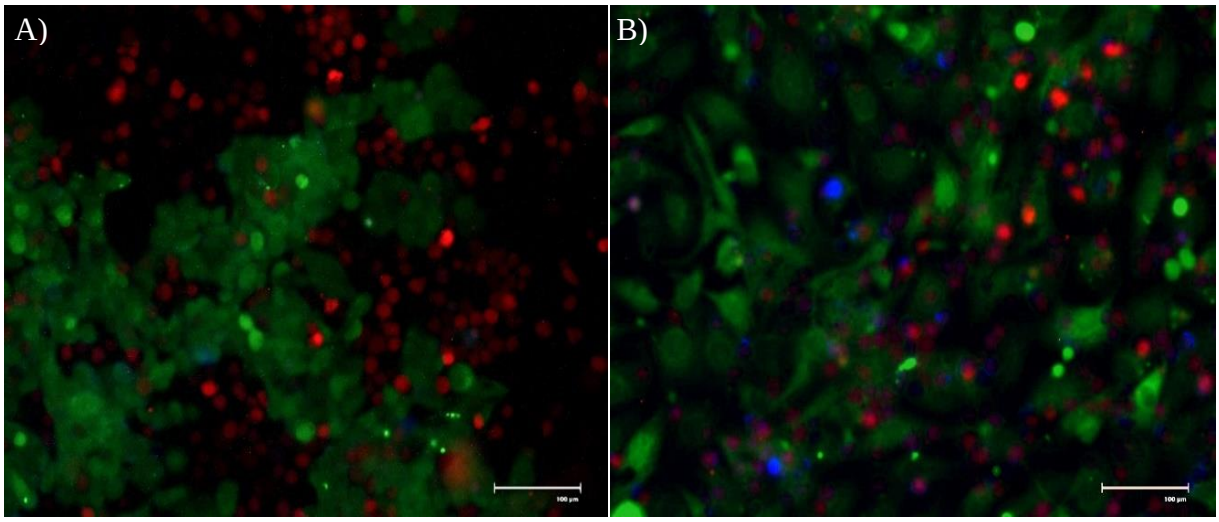

Figure 21: Both anti her-2 & mCherry transduced Jurkat cells (red and blue) co-cultured 24 hours with A)HEK293T (Her-2 negative) and B) SKOV-3(Her-2 positive) cell lines (green).

3.13) Physical characterization of CAR-T-MNPs

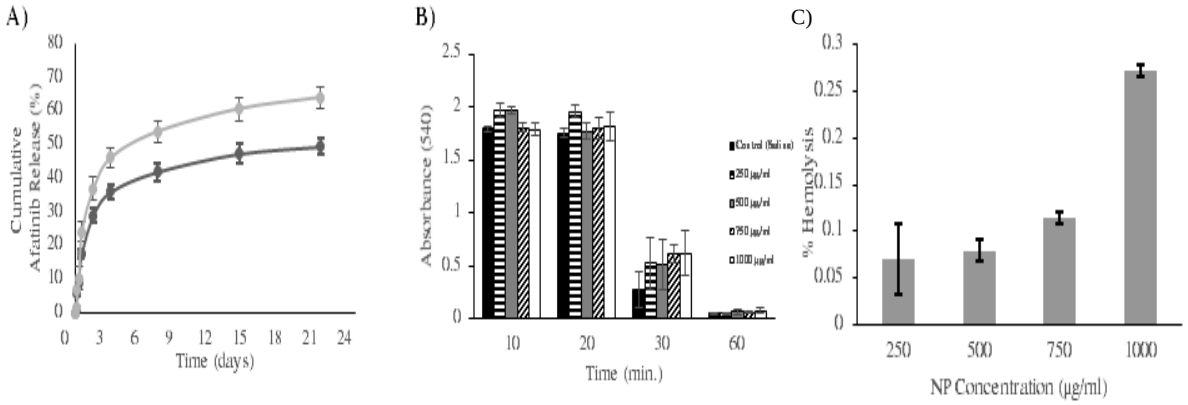

Figure 22: Physiological Characterization of CAR-T-MNPs. A) Drug release comparison of CAR-T-MNP vs bare PLGA NPs. B) Blood clotting trend of CART-MNPs compared to saline group. C) Hemolysis graph of CAR-T-MNPs.

CAR-T-MNPs were synthesized with a two-step process: 1- CAR-T membrane isolation from genetically engineered Jurkat cells and co-extrusion with afatinib loaded PLGA NPs. First, anti her-2 CAR-T-cell membranes were collected via hypotonic membrane extraction method. Second, afatinib loaded PLGA nanoparticles were synthesized via double emulsion method. Isolated anti her-2 CAR-T-MNPs were then reconstituted and co-extruded through a 400-nm polycarbonate

A)

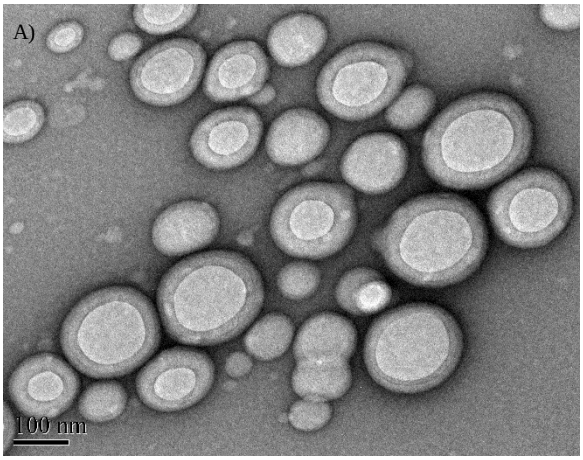

B)	Bare PLGA	CAR-T-MNPs	Anti her-2 PLGA NPs
Size Before Extrusion	130 nm	132 nm	283 nm
Size After Extrusion (conjugation)	330 nm	350 nm	310 nm
Polydispersity	0.156	0.234	0.227
Zeta Potential (mV)	-5.3 mV	-7.2 mV	-5.7 mV

Figure 23: Physical characterization of CAR-T-MNPs. A) TEM image of CAR-T-MNPs. B) size zeta potential and polydispersity chart of NP formulations.

membrane with afatinib loaded PLGA NPs to form CAR-T-MNPs. The extruded NPs were hemocompatible, and the blood clotting graph and *in vitro* drug release profile are also shown in **Figure 22**. TEM images of both bare PLGA NPs and CAR-T-MNPs revealed core shell or onion like structure on the CAR-T-MNP group while bare PLGA NPs were shown as spheres (**Fig 23**). The average diameter of the final afatinib loaded PLGA NPs was 350 nm (PDI =0.234). Zeta potential of both extruded and bare PLGA NPs found to be in between -7 to -5 mV (**Fig. 23**).

3.14) Detection of mAbs on the surface of nanoparticles

3.14.1) Indirect ELISA & Western Blot assays

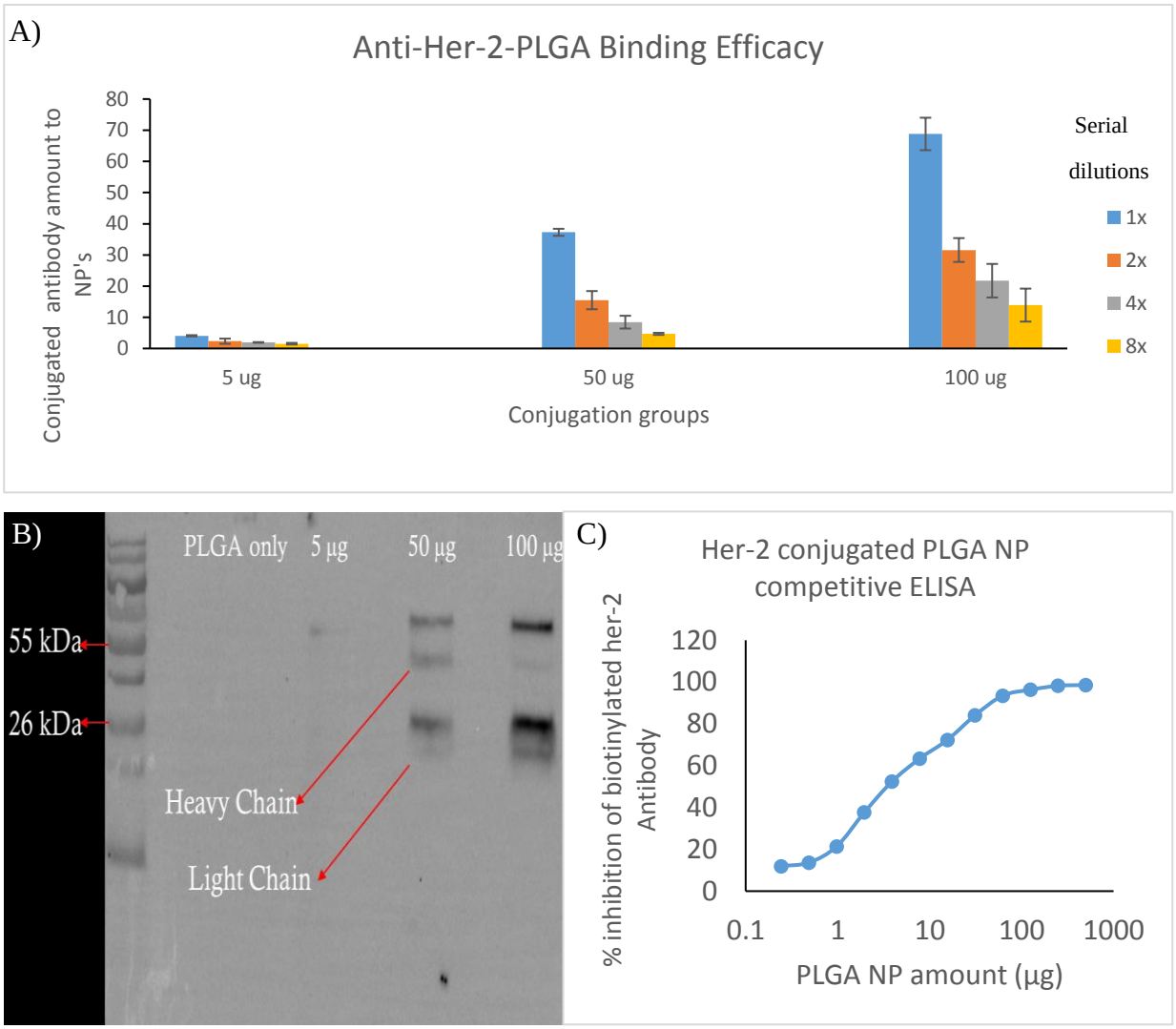

Figure 24: Characterization of anti her-2 PLGA NPs. A) Indirect ELISA. B) Western Blot measurements of anti Her-2 conjugated PLGA NPs**. C)** Her-2 protein binding results of the particles against biotinylated anti her-2 antibodies.

Indirect ELISA measurement of anti her-2 antibody conjugated PLGA NPs indicated the average efficiency of antibodies to PLGA nanoparticle conjugation was between 65-75%. We observed that when the antibody amount increased, the conjugation efficacy slightly decreased. The same groups were also subjected to Western Blot analysis (**Fig. 24**), and for that, conjugated particles were washed, run on SDS-PAGE and transferred to a nitrocellulose membrane.

Following, protein blotted membranes were incubated with HRP conjugated anti mouse IgG (H+L chain) antibodies (Jackson Laboratories). As shown in **Figure 23B**, 5 µg PLGA group is not given distinguishable band on the membrane. On the other hand, 50µg and 100µg antibody-conjugated NP groups produced highly distinguishable bands. As seen in the figure, there are 4 bands in each group. In general, it is expected that antibodies create 2 bands in the Western Blot (one just below 55kDa and another below 26kDa). However, in these results, we observed two additional bands just below the expected bands. It might be that the conjugation of the antibody to the nanoparticles changed the overall size of the unit, and the conjugated particles were dragged in the gel to run slower. This information also demonstrated the conjugation efficacy of the particles with antibodies.

To measure whether fabricated NPs are able to engage with her-2 protein, competitive ELISA assays were performed with anti her-2 conjugated PLGA NPs. As shown in **Figure 23C**, the higher concentration of PLGA NPs (500µg to 1000µg) almost outraces the biotinylated her-2 antibody to bind her-2. Below the 100µg threshold, biotinylated antibody was able to be detected in the wells via streptavidin-HRP binding reactions in respect to the PLGA concentration decrease. In addition, below 1 µg biotinylated anti her-2 antibody mainly outcompeted the PLGA NPs to engage coated her-2 proteins in the wells. Therefore, this competitive ELISE demonstrated the binding ability of anti her-2 conjugated PLGA NPs to her-2 protein *in vitro*. However, during the conjugation studies, we observed that the antibody amount used in the reaction was significantly affecting the nanoparticle size, whereas an excessive antibody caused NP aggregations during the reaction. Following DLS measurement of the antibody conjugated NPs, it was demonstrated that there were size discrepancies among the conjugation groups especially the 100µg antibody group. Therefore, for further studies, the 50µg group was chosen and studies continued with this group.

3.15) Jurkat CAR-T MNP membrane extruded PLGA NP coating efficacy optimization by flow cytometry and fluorescent imaging

After extrusion of PLGA NPs with isolated membranes, membrane coating efficacy was measured via spectral fluorescent microscopy and flow cytometry. Coumarin-6 loaded PLGA NPs were used for detecting PLGA NPs (FITC channel). After extrusion, membranes were stained with lipophillic DiD dye to detect coating efficacy (APC channel), and CAR-T-MNPs were quantified using the flow cytometry (**Fig. 25**).

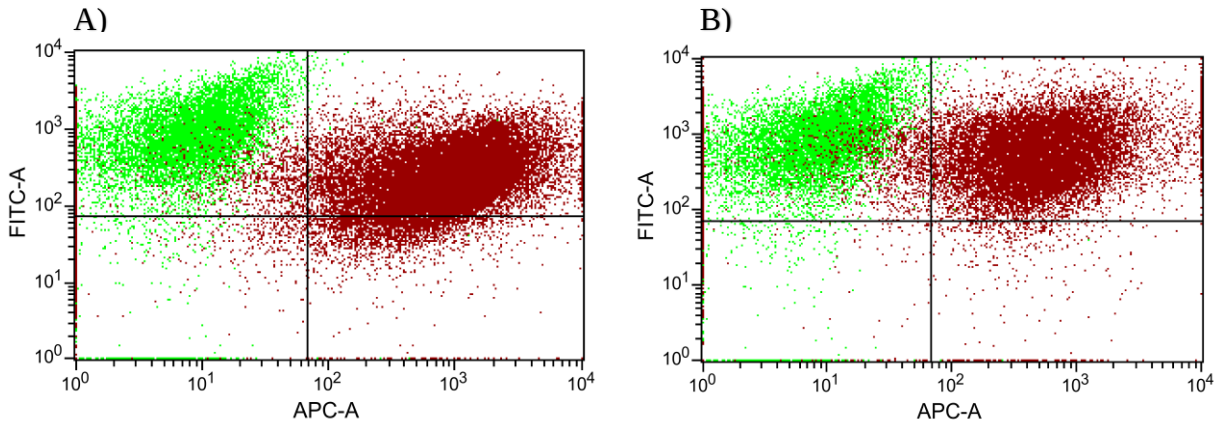

Figure 25: Coating efficacy of CAR-T-MNPs. Bare Coumarin-6 PLGA NPs (as green) used in non-transduced (A) and transduced (B) Jurkat CAR T-cell membrane coated Coumarin-6 PLGA NPs (as red).

A)

Total events: 50000
Gate: G0
x-Parameter: APC-A
y-Parameter: FITC-A

Label	Events	Percent gated	Percent total
all	12860	100.00	25.72
APC-A- FITC-A-	887	6.90	1.77
APC-A+ FITC-A-	6	0.05	0.01
APC-A- FITC-A+	11919	92.68	23.84
APC-A+ FITC-A+	48	0.37	0.10
Extruded Particle Population	12860	100.00	25.72
Plain Jurkat-PLGA C6-	11238	87.39	22.48
G0	12860	100.00	25.72

Total events: 50000
Gate: G0
x-Parameter: APC-A
y-Parameter: FITC-A

Label	Events	Percent gated	Percent total
all	12860	100.00	25.72
APC-A- FITC-A-	856	6.66	1.71
APC-A+ FITC-A-	6	0.05	0.01
APC-A- FITC-A+	11950	92.92	23.90
APC-A+ FITC-A+	48	0.37	0.10
Extruded Particle Population	12860	100.00	25.72
Plain Jurkat-PLGA C6-	11238	87.39	22.48
G0	12860	100.00	25.72

Total events: 50000
Gate: G0
x-Parameter: APC-A
y-Parameter: FITC-A

Label	Events	Percent gated	Percent total
all	33152	100.00	66.30
APC-A- FITC-A-	894	2.70	1.79
APC-A+ FITC-A-	2760	8.33	5.52
APC-A- FITC-A+	3726	11.24	7.45
APC-A+ FITC-A+	25772	77.74	51.54
Extruded Particle Population	33152	100.00	66.30
Plain Jurkat-PLGA C6-	31976	96.45	63.95
G0	33152	100.00	66.30

Total events: 50000
Gate: G0
x-Parameter: APC-A
y-Parameter: FITC-A

Label	Events	Percent gated	Percent total
all	22369	100.00	44.74
APC-A- FITC-A-	364	1.63	0.73
APC-A+ FITC-A-	471	2.11	0.94
APC-A- FITC-A+	5375	24.03	10.75
APC-A+ FITC-A+	16159	72.24	32.32
Extruded Particle Population	22369	100.00	44.74
Plain Jurkat-PLGA C6-	18972	84.81	37.94
G0	22369	100.00	44.74

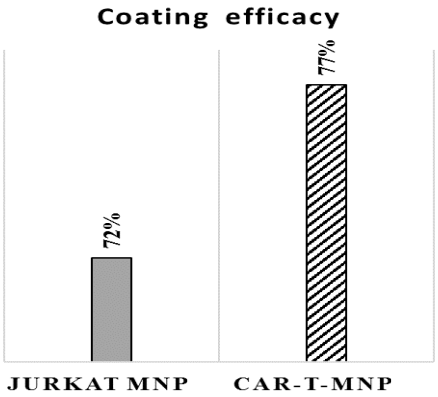

Figure 26: Flow cytometric coating efficacy statistics of CAR-T-MNPs.

Based on flow cytometry statistic data, coating efficacy of Coumarin-6 PLGA NPs with cell membranes was between 72-77% on both transduced and non-transduced CAR-T-cell membrane extruded groups. For additional confirmation, coating efficacy of CAR-T-cell membranes with PLGA NPs was assessed via spectral fluorescent microscopy (**Fig. 25**). As shown in **Figure 27,** CAR-T-MNPs loaded with Coumarin-6 and stained with DiD were able to be imaged under FITC

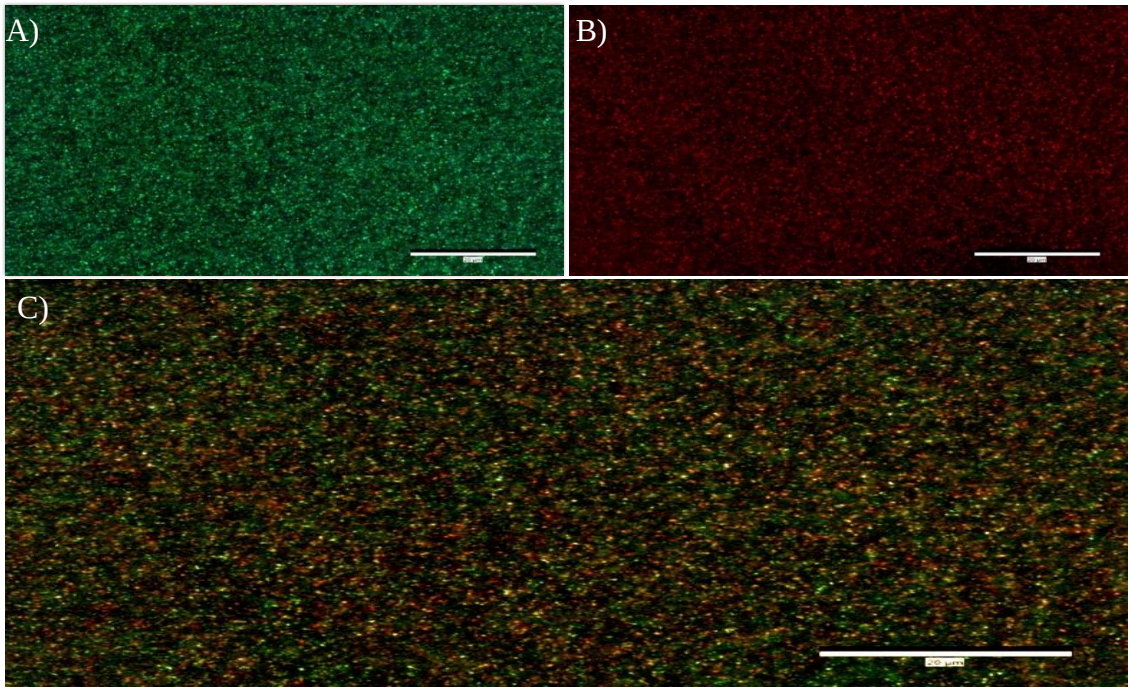

Figure 27: Coumarin-6 PLGA NPs extruded with CAR-T-MNPs and stained with lipophilic DiD dye. A) PLGA NPs (FITC channel) B) Stained exterior membranes (Red channel) C) merged image (TRITC- channel).

and red channels. In addition, in the merged channel we obtained yellow looking NP's which confirms the coating of the NPs with membranes.

3.16) Anti her-2 TCR existence confirmation on extruded NPs

For the confirmation of anti her-2 CAR receptor of extruded NPs, CAR-T-MNPs were checked on flow cytometry in terms of anti her-2 CAR existence on their surfaces. Based on the flow

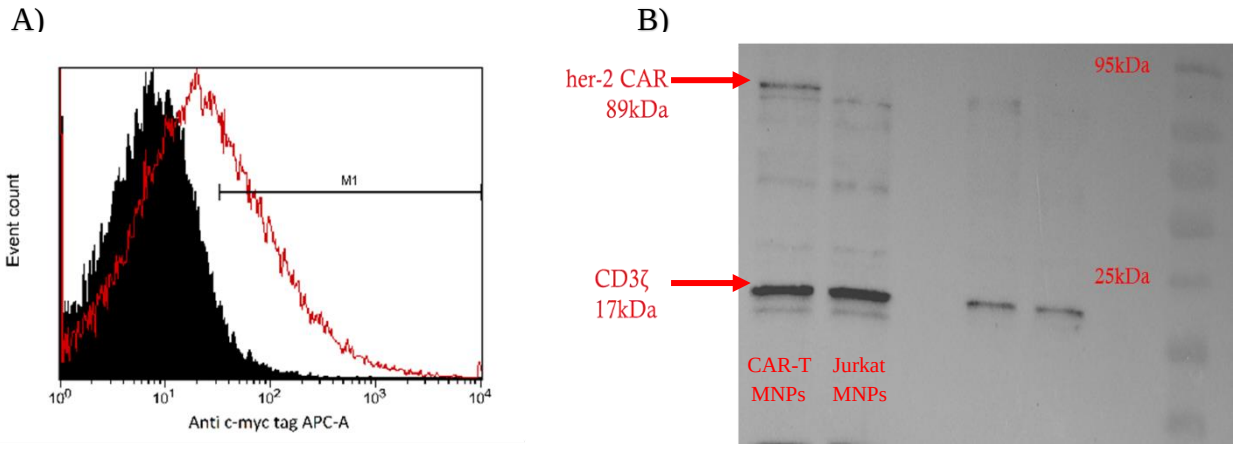

Figure 28: Anti her-2 existence confirmation on isolated and extruded CAR-T-MNPs.

cytometry results (**Fig. 28A**), CAR-T membrane coated PLGA NPs showed a distinctive shift compared to that of the non-transduced T-cell membrane NP group and consisted of 55%-60% anti her-2 positive NP population. In addition, **in Figure 28B,** Western Blot analysis of isolated CAR-T membranes also showed bands respective to both CD3 and anti her-2 CAR molecules. Thus, engineered anti her-2 CAR molecule existence on isolated Jurkat membranes has been shown **(Fig. 28B)**.

3.17) *In vitro* uptake studies of CAR-T-MNPs

Coumarin-6 loaded PLGA NPs either conjugated with anti her-2 antibodies coated with CAR-T-MNPs or Jurkat-T-MNPs. NPs were incubated 30 minutes with A549 lung cancer cells. Microscopy images of cells after incubation (**Fig. 30**) indicate that both anti her-2 CAR-T-MNPs

and anti her-2 PLGA NPs were uptaken more by the A549 lung cancer cells compared to that of the Jurkat-T-MNPs group.

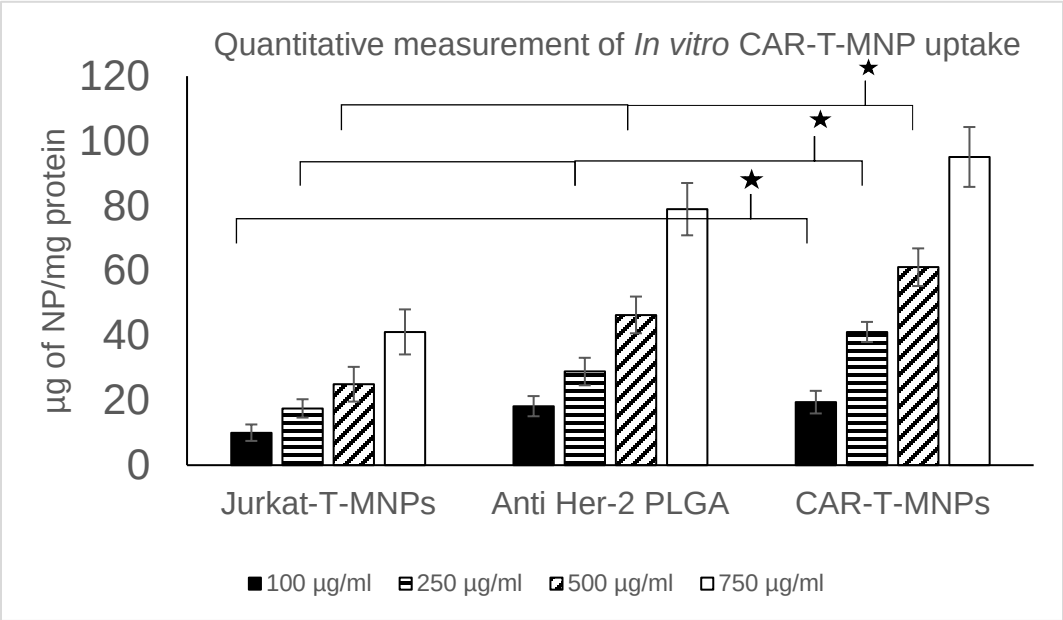

Figure 29: Spectrophotometric analysis of different NP group's uptake trend (★*p<0.05).*

Spectrophotometric analysis of lysis cell samples in cell uptake studies revealed that anti her-2 PLGA NPs and CAR-T-MNPs had been uptaken more by cancer cells for all concentrations compared to that of Jurkat-T-MNPs as shown in **Figure 29**. When anti her-2 PLGA NPs and CAR-T-MNPs were compared with each other, CAR-T-MNPs showed significantly more uptake in 250

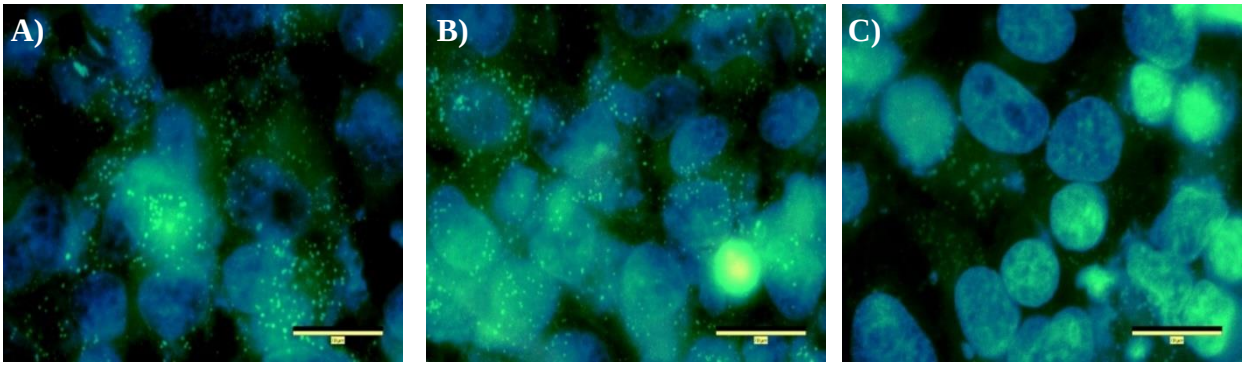

Figure 30: Fluorescent uptake images of CAR-T-MNPs by A549. A) Anti Her-2 CAR-T-MNPs. B) Anti Her-2 PLGA NPs. C) Jurkat- T-MNPs.

µg/ml and 500 µg/ml concentrations. As a result, spectrophotometric analysis of uptake (**Fig. 29**) confirmed the microscopic uptake analysis data.

3.18) *In vitro* tumor cell killing studies of CAR-T-MNPs

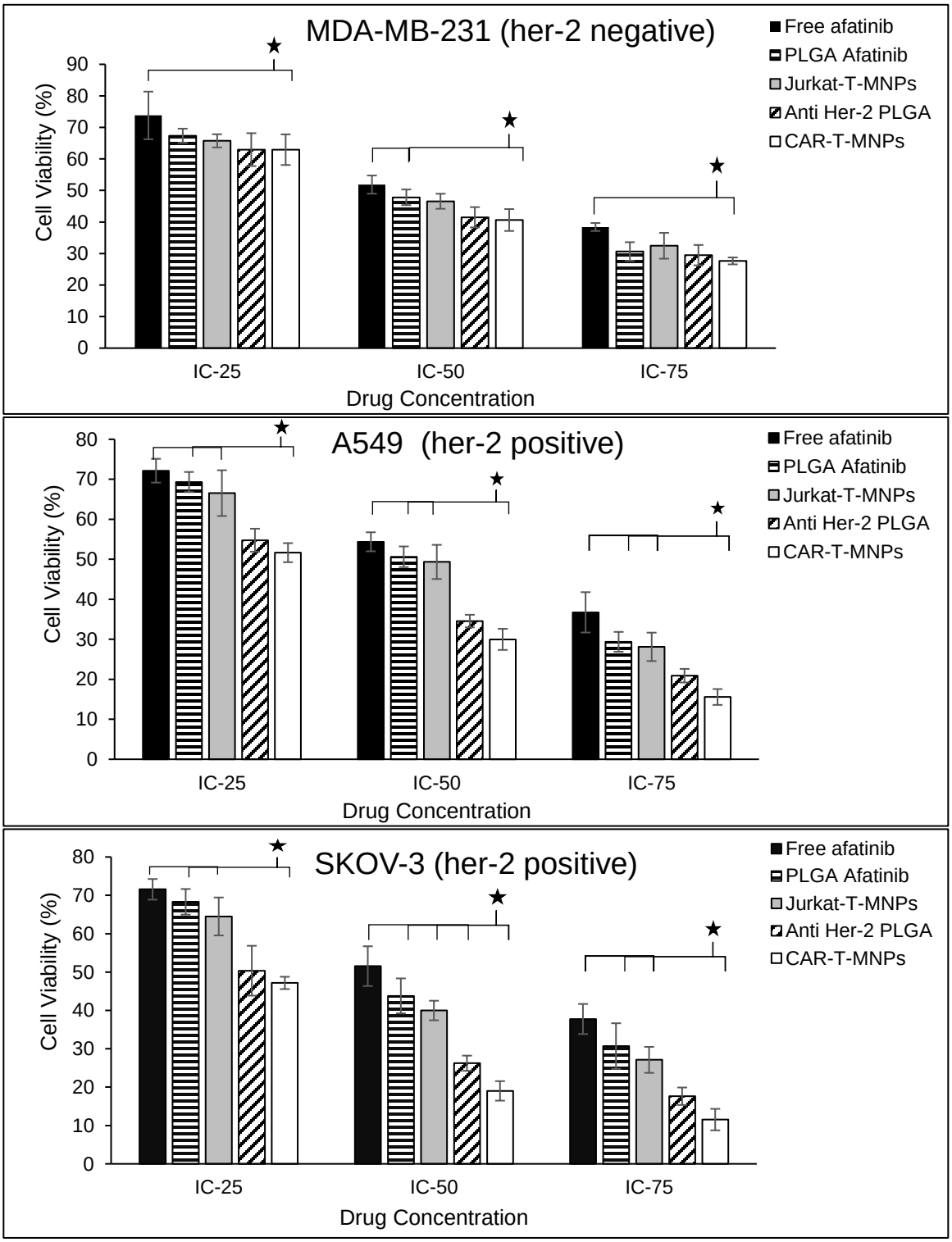

Figure 31: *In vitro* tumor cell killing properties of CAR-T-MNPs. A) MDA-MB-231; B) A549 and C) SKOV-3 cells exposed to free afatinib, PLGA NPs, Jurkat-T-MNPs, anti her-2 PLGA NPs and CAR-T-MNPs for 48 hours. Cell viability was quantified via MTT assays after the exposure (n=4, ★$p<0.05$).

The IC50 (half maximal inhibitory concentration) values of afatinib for A549, SKOV-3 and MDA-MB-231 cells were 4.3, 1.4, and 3.7 μM, respectively. MTT readings were taken of cells exposed to free drug or drug-loaded NPs at the 48 hour time point. Free afatinib, afatinib PLGA NPs and afatinib-loaded CAR-T-MNPs exhibited dose-dependent cytotoxicity in A549, SKOV-3 and MDA-MB231 cells (**Fig. 31**). Viability reduction of CAR-T-MNPs on SKOV-3 and A549 cells was significantly different when compared between the groups.

3.19) *In vitro* live-dead assays

A549 cells were seeded (5×10^3 cells/well) in 96-well plates and incubated overnight. As shown in **Figure 32**, free afatinib and afatinib-loaded PLGA NPs induced relatively low cell death compared to anti her-2 PLGA NPs and CAR-T-MNPs. When membrane and antibody groups were compared with each other, Jurkat-T-MNPs and anti her-2-PLGA NPs loaded with afaninib showed similar

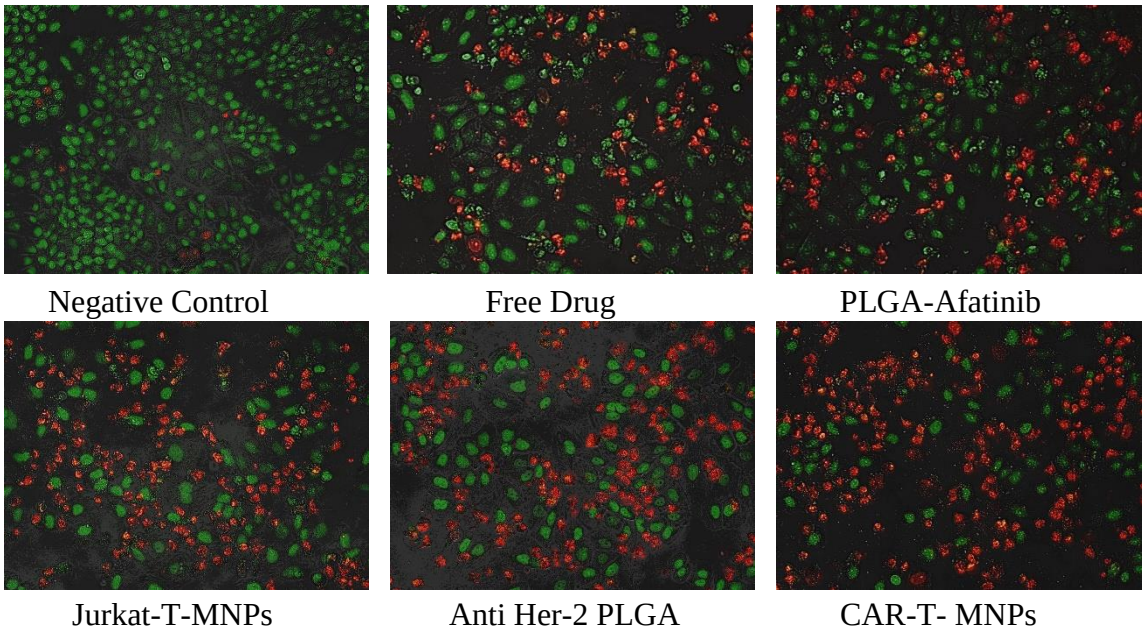

Figure 32: Fluorescent live/dead assay images of all treatment groups.

cell killing trends but were still lower than that of the CAR-T-MNP group. When image analysis was conducted via image J software on all groups (n=4 for each group), the CAR-T-MNP group

showing statistically higher dead/live ratio in exposed cells compared to other groups (**Fig. 33**). These results indicate that CAR-T-MNPs have superior cell killing ability compared to the bare membrane coated or antibody conjugated nanoparticle groups. This low effect of antibody conjugated nanoparticle group might be due to the wrong orientation via NHS conjugation method on the PLGA NPs, which might alter the interaction of anti her-2 antibody molecules to the targets and inhibit their binding activity on the cells.

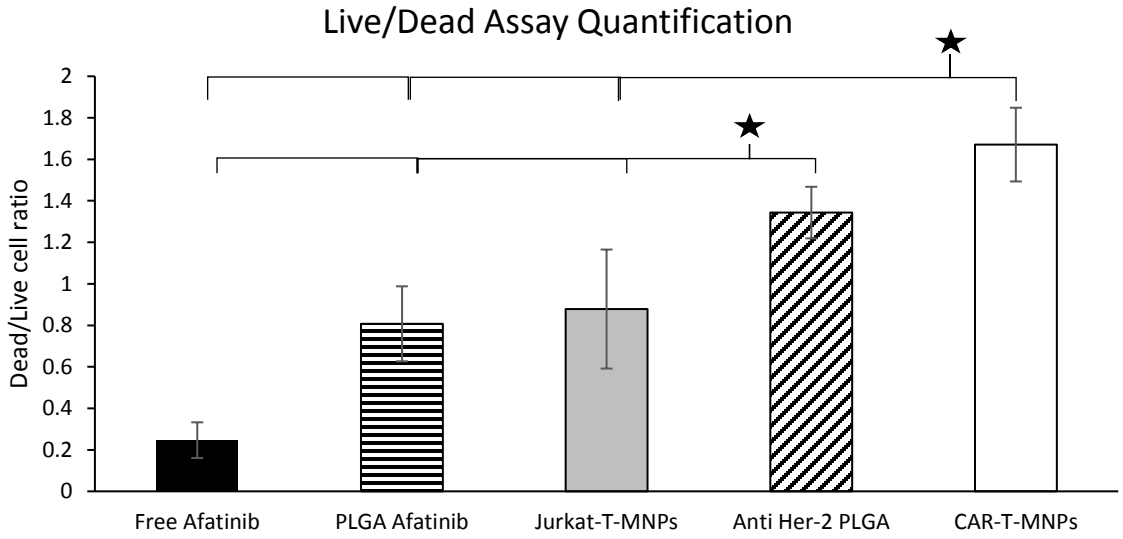

Figure 33: Live/dead assay image analyis quantification of all treatment groups *(★$p<0.05$).*

3.20) *In vivo* near-infrared fluorescence imaging

PLGA NPs were loaded with ICG dyes and then conjugated with anti her-2 antibody or coated with either anti her-2 CAR-T-cell or Jurkat cell membranes. *In vivo* biodistribution studies were used to examine whether intravenously injected CAR-T-MNPs in subcutaneous tumors shrunk

over the time. To ascertain whether the CAR-T-MNPs could efficiently accumulate at tumor sites, their biodistribution in a xenograft mouse model was assessed (**Figs. 34-37**).

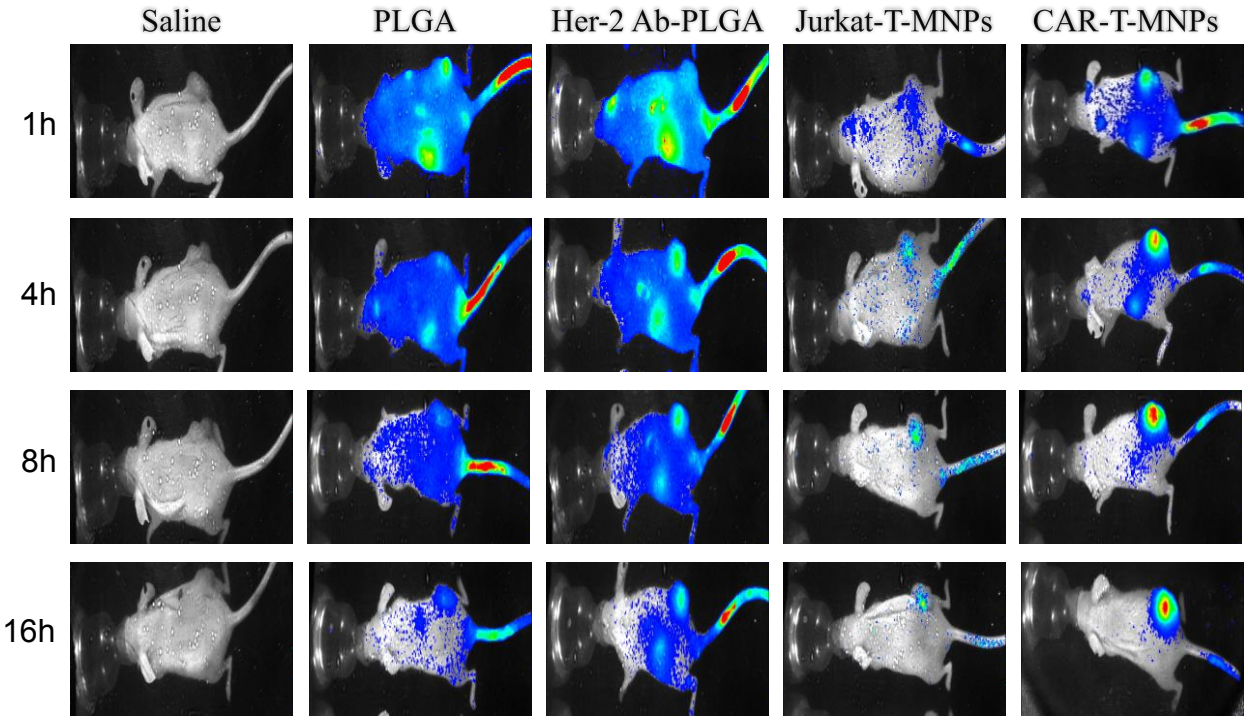

Figure 1: *In vivo* biodistribution of PLGA NP, Anti Her-2 PLGA, Jurkat-T-MNPs and CAR-T-MNPs

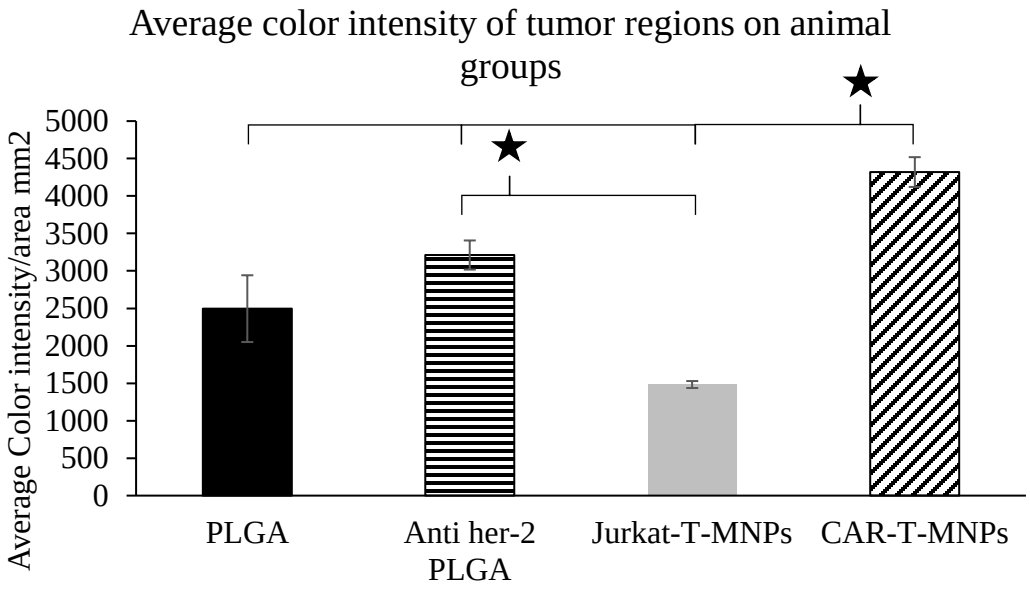

Figure 2: Color intensity measurement of tumor regions on animals.

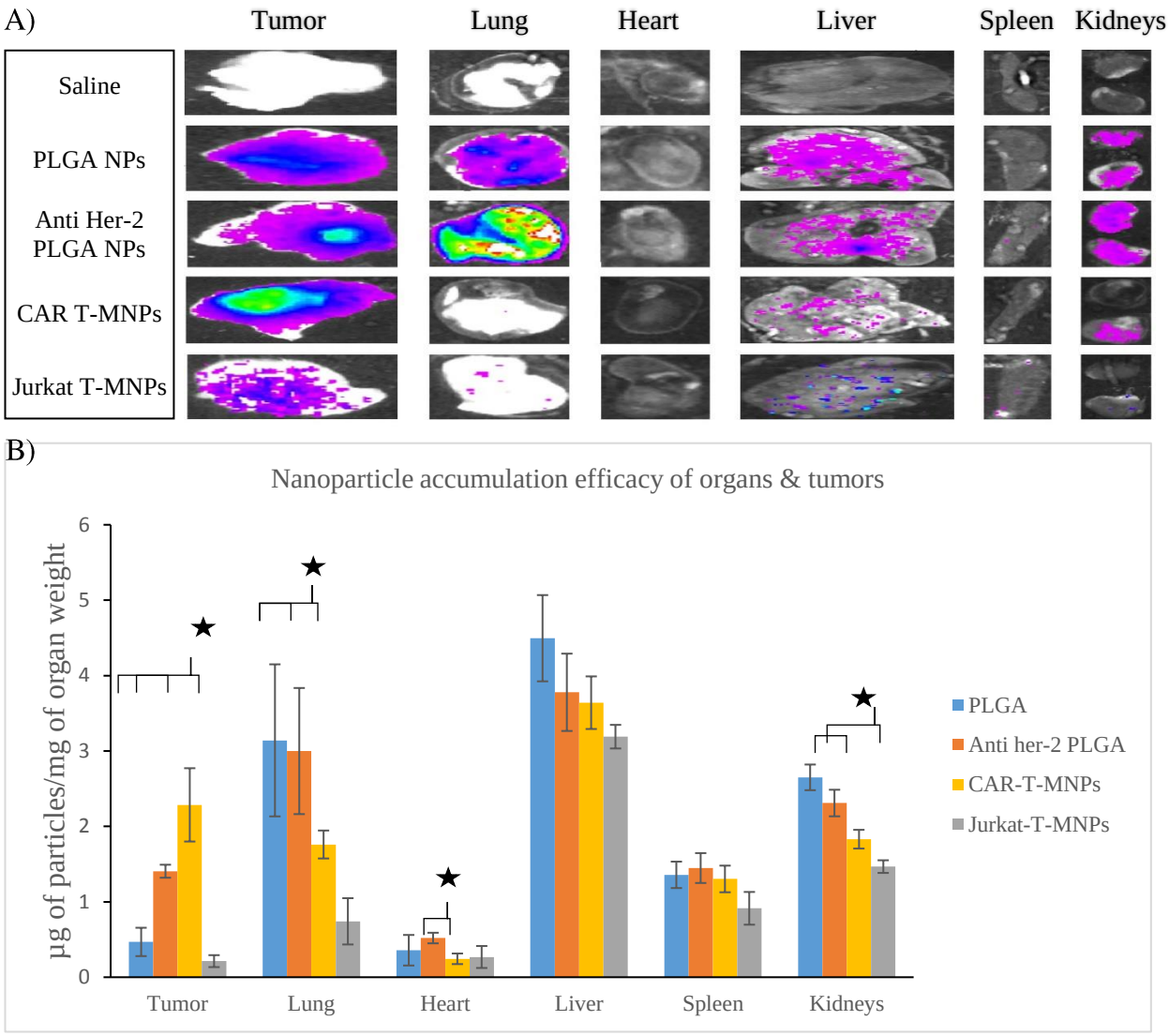

Figure 36: CAR-T-MNPs localized more in tumors compared to other groups *in vivo* studies. **A)** Representative *ex vivo* organ images of all biodistribution study groups. **B)** Accumulation efficiency of fabricated nanoparticle systems in individual organs and tumors.*(★p<0.05)*

At the end time point, all mice were sacrificed, and tumors and major organs were carefully collected and weighted. The fluorescence signals of tumors and each organ were recoded using the Kodak FX/Pro imaging system. All the particles were accumulated mainly liver and spleen in 1 hour. However, PLGA NPs gradually cleared from systemic circulation and from all organs including tumors. On the other hand, anti her-2-PLGA and CAR-T-MNP groups showed gradual increases of fluorescence in tumors over the course of study and slightly started to be cleared from the system after 8 hour (**Fig. 34**). Intensities of the implanted tumors also shows similar trend

to *in vivo* images **(Fig. 35)**. As shown in the *ex vivo* organ and tumor images, all groups have shown kidney and liver accumulation (**Fig. 36A**). Spectrophotometric analysis of whole organs showed a similar trend of both *in vivo* and *ex vivo* measurements (**Fig. 36B**). In the liver and spleen, despite a trend of low accumulation of membrane coated groups, the amount of particle per mg of organ remained relatively similar in all groups. In the kidney and heart, membrane coated NPs showed lower accumulation compared to the anti her-2 PLGA NP group. Lastly, when tumor accumulation is compared, CAR-T-MNPs have significantly higher accumulation in the tumor tissues compared to that of the anti her-2 PLGA NP group.

3.21) Discussion of results

In this research, we have successfully created the anti her-2 CAR expressing Jurkat cell line via lentiviral transduction. In transduction studies, Lenti-X cell line is used to produce lentiviral particles carrying anti her-2 CAR gene. Lentivirus titer measured using anti-p24 ELISA kit and found lenti-X cells were able to produce 10^8 lentiviral titer (TU). Based on lentiviral transduction results and optimization studies (**Fig. 11**), 10 multiplicity of infection (MOI) was chosen to transduce 10^5 Jurkat cells. After transduction, we observed red fluorescent cells in the culture after 48 hours (**Fig. 13**). Flow cytometric analyses showed that cells were able to achieve stable expression of both mCherry and anti her-2 CAR receptors over 90% (**Figs. 17-20**).

In the scope of the proposal, anti her-2 CAR-T-cells were fabricated and characterized, and then anti her-2 CAR-T-cell membrane isolation and extrusion with PLGA NPs to formulate CAR-T-MNPs were performed. The zeta potential of the CAR-T-MNPs was approximately -7.2 mV. The size of the CAR-T-MNPs was monitored using dynamic light scattering and was found to be 330 nm, with approximately a 20-nm increase compared to the Bare PLGA NPs (130 nm) (**Fig. 23C**). In addition, in the literature researchers found membrane coated PLGA nanoparticles were

stable up to 15 days [78]. The loading efficiency of the CAR-T-MNPs was observed to be approximately 48% and the drug release kinetics displayed an initial burst release followed by a sustained release up to 21 days of incubation at 37 ℃ in PBS (pH 7.2). The rate of release kinetics differed across bare PLGA and the CAR-T-MNPs (**Fig. 22A**). This result might be due to the diffusion barrier effect of the membrane layer. Additional coating of cell membranes on the PLGA NPs might either have slowed down the degradation process of the PLGA NPs or drug diffusion to the surrounding. CAR-T-MNPs were tested for blood clotting and hemolytic properties. CAR-T-MNPs-induced blood hemolysis was observed to be < 1% up to 1000 ug/mL (**Fig. 22C**). Effects of CAR-T-MNPs on blood clotting characteristics were also tested and found no significant effect on the blood clotting cascade up to 1000 ug/mL when compared to the saline control (**Fig. 22B**). In addition, TEM images revealed that membrane coated NPs had shown as core shell or onion like structures, which confirms the membrane coating on the surface of PLGA NPs (**Fig. 23A, 23B**). To identify the specific anti her-2 CAR receptor in the CAR-T-MNPs formulations, the particles were stained with anti c-myc tag antibody to detect ScFv on the particle surface. The samples were analyzed using a flow cytometer without SSC threshold. Compared to the unstained control, stained T-MNP samples displayed a significant mean fluorescence intensity shift (~%70) (**Fig. 27**). Therefore, CAR-T-MNP formulation processes were optimized to obtain engineered cell membrane coated nanoparticles, and CAR-T-MNPs were characterized in terms of coating efficacy, ligand existence on the surface, drug loading/release and hemocompatibility.

In addition, anti her-2 antibody purification, optimization and conjugation to PLGA NPs had been conducted as a comparison group for our experiments. Indirect ELISA results of anti her-2 PLGA NP conjugation revealed that we have achieved ~%70 conjugation efficacy (**Fig. 24A**). On the other hand, Western Blot analysis showed two distinctive bands respective to heavy and

light chain of the antibodies (**Fig. 24B**). Interestingly, we have noticed two consecutive bands of both chains of antibodies. We estimate that those bands belong to PLGA NPs conjugated antibody chains which they dragged behind the free chains during the SDS-PAGE electrophoresis. Competitive ELISA confirmed that conjugated antibodies were able to compete with free anti her-2 antibodies and bind to its target (her-2 protein) between the concentrations of 1-100 µg/ml (**Fig. 24C**).

A549 cell lines were utilized to examine the CAR-T-MNPs uptake effect in comparison with anti her-2 PLGA NPs and Jurkat-T-MNPs (**Figs. 29-30**). All nanoparticles were tested at different concentrations (100 ug/mL-750 ug/mL). The uptake of CAR-T-MNPs was significantly higher than the Jurkat-T-MNPs (**Fig. 29**) in all concentrations. The cellular uptake of the CAR-T-MNPs was increased with increasing concentration. In addition, uptake of CAR-T-MNPs was significantly higher than anti her-2 PLGA NPs in moderate concentrations (250 ug/mL and 500 ug/mL). This might be due to the static uptake conditions and saturation of the cell samples with targeting molecules. Due to the enhanced uptake of CAR-T-MNPs, it was proposed that the CAR-T-MNPs could present functional anti her-2 molecules on their surface that are contributing to the NP uptake significantly.

The cancer cell killing properties of these CAR-T-MNPs were investigated; we found them to be effective against A549, SKOV and MDA-MB-231 cell lines *in vitro*. Before the cancer cell killing studies, flow cytometry studies verified the presence of her-2 antigen on the A549 cancer cells. *Bunn et al.* previously described her-2 expression levels of various N-SCLC cell lines via different methods and found A549 cell line is moderate to high expression of her-2 protein even if it does not contain gene amplification [155]. Furthermore, the group also provided evidence of anti

her-2 antibody binding and the synergistic effect of trastuzumab and different chemotherapeutic drugs on the A549 cell line. Similar to the above-mentioned literature, A549 cells stained with purified anti her-2 antibodies showed a moderate to high shift (~%75 to %90) in the flow cytometry histogram. In addition, her-2 overexpressing SKOV-3 and her-2 negative MDA-MB-231 cell line were also checked for their expression levels and it was been found that SKOV-3 cells showed a distinctive shift, whereas MDA-MB-231 did not show a significant shift in the flow cytometric histogram in terms of her-2 binding (PE channel) (**Appendix 1**).

In the literature, inhibitor concentration at 50% cell viability (IC-50) for afatinib against different cell lines has been described. To verify the IC50, a pharmacokinetics study on afatinib was carried out by exposing the SKOV-3, A549 and MDA-MB-231 cell lines to varying afatinib concentrations over a 48 hour period. IC50 values of afatinib for SKOV-3, A549 and MDA-MB-231 were found to be approximately 1.4 µM, 4.3 µM, and 3.7 µM, respectively (**Appendix 2**). Following, to test the therapeutic efficiency of CAR-T-MNPs on SKOV-3, A549 and MDA-MB-231 cell lines, the cells were incubated with afatinib-loaded PLGA-NPs, Jurkat-T-MNPs, anti her-2 PLGA, CAR-T-MNPs and free afatinib for 48 hours at IC25, IC50 and IC75 drug concentrations (**Fig. 31**).

For cancer cell killing studies, Jurkat-T-MNPs served as membrane-coated negative controls. PLGA NPs served as a non-membrane coated negative control. A free drug group was also included to control against nanoparticle delivery systems. Both anti her-2 PLGA and CAR-T-MNPs were found to be significantly more efficient than any of the negative control groups, including the free afatinib at all concentrations on high her-2 expressing cell lines (SKOV-3 and A549) (**Figs. 31B-C**). On the other hand, on low her-2 expressing cell line MDA-MB 231, anti

her-2 PLGA and CAR-T-MNPs showed significant efficiency only in higher concentrations (IC50 and IC75) compared to free afatinib only (**Fig. 31A**). This effect might be the result of a low available number of her-2 protein on the surface of the cells, leading to lower uptake and killing efficacy compared to higher her-2 expressing cell lines. When CAR-T-MNPs compared to anti her-2 PLGA NPs, membrane coated NPs showed significant higher killing efficacy on SKOV-3 and A549 cell lines at higher concentrations (IC50 & IC75) (**Figs. 31B-C**). It is estimated that the non-significant results on lower concentrations might be due to the relatively low NP uptake number. Additionally, significantly higher killing efficacy of CAR-T-MNPs might have resulted from a higher number of uptake due to either a higher number of copies on the surface of CAR-T-MNPs, or the correct orientation (ScFv towards to the target molecule) of the anti her-2 molecules on the NP surface, or other surface protein interactions might serve as synergistic enhanced binding to target cells. As a second confirmation of the cell killing efficacy of CAR-T-MNPs, live/dead fluorescent cell killing assays were performed and revealed parallel results with MTT assays (**Figs. 32-33**). Based on the live/dead cell killing assay, both anti her-2 PLGA NPs and CAR-T-MNPs showed significant dead/live cell ratios (~1.3 and 1.6, respectively) compared to negative controls (**Fig. 33**).

The biodistribution study examined whether intravenously injected CAR-T-MNPs targeted subcutaneous tumors in the tumor implanted mice. A549 cells were injected into NGC mice at 2 $\times 10^6$ cells/mouse via subcutaneously to develop a lung cancer model. All the particles were accumulated mainly in the liver and spleen in 1 hour. However, PLGA NPs gradually cleared from systemic circulation and from all organs including tumors. On the other hand, anti her-2-PLGA and CAR-T-MNP groups showed gradual increases of fluorescence in tumors over the course of study and slightly started to be cleared from the system after 8 hours (**Fig. 34**). Additionally, CAR-

T-MNPs showed significantly higher accumulation on the tumor regions compared to anti her-2 PLGA NPs (**Fig. 35**). At the end time point, all animals were autopsied and *ex vivo* organ images taken to be analyzed. First, the imaging system was not able to pick fluorescent data from the spleen and heart. This might be due to a relatively small concentration or the clearance of the drug in these organs at that time point. Significant accumulation of the nanoparticles in lung tissues of both PLGA and anti her-2 PLGA NP groups have also been observed. On the other hand, CAR-T-MNPs and anti her-2 PLGA NP groups showed relatively higher accumulation of NPs in the tumor tissues (**Fig. 36A**).

Spectrophotometric analysis of homogenized organs showed a similar trend of both *in vivo* and *ex vivo* imaging measurements (**Fig. 36B**). In the liver and spleen, despite a trend of low accumulation of membrane coated groups, the amount of particle per mg of organ remained relatively similar in all groups. In the kidney, heart and lungs, membrane coated NPs showed lower accumulation compared to the anti her-2 PLGA NP group. Lastly, when tumor accumulation is compared, CAR-T-MNPs had significantly higher accumulation in the tumor tissue compared to that of the anti her-2 PLGA NP group (2.3 and 1.4 μg of particle/mg of tumor tissues, respectively).

CHAPTER 4

Conclusions, Limitations, and Future Work

In conclusion, we have successfully engineered and characterized Jurkat T lymphoma cells with chimeric antigenic receptor, and anti her-2 CAR engineered T-cell membrane coated afatinib-PLGA nanoparticles were successfully synthesized. These CAR-T-MNP membrane coated NPs displayed a high drug encapsulations efficiency of 61% and could release the drug in a sustained fashion over a period of 21 days. The drug release profile was found to be dependent on the existence of membrane on the particles in which the membrane coated nanoparticles provided a slower release. It might be due to the barrier effect of the additional membrane layer. Fabricated CAR T-MNPs were characterized in terms of size (< 400 nm), cell combability (up to 1000 ug/mL), stability and hemocompatibility (up to 500 ug/mL).

Moreover, cellular uptake studies showed that CAR-T-MNPs demonstrated superior uptake kinetics compared to bare particles and anti her-2 conjugated synthetic PLGA NPs. With the help of the anti her-2 CAR receptor, particles showed selective uptake by her-2 positive lung cancer cells when compared to anti her-2 negative Jurkat membrane coated PLGA and chemically conjugated anti her-2 PLGA NPs. These findings also correlated with enhanced therapeutic efficiencies of CAR-T-MNPs. Their cancer killing efficiencies agreed with uptake characteristics. However, detailed uptake binding kinetics of the ScFv's and antibodies is necessary for quantitative assessment and comparison of both systems such as targeting molecule per carrier conjugation direction to the surface and others. Therefore, CAR engineered membrane coated NPs

system could be a promising cell mimicking drug carrier that can improve the therapeutic outcomes of non-small lung cancer treatments.

Although cell membrane coated nanocarriers have a great potential to deliver drugs at the desired location, we need to consider the limitations and challenges associated with this approach. The cell membrane is comprised of various proteins, some of which are required for targeting, evading immune response while the other abundant proteins have unknown interactions in the host environment where the biodistribution, immune responses, and toxicity profiles have not been studied. Cell lines required for extracting the cell membrane need to tightly be monitored for their homogeneity, especially in stem cells where heterogeneous populations have been observed in a clonal cell population [32]. On the other hand, based on our observations in biodistribution studies, between the anti her-2 PLGA vs. CAR-T-MNP group, expected tumor accumulation difference in fold wise could not be obtained. Therefore, this similar accumulation effect reflects room for further development and investigation necessities for membrane-based drug carrier platforms. One of the possible improvements might be intracellular and extracellular facing ScFv bearing chimeric antigenic receptor development. This new strategy which is under investigation in our lab (data not shown) might be a new way to further develop the existing design. Therefore, isolated membranes are going to have targeting ScFv's on both sides of their lipid bilayer and when it is extruded along with NPs, the out layer of the membrane is always going to have outfacing ScFv's. With this method, targeting molecule number can be increased on the particle surface via integrating these "bidirectional CARs" (BiCARs) to the existing research. So far, integrating this BiCARs to existing research is under investigation by our lab for future developments. By this way, we are hoping to improve proposed drug carrier system's tumor accumulation efficiency without compromising its features.

Cell membrane isolation procedures are not robust and are majorly limited to a laboratory setting which can be a challenge in clinical translation of the cell membrane coated nanoparticles. Therefore, quality control such as maintaining the functional and structural aspects of cell membranes during membrane isolation techniques needs to be investigated. Some of the functionalized nanoparticles have already entered clinical trials, and the CMCNP have shown promising results in therapy with a potential for testing in clinical trials.

Even though the characterization *in vitro* and *in vivo* studies demonstrated positive results, as we mention above and have been realized during the research and development process, certain shortcomings and limitations need to be addressed and overcome.

- In preparation of the CAR-T-MNP particles, a vast number of transduced cells is necessary to provide enough cell membranes to cover the entire surface of NPs.
- During the extrusion process, inside-out or outside-in membrane vesicles are possibly coating the PLGA nanoparticles, and this will reduce the targeting moiety on the surface of the particles, leading to lower targeting efficacy.
- Due to the complex nature of membrane isolation and extrusion processes, considerable amounts of target proteins might have been damaged/lost during these processes. Membrane extraction protocol optimization is necessary to improve the yield of membrane protein.

Therefore, future work for this project is going to include the following studies to address above-mentioned limitations of the proposed research:

- Number targeting moiety assessment per particle (with the comparison of conventional targeting systems).
- Improvement of ligand number on the particle surface via integrating “double sided

(intracellular and extracellular facing ScFv modified CAR's) to the existing research. Thus, membrane-particle extrusions via extra-intra cellular facing ScFv CAR engineered membranes can drastically improve the outcomes of proposed research to a completely new level. For this purpose, preliminary studies have been done and the assessment of double-sided CAR molecules on the cells and extrusion studies are being investigated.

- CAR-T-MNPs are being formulated using engineered T-cells isolated from donors. Transduction and characterization studies of healthy T-cells have been done. Their potential in drug delivery application will be investigated as future steps of proposed drug delivery system for personalized cancer therapy.

REFERENCES

1. *Lung Anatomy*. [cited 2018; Available from: https://www.physio-pedia.com/Lung_Anatomy.
2. Ranganathan, R. and M.C. Foster, *The Limitations and Promise of Immunotherapy With Chimeric Antigen-Modified T Cells*. 2016, UBM MEDICA 535 CONNECTICUT AVE, STE 300, NORWALK, CT 06854 USA.
3. CDC. *Leading Cancer Cases and Deaths, Male and Female, 2015*. 2015 [cited 2018; Available from: https://gis.cdc.gov/Cancer/USCS/DataViz.html.
4. Zappa, C. and S.A. Mousa, *Non-small cell lung cancer: current treatment and future advances.* Translational lung cancer research, 2016. **5**(3): p. 288.
5. Detterbeck, F.C., D.J. Boffa, and L.T. Tanoue, *The new lung cancer staging system.* Chest, 2009. **136**(1): p. 260-271.
6. Molina, J.R., et al. *Non-small cell lung cancer: epidemiology, risk factors, treatment, and survivorship*. in *Mayo Clinic Proceedings*. 2008. Elsevier.
7. Sailor, M.J. and J.H. Park, *Hybrid nanoparticles for detection and treatment of cancer.* Advanced materials, 2012. **24**(28): p. 3779-3802.
8. Lindner, L.H., et al., *Novel temperature-sensitive liposomes with prolonged circulation time.* Clinical Cancer Research, 2004. **10**(6): p. 2168-2178.
9. Simões, S., et al., *Cationic liposomes for gene delivery.* Expert opinion on drug delivery, 2005. **2**(2): p. 237-254.
10. Babu, A., et al., *Nanoparticle-based drug delivery for therapy of lung cancer: progress and challenges.* Journal of Nanomaterials, 2013. **2013**: p. 14.
11. Rami-Porta, R., et al., *Complete resection in lung cancer surgery: proposed definition.* Lung Cancer, 2005. **49**(1): p. 25-33.
12. Wang, Y., et al., *Detection of micrometastases in lung cancer with magnetic nanoparticles and quantum dots.* International Journal of Nanomedicine, 2012. **7**: p. 2315.
13. Sundarraj, S., *EGFR antibody conjugated mesoporous silica nanoparticles for cytosolic phospholipase A2α targeted nonsmall lung cancer therapy.* Journal of Cell Science and Therapy, 2012. **3**(7).
14. Maciejczyk, A., I. Skrzypczyńska, and M. Janiszewska, *Lung cancer. Radiotherapy in lung cancer: Actual methods and future trends.* Reports of Practical Oncology & Radiotherapy, 2014. **19**(6): p. 353-360.
15. Timmerman, R., et al., *Excessive toxicity when treating central tumors in a phase II study of stereotactic body radiation therapy for medically inoperable early-stage lung cancer.* Journal of Clinical Oncology, 2006. **24**(30): p. 4833-4839.

16. Pérez-Herrero, E. and A. Fernández-Medarde, *Advanced targeted therapies in cancer: drug nanocarriers, the future of chemotherapy.* European Journal of Pharmaceutics and Biopharmaceutics, 2015. **93**: p. 52-79.
17. Peer, D., et al., *Nanocarriers as an emerging platform for cancer therapy.* Nature Nanotechnology, 2007. **2**(12): p. 751.
18. Brannon-Peppas, L. and J.O. Blanchette, *Nanoparticle and targeted systems for cancer therapy.* Advanced drug delivery reviews, 2012. **64**: p. 206-212.
19. Wicki, A., et al., *Nanomedicine in cancer therapy: challenges, opportunities, and clinical applications.* Journal of Controlled Release, 2015. **200**: p. 138-157.
20. Raez, L.E., S. Fein, and E.R. Podack, *Lung cancer immunotherapy.* Clinical Medicine & Research, 2005. **3**(4): p. 221-228.
21. Cho, J.H., *Immunotherapy for non-small-cell lung cancer: current status and future obstacles.* Immune Network, 2017. **17**(6): p. 378-391.
22. Karmakar, S., *Cell Based Immunotherapy: As a Promising Futuristic Solution for Effective Cancer Therapy.* Single Cell Biol, 2014. **4**(105): p. 2.
23. Sabado, R.L., S. Balan, and N. Bhardwaj, *Dendritic cell-based immunotherapy.* Cell Research, 2017. **27**(1): p. 74.
24. Fang, F., W. Xiao, and Z. Tian. *NK cell-based immunotherapy for cancer*. in *Seminars in immunology*. 2017. Elsevier.
25. Houot, R., et al., *T-cell–based immunotherapy: adoptive cell transfer and checkpoint inhibition.* Cancer Immunology Research, 2015. **3**(10): p. 1115-1122.
26. Androulla, M.N. and P.C. Lefkothea, *CAR T-cell therapy: a new era in cancer immunotherapy.* Current Pharmaceutical Biotechnology, 2018. **19**(1): p. 5-18.
27. Weiner, L.M., R. Surana, and S. Wang, *Monoclonal antibodies: versatile platforms for cancer immunotherapy.* Nature Reviews Immunology, 2010. **10**(5): p. 317.
28. Pardoll, D.M., *The blockade of immune checkpoints in cancer immunotherapy.* Nature Reviews Cancer, 2012. **12**(4): p. 252.
29. Lambour, J., et al., *Converting monoclonal antibody-based immunotherapies from passive to active: bringing immune complexes into play.* Emerging Microbes & Infections, 2016. **5**(8): p. e92.
30. Scott, A.M., J.D. Wolchok, and L.J. Old, *Antibody therapy of cancer.* Nature Reviews Cancer, 2012. **12**(4): p. 278.
31. Tarazona, R., et al., *Immunosenescence: limitations of natural killer cell-based cancer immunotherapy.* Cancer Immunology, Immunotherapy, 2017. **66**(2): p. 233-245.
32. Sciavolino, P.J., *Autoimmunity and limitations of cancer vaccines.* Targeted Oncology, 2014.
33. Ghoneim, H.E., et al., *Cell-intrinsic barriers of T cell-based immunotherapy.* Trends in Molecular Medicine, 2016. **22**(12): p. 1000-1011.
34. Singh, S., et al., *Nanoparticle based drug delivery system: advantages and applications.* Indian Journal of Science and Technology, 2011. **4**(3): p. 177-180.
35. Conde, J., G. Doria, and P. Baptista, *Noble metal nanoparticles applications in cancer.* Journal of Drug Delivery, 2012. **2012**.

36. Sun, W., et al., *Endocytosis of a single mesoporous silica nanoparticle into a human lung cancer cell observed by differential interference contrast microscopy.* Analytical and Bioanalytical Chemistry, 2008. **391**(6): p. 2119.
37. Bartlett, D.W., et al., *Impact of tumor-specific targeting on the biodistribution and efficacy of siRNA nanoparticles measured by multimodality in vivo imaging.* Proceedings of the National Academy of Sciences, 2007. **104**(39): p. 15549-15554.
38. Pirollo, K.F. and E.H. Chang, *Does a targeting ligand influence nanoparticle tumor localization or uptake?* Trends in Biotechnology, 2008. **26**(10): p. 552-558.
39. Qiu, L., et al., *A cell-targeted, size-photocontrollable, nuclear-uptake nanodrug delivery system for drug-resistant cancer therapy.* Nano Letters, 2014. **15**(1): p. 457-463.
40. Zhong, Y., et al., *Ligand-directed active tumor-targeting polymeric nanoparticles for cancer chemotherapy.* Biomacromolecules, 2014. **15**(6): p. 1955-1969.
41. Ramzy, L., et al., *Cancer nanotheranostics: a review of the role of conjugated ligands for overexpressed receptors.* European Journal of Pharmaceutical Sciences, 2017. **104**: p. 273-292.
42. Nukolova, N.V., et al., *Folate-decorated nanogels for targeted therapy of ovarian cancer.* Biomaterials, 2011. **32**(23): p. 5417-5426.
43. Hong, M., et al., *Novel anti-tumor strategy: PEG-hydroxycamptothecin conjugate loaded transferrin-PEG-nanoparticles.* Journal of Controlled Release, 2010. **141**(1): p. 22-29.
44. Guo, J., et al., *Aptamer-functionalized PEG–PLGA nanoparticles for enhanced anti-glioma drug delivery.* Biomaterials, 2011. **32**(31): p. 8010-8020.
45. Xin, H., et al., *Angiopep-conjugated poly (ethylene glycol)-co-poly (ε-caprolactone) nanoparticles as dual-targeting drug delivery system for brain glioma.* Biomaterials, 2011. **32**(18): p. 4293-4305.
46. Biswas, S., et al., *Liposomes loaded with paclitaxel and modified with novel triphenylphosphonium-PEG-PE conjugate possess low toxicity, target mitochondria and demonstrate enhanced antitumor effects in vitro and in vivo.* Journal of Controlled Release, 2012. **159**(3): p. 393-402.
47. Warenius, H., et al., *Attempted targeting of a monoclonal antibody in a human tumour xenograft system.* European Journal of Cancer and Clinical Oncology, 1981. **17**(9): p. 1009-1015.
48. Valencia, P.M., et al., *Effects of ligands with different water solubilities on self-assembly and properties of targeted nanoparticles.* Biomaterials, 2011. **32**(26): p. 6226-6233.
49. Elias, D.R., et al., *Effect of ligand density, receptor density, and nanoparticle size on cell targeting.* Nanomedicine: Nanotechnology, Biology and Medicine, 2013. **9**(2): p. 194-201.
50. Juweid, M., et al., *Micropharmacology of monoclonal antibodies in solid tumors: direct experimental evidence for a binding site barrier.* Cancer Research, 1992. **52**(19): p. 5144-5153.
51. Ghitescu, L. and M. Bendayan, *Immunolabeling efficiency of protein A-gold complexes.* Journal of Histochemistry & Cytochemistry, 1990. **38**(11): p. 1523-1530.
52. Muro, S., *Challenges in design and characterization of ligand-targeted drug delivery systems.* Journal of Controlled Release, 2012. **164**(2): p. 125-137.

53. Yumura, K., et al., *Mutations for decreasing the immunogenicity and maintaining the function of core streptavidin.* Protein Science, 2013. **22**(2): p. 213-221.
54. Colombo, G., et al., *Structure-activity relationships of linear and cyclic peptides containing the NGR tumor-homing motif.* Journal of Biological Chemistry, 2002. **277**(49): p. 47891-47897.
55. Thanuja, M., C. Anupama, and S.H. Ranganath, *Bioengineered cellular and cell membrane-derived vehicles for actively targeted drug delivery: So near and yet so far.* Advanced Drug Delivery Reviews, 2018.
56. Yu, X., et al., *Design of nanoparticle-based carriers for targeted drug delivery.* Journal of Nanomaterials, 2016. **2016**.
57. Kroll, A.V., R.H. Fang, and L. Zhang, *Biointerfacing and applications of cell membrane-coated nanoparticles.* Bioconjugate Chemistry, 2016. **28**(1): p. 23-32.
58. Gajewski, T.F., H. Schreiber, and Y.-X. Fu, *Innate and adaptive immune cells in the tumor microenvironment.* Nature Immunology, 2013. **14**(10): p. 1014.
59. Roybal, K.T., et al., *Engineering T cells with customized therapeutic response programs using synthetic notch receptors.* Cell, 2016. **167**(2): p. 419-432. e16.
60. Baeumler, T.A., A.A. Ahmed, and T.A. Fulga, *Engineering synthetic signaling pathways with programmable dCas9-based chimeric receptors.* Cell Reports, 2017. **20**(11): p. 2639-2653.
61. Schmid, D., et al., *T cell-targeting nanoparticles focus delivery of immunotherapy to improve antitumor immunity.* Nature Communications, 2017. **8**(1): p. 1747.
62. Paulitschke, M., et al., *Perturbation of red blood cell membrane rigidity by extracellular ligands.* Blood, 1995. **86**(1): p. 342-348.
63. Orbach, A., et al., *Biophysical and biochemical markers of red blood cell fragility.* Transfusion Medicine and Hemotherapy, 2017. **44**(3): p. 183-187.
64. Morera, D. and S.A. MacKenzie, *Is there a direct role for erythrocytes in the immune response?* Veterinary Research, 2011. **42**(1): p. 89.
65. Mengesha, A., et al., *Potential and limitations of bacterial-mediated cancer therapy.* Front Biosci, 2007. **12**: p. 3880-3891.
66. Mohr, A. and R. Zwacka, *The future of mesenchymal stem cell-based therapeutic approaches for cancer–From cells to ghosts.* Cancer Letters, 2017.
67. Li, R., et al., *Cell membrane-based nanoparticles: a new biomimetic platform for tumor diagnosis and treatment.* Acta Pharmaceutica Sinica B, 2017.
68. von Roemeling, C., et al., *Breaking down the barriers to precision cancer nanomedicine.* Trends in Biotechnology, 2017. **35**(2): p. 159-171.
69. Hu, C.-M.J., et al., *Erythrocyte membrane-camouflaged polymeric nanoparticles as a biomimetic delivery platform.* Proceedings of the National Academy of Sciences, 2011. **108**(27): p. 10980-10985.
70. Gao, M., et al., *Erythrocyte-Membrane-Enveloped Perfluorocarbon as Nanoscale Artificial Red Blood Cells to Relieve Tumor Hypoxia and Enhance Cancer Radiotherapy.* Advanced Materials, 2017. **29**(35): p. 1701429.
71. Dehaini, D., et al., *Erythrocyte–platelet hybrid membrane coating for enhanced nanoparticle functionalization.* Advanced Materials, 2017. **29**(16): p. 1606209.

72. Wang, D., et al., *Erythrocyte–Cancer Hybrid Membrane Camouflaged Hollow Copper Sulfide Nanoparticles for Prolonged Circulation Life and Homotypic-Targeting Photothermal/Chemotherapy of Melanoma.* ACS nano, 2018. **12**(6): p. 5241-5252.
73. Zhang, D., J. Wang, and D. Xu, *Cell-penetrating peptides as noninvasive transmembrane vectors for the development of novel multifunctional drug-delivery systems.* Journal of Controlled Release, 2016. **229**: p. 130-139.
74. Hu, C.-M.J., et al., *A biomimetic nanosponge that absorbs pore-forming toxins.* Nature Nanotechnology, 2013. **8**(5): p. 336.
75. Kang, T., et al., *Nanoparticles coated with neutrophil membranes can effectively treat cancer metastasis.* ACS Nano, 2017. **11**(2): p. 1397-1411.
76. Spicer, J.D., et al., *Neutrophils promote liver metastasis via Mac-1 mediated interactions with circulating tumor cells.* Cancer Research, 2012: p. canres. 2393.2011.
77. Strell, C., et al., *Surface molecules regulating rolling and adhesion to endothelium of neutrophil granulocytes and MDA-MB-468 breast carcinoma cells and their interaction.* Cellular and Molecular Life Sciences, 2007. **64**(24): p. 3306-3316.
78. Fang, R.H., et al., *Cancer cell membrane-coated nanoparticles for anticancer vaccination and drug delivery.* Nano Letters, 2014. **14**(4): p. 2181-2188.
79. Angsantikul, P., et al., *Cell membrane-coated nanoparticles as an emerging antibacterial vaccine platform.* Vaccines, 2015. **3**(4): p. 814-828.
80. Fontana, F., et al., *Multistaged nanovaccines based on porous silicon@ acetalated dextran@ cancer cell membrane for cancer immunotherapy.* Advanced Materials, 2017. **29**(7): p. 1603239.
81. Beatty, G.L. and W.L. Gladney, *Immune escape mechanisms as a guide for cancer immunotherapy.* Clinical Cancer Research, 2015. **21**(4): p. 687-692.
82. Cao, H., et al., *Liposomes coated with isolated macrophage membrane can target lung metastasis of breast cancer.* ACS Nano, 2016. **10**(8): p. 7738-7748.
83. Zhu, J.-Y., et al., *Preferential cancer cell self-recognition and tumor self-targeting by coating nanoparticles with homotypic cancer cell membranes.* Nano Letters, 2016. **16**(9): p. 5895-5901.
84. Kroll, A.V., et al., *Nanoparticulate delivery of cancer cell membrane elicits multiantigenic antitumor immunity.* Advanced Materials, 2017. **29**(47): p. 1703969.
85. Zhang, L., et al., *Human cytotoxic T-lymphocyte membrane-camouflaged nanoparticles combined with low-dose irradiation: a new approach to enhance drug targeting in gastric cancer.* International Journal of Nanomedicine, 2017. **12**: p. 2129.
86. Parodi, A., et al., *Synthetic nanoparticles functionalized with biomimetic leukocyte membranes possess cell-like functions.* Nature Nanotechnology, 2013. **8**(1): p. 61.
87. Pasto, A., et al., *Cell membrane protein functionalization of nanoparticles as a new tumor-targeting strategy.* Clinical and translational medicine, 2019. **8**(1): p. 8.
88. Stephan, M.T., et al., *Synapse-directed delivery of immunomodulators using T-cell-conjugated nanoparticles.* Biomaterials, 2012. **33**(23): p. 5776-5787.
89. Mitchell, M.J., et al., *TRAIL-coated leukocytes that kill cancer cells in the circulation.* Proceedings of the National Academy of Sciences, 2014. **111**(3): p. 930-935.

90. Thanuja, M., C. Anupama, and S.H. Ranganath, *Bioengineered cellular and cell membrane-derived vehicles for actively targeted drug delivery: So near and yet so far.* Advanced Drug Delivery Reviews, 2018. **132**: p. 57-80.
91. Xuan, M., et al., *Nanocapsules: macrophage cell membrane camouflaged mesoporous silica nanocapsules for in vivo cancer therapy (Adv. Healthcare Mater. 11/2015).* Advanced Healthcare Materials, 2015. **4**(11): p. 1578-1578.
92. Thamphiwatana, S., et al., *Macrophage-like nanoparticles concurrently absorbing endotoxins and proinflammatory cytokines for sepsis management.* Proceedings of the National Academy of Sciences, 2017. **114**(43): p. 11488-11493.
93. Munich, S., et al., *Dendritic cell exosomes directly kill tumor cells and activate natural killer cells via TNF superfamily ligands.* Oncoimmunology, 2012. **1**(7): p. 1074-1083.
94. Xue, J., et al., *Neutrophil-mediated anticancer drug delivery for suppression of postoperative malignant glioma recurrence.* Nature Nanotechnology, 2017. **12**(7): p. 692.
95. Krishnamurthy, S., et al., *Monocyte cell membrane-derived nanoghosts for targeted cancer therapy.* Nanoscale, 2016. **8**(13): p. 6981-6985.
96. Li, R., et al., *Cell membrane-based nanoparticles: a new biomimetic platform for tumor diagnosis and treatment.* Acta Pharmaceutica Sinica B, 2018. **8**(1): p. 14-22.
97. Fang, R.H., et al., *Cell membrane coating nanotechnology.* Advanced Materials, 2018. **30**(23): p. 1706759.
98. Luk, B.T., et al., *Safe and immunocompatible nanocarriers cloaked in RBC membranes for drug delivery to treat solid tumors.* Theranostics, 2016. **6**(7): p. 1004.
99. Wang, F., et al., *Nanoparticle-based antivirulence vaccine for the management of methicillin-resistant Staphylococcus aureus skin infection.* Advanced Functional Materials, 2016. **26**(10): p. 1628-1635.
100. Danesh, A., et al., *Exosomes from red blood cell units bind to monocytes and induce proinflammatory cytokines, boosting T-cell responses in vitro.* Blood, 2014. **123**(5): p. 687-696.
101. Gao, W., et al., *Surface functionalization of gold nanoparticles with red blood cell membranes.* Advanced Materials, 2013. **25**(26): p. 3549-3553.
102. Wu, H.-H., et al., *Mesenchymal stem cell-based drug delivery strategy: from cells to biomimetic.* Journal of Controlled Release, 2018.
103. Sadhukha, T., T.D. O'brien, and S. Prabha, *Nano-engineered mesenchymal stem cells as targeted therapeutic carriers.* Journal of Controlled Release, 2014. **196**: p. 243-251.
104. Wang, X., et al., *Mesenchymal stem cells loaded with paclitaxel-poly (lactic-co-glycolic acid) nanoparticles for glioma-targeting therapy.* International Journal of Nanomedicine, 2018. **13**: p. 5231.
105. Gao, C., et al., *Stem cell membrane-coated nanogels for highly efficient in vivo tumor targeted drug delivery.* Small, 2016. **12**(30): p. 4056-4062.
106. Sun, H., et al., *Cancer cell membrane-coated gold nanocages with hyperthermia-triggered drug release and homotypic target inhibit growth and metastasis of breast cancer.* Advanced Functional Materials, 2017. **27**(3): p. 1604300.
107. Poetsch, A. and D. Wolters, *Bacterial membrane proteomics.* Proteomics, 2008. **8**(19): p. 4100-4122.

108. Lee, E.Y., et al., *Global proteomic profiling of native outer membrane vesicles derived from Escherichia coli.* Proteomics, 2007. **7**(17): p. 3143-3153.
109. Kuehn, M.J. and N.C. Kesty, *Bacterial outer membrane vesicles and the host–pathogen interaction.* Genes & Development, 2005. **19**(22): p. 2645-2655.
110. Gao, W., et al., *Modulating antibacterial immunity via bacterial membrane-coated nanoparticles.* Nano Letters, 2015. **15**(2): p. 1403-1409.
111. Muralinath, M., et al., *Immunization with Salmonella enterica serovar Typhimurium-derived outer membrane vesicles delivering the pneumococcal protein PspA confers protection against challenge with Streptococcus pneumoniae.* Infection and Immunity, 2011. **79**(2): p. 887-894.
112. Kim, O.Y., et al., *Bacterial outer membrane vesicles suppress tumor by interferon-γ-mediated antitumor response.* Nature Communications, 2017. **8**(1): p. 626.
113. Gujrati, V., et al., *Bioengineered bacterial outer membrane vesicles as cell-specific drug-delivery vehicles for cancer therapy.* ACS Nano, 2014. **8**(2): p. 1525-1537.
114. Fantappie, L., et al., *Antibody-mediated immunity induced by engineered Escherichia coli OMVs carrying heterologous antigens in their lumen.* Journal of Extracellular Vesicles, 2014. **3**(1): p. 24015.
115. Tsai, R.K., P.L. Rodriguez, and D.E. Discher, *Self inhibition of phagocytosis: the affinity of 'marker of self'CD47 for SIRPα dictates potency of inhibition but only at low expression levels.* Blood Cells, Molecules, and Diseases, 2010. **45**(1): p. 67-74.
116. Ma, Y.Q., J. Qin, and E. Plow, *Platelet integrin αIIbβ3: activation mechanisms.* Journal of Thrombosis and Haemostasis, 2007. **5**(7): p. 1345-1352.
117. Bu, L.L., et al., *Cancer stem cell-platelet hybrid membrane-coated magnetic nanoparticles for enhanced photothermal therapy of head and neck squamous cell carcinoma.* Advanced Functional Materials, 2019. **29**(10): p. 1807733.
118. Cao, X., et al., *Neutrophil-mimicking therapeutic nanoparticles for targeted chemotherapy of pancreatic carcinoma.* Acta Pharmaceutica Sinica B, 2019. **9**(3): p. 575-589.
119. Zhang, Y., et al., *Macrophage-membrane-coated nanoparticles for tumor-targeted chemotherapy.* Nano Letters, 2018. **18**(3): p. 1908-1915.
120. Jin, J., et al., *Human cancer cell membrane coated biomimetic nanoparticles reduce fibroblast-mediated invasion and metastasis, and induce T cells.* ACS Applied Materials & Interfaces, 2019.
121. Felgner, S., et al., *Engineered Salmonella enterica serovar Typhimurium overcomes limitations of anti-bacterial immunity in bacteria-mediated tumor therapy.* Oncoimmunology, 2018. **7**(2): p. e1382791.
122. Moghimi, S.M. and J. Szebeni, *Stealth liposomes and long circulating nanoparticles: critical issues in pharmacokinetics, opsonization and protein-binding properties.* Progress in Lipid Research, 2003. **42**(6): p. 463-478.
123. Immordino, M.L., F. Dosio, and L. Cattel, *Stealth liposomes: review of the basic science, rationale, and clinical applications, existing and potential.* International Journal of Nanomedicine, 2006. **1**(3): p. 297.

124. Lundqvist, M., et al., *Nanoparticle size and surface properties determine the protein corona with possible implications for biological impacts.* Proceedings of the National Academy of Sciences, 2008. **105**(38): p. 14265-14270.
125. Monopoli, M.P., et al., *Physical− chemical aspects of protein corona: relevance to in vitro and in vivo biological impacts of nanoparticles.* Journal of the American Chemical Society, 2011. **133**(8): p. 2525-2534.
126. Corbo, C., et al., *The impact of nanoparticle protein corona on cytotoxicity, immunotoxicity and target drug delivery.* Nanomedicine, 2016. **11**(1): p. 81-100.
127. Feliu, N., et al., *In vivo degeneration and the fate of inorganic nanoparticles.* Chemical Society Reviews, 2016. **45**(9): p. 2440-2457.
128. Zanganeh, S., et al., *Protein corona: Opportunities and challenges.* The international journal of biochemistry & cell biology, 2016. **75**: p. 143-147.
129. Yin, H., et al., *Reducing the cytotoxicity of ZnO nanoparticles by a pre-formed protein corona in a supplemented cell culture medium.* RSC Advances, 2015. **5**(90): p. 73963-73973.
130. Escamilla-Rivera, V., et al., *Protein corona acts as a protective shield against Fe3O4-PEG inflammation and ROS-induced toxicity in human macrophages.* Toxicology Letters, 2016. **240**(1): p. 172-184.
131. Weidner, A., et al. *Formation of a biocompatible protein corona on magnetic nanoparticles*. in *Magnetic Particle Imaging (IWMPI), 2015 5th International Workshop on*. 2015. IEEE.
132. Mahmoudi, M., *Protein corona: The golden gate to clinical applications of nanoparticles.* International Journal of Biochemistry and Cell Biology, 2016(75): p. 141-142.
133. Hühn, J., et al., *Dissociation coefficients of protein adsorption to nanoparticles as quantitative metrics for description of the protein corona: A comparison of experimental techniques and methodological relevance.* The International Journal of Biochemistry & Cell Biology, 2016. **75**: p. 148-161.
134. Parodi, A., et al., *Bio-inspired engineering of cell-and virus-like nanoparticles for drug delivery.* Biomaterials, 2017. **147**: p. 155-168.
135. Yoo, J.-W., et al., *Bio-inspired, bioengineered and biomimetic drug delivery carriers.* Nature Reviews Drug discovery, 2011. **10**(7): p. 521.
136. Barenholz, Y., *Sphingomyelin and cholesterol: from membrane biophysics and rafts to potential medical applications*, in *Membrane Dynamics and Domains*. 2004, Springer. p. 167-215.
137. Langer, R. and D.A. Tirrell, *Designing materials for biology and medicine.* Nature, 2004. **428**(6982): p. 487.
138. Irvine, D.J., M.A. Swartz, and G.L. Szeto, *Engineering synthetic vaccines using cues from natural immunity.* Nature Materials, 2013. **12**(11): p. 978.
139. Manchester, M. and P. Singh, *Virus-based nanoparticles (VNPs): platform technologies for diagnostic imaging.* Advanced Drug Delivery Reviews, 2006. **58**(14): p. 1505-1522.
140. Merkel, T.J., et al., *Using mechanobiological mimicry of red blood cells to extend circulation times of hydrogel microparticles.* Proceedings of the National Academy of Sciences, 2011. **108**(2): p. 586-591.

141. Von Maltzahn, G., et al., *Nanoparticles that communicate in vivo to amplify tumour targeting.* Nature Materials, 2011. **10**(7): p. 545.
142. Toledano Furman, N.E., et al., *Reconstructed stem cell nanoghosts: a natural tumor targeting platform.* Nano Letters, 2013. **13**(7): p. 3248-3255.
143. Piao, J.-G., et al., *Erythrocyte membrane is an alternative coating to polyethylene glycol for prolonging the circulation lifetime of gold nanocages for photothermal therapy.* ACS Nano, 2014. **8**(10): p. 10414-10425.
144. Hirsh, V., *Next-generation covalent irreversible kinase inhibitors in NSCLC: focus on afatinib.* BioDrugs, 2015. **29**(3): p. 167-183.
145. Trinidad, A.J., et al., *Combined concurrent photodynamic and gold nanoshell loaded macrophage-mediated photothermal therapies: An in vitro study on squamous cell head and neck carcinoma.* Lasers in Surgery and Medicine, 2014. **46**(4): p. 310-318.
146. Bahmani, B., D. Bacon, and B. Anvari, *Erythrocyte-derived photo-theranostic agents: hybrid nano-vesicles containing indocyanine green for near infrared imaging and therapeutic applications.* Scientific Reports, 2013. **3**: p. 2180.
147. Baek, S.-K., et al., *Photothermal treatment of glioma; an in vitro study of macrophage-mediated delivery of gold nanoshells.* Journal of Neuro-Oncology, 2011. **104**(2): p. 439-448.
148. Springer, T.A., *Traffic signals for lymphocyte recirculation and leukocyte emigration: the multistep paradigm.* Cell, 1994. **76**(2): p. 301-314.
149. Baggiolini, M., *Chemokines and leukocyte traffic.* Nature, 1998. **392**(6676): p. 565.
150. Panés, J., M. Perry, and D.N. Granger, *Leukocyte-endothelial cell adhesion: avenues for therapeutic intervention.* British Journal of Pharmacology, 1999. **126**(3): p. 537-550.
151. Ley, K., *Molecular mechanisms of leukocyte recruitment in the inflammatory process.* Cardiovascular Research, 1996. **32**(4): p. 733-742.
152. Huang, Y., X. Gao, and J. Chen, *Leukocyte-derived biomimetic nanoparticulate drug delivery systems for cancer therapy.* Acta Pharmaceutica Sinica B, 2018. **8**(1): p. 4-13.
153. Mitchell, M.J. and M.R. King, *Leukocytes as carriers for targeted cancer drug delivery.* Expert Opinion on Drug Delivery, 2015. **12**(3): p. 375-392.
154. Crittenden, M., et al., *Pharmacologically regulated production of targeted retrovirus from T cells for systemic antitumor gene therapy.* Cancer Research, 2003. **63**(12): p. 3173-3180.
155. Bunn, P.A., et al., *Expression of Her-2/neu in human lung cancer cell lines by immunohistochemistry and fluorescence in situ hybridization and its relationship to in vitro cytotoxicity by trastuzumab and chemotherapeutic agents.* Clinical Cancer Research, 2001. **7**(10): p. 3239-3250.

APPENDIX 1

Flow cytometric Her-2 expression level analysis of cell lines used in pharmakokinetic studies

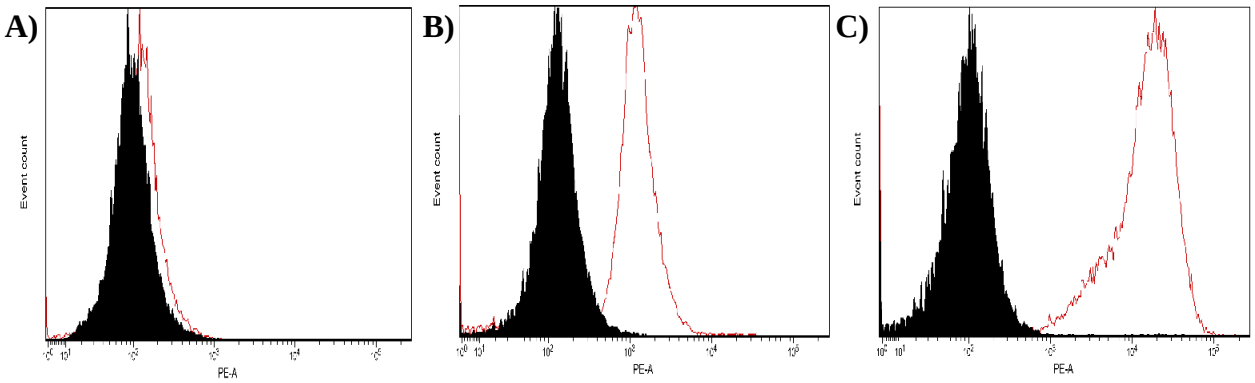

Figure 37: Appendix.1 Flow cytometric Her-2 expression level analysis of A) MDA-MB-231, B) A549 and C) SKOV-3 cell lines.

APPENDIX 2

Pharmacokinetic measurement of free afatinib on A) MDA-MB-231, B) A549 and C) SKOV-3 cell lines.

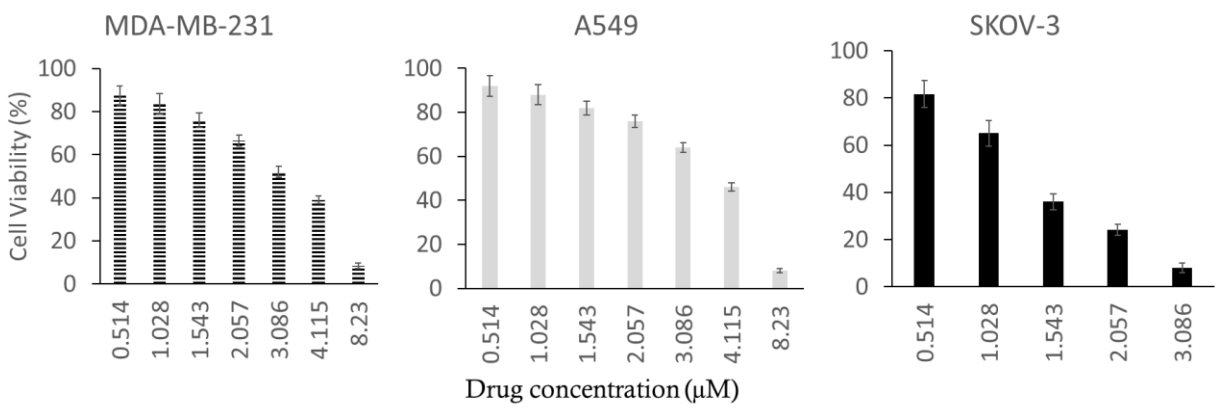

Figure 38: Appendix 2. Pharmacokinetic measurement of free afatinib on A) MDA-MB-231, B) A549 and C) SKOV-3 cell lines.

Serkan Yaman pursued his bachelor's in molecular biology and genetics from Istanbul University in Turkey. He worked as an undergraduate researcher attempting to purify DNA and protein from operant conditioned rats to investigate changes of c-AMP response element binding (CREB) protein in the brain. Following a year working at RAS, he started to pursue a master's degree in bioengineering at Yıldız Technical University and was involved with several different projects in Dr. Allahverdiyev's research group. He worked extensively in cell cultures, identification, differentiation, separating and cryopreserving techniques, antibody development, purification techniques, and animal experiments. He also took part in several research projects associated with developing new vaccines and diagnostics. After his graduation, he secured a scholarship from the Turkish ministry of education to pursue doctoral degree in the U.S.A. He joined Dr. Kytai T. Nguyen's lab to pursue a doctorate in biomedical engineering with an emphasis on tissue engineering in the year 2014. Since then, he has been working with Dr. Nguyen and Dr. Weidanz on their collaboration project to develop a biomimetic drug carrier for superior drug delivery applications. Throughout his Ph.D. program, he also served as a lab safety and training officer. He has worked on several different projects such as the development of responsive drug delivery nanoparticle systems, development of immunotherapy applications for lung cancer, CAR-T-cell development, *in vitro* therapeutic activities of chemo-drugs, *in vitro* therapeutic activities of immunotherapy applications, cell sorting techniques, and animal experiments regarding drug delivery, immunotherapy and biodistribution aspects. The efforts on the research projects have yielded several conference publications in national meetings of BMES (2014-2018), and several peer reviewed papers are under the submission process (2019). In addition, Serkan also has been awarded 2nd runner-up and price money ($4,000) in the International Food R&D Brokerage Event with the "fabrication of fast, sensitive and point of care detection kits for detecting contaminations of meat and meat products" (organized by Assembly of Turkish Exporters). The same project was also passed the election process to be awarded $50,000 for an individual entrepreneurship project proposal (Project No :194) titled "The Fabrication of Fast, Sensitive and Point of Care Detection Kits to Detect Contamination of Meat and Meat Products" by the scientific and technological research council of Turkey (TUBITAK) (2012). Lastly, he has been granted a full graduate scholarship award for Ph.D. studies in biomedical engineering field from the Turkish Government (Ministry of Education) (2013-2019).